CARBOXYLATO COMPOUNDS OF CHROMIUM, COPPER, RHODIUM AND MOLYBDENUM AND NEW ADVANCES IN THE CHEMISTRY OF $V_2(NXN)_4$

A Dissertation

by

ELIZABETH ANNE HILLARD

Submitted to the Office of Graduate Studies of
Texas A&M University
in partial fulfillment of the requirements for the degree of

DOCTOR OF PHILOSOPHY

May 2003

Major Subject: Chemistry

CARBOXYLATO COMPOUNDS OF CHROMIUM, COPPER, RHODIUM AND MOLYBDENUM AND NEW ADVANCES IN THE CHEMISTRY OF $V_2(NXN)_4$

A Dissertation

by

ELIZABETH ANNE HILLARD

Submitted to the Office of Graduate Studies of
Texas A&M University
in partial fulfillment of the requirements for the degree of

DOCTOR OF PHILOSOPHY

Approved as to style and content by:

F. A. Cotton (Chair of Committee)	Marlan Scully (Member)
Marcetta Darensbourg (Member)	Rand Watson (Member)
E. A. Schweikert (Head of Department)	

May 2003

Major Subject: Chemistry

ABSTRACT

Carboxylato Compounds of Chromium, Copper, Rhodium and

Molybdenum and New Advances in the Chemistry of $V_2(NXN)_4$. (May 2003)

Elizabeth Anne Hillard, B.A.; B.S., University of Alaska-Fairbanks

Chair of Advisory Committee: Dr. F. Albert Cotton

This dissertation comprises the investigation of two subjects in the field of dimetal paddlewheel-type compounds containing metal-metal bonds: unsolvated transition metal carboxylates and triply bonded divanadium compounds. The first subject is very mature; dichromium tetraacetate was first synthesized in 1844, and hundreds of dimetal tetracarboxylates have been structurally characterized to date. A general question concerning the complexes of the type $M_2L_4{\cdot}X_n$ (where n = 0 to 2) is the extent to which the M–M distances are influenced by the presence of axial ligands, X. However, virtually none of the carboxylato complexes crystallize without axial ligands. In the solid state, in the absence of a coordinating solvent, the dimetal units often act as axial ligands to one another. In order to exclude axial coordination, both from donor solvent molecules, and from the aggregation of M_2^{4+} units, we have successfully used the bulky 2,4,6-triisopropylbenzoate ligand to bridge the dimetal core. We have investigated the triisopropylbenzoato complexes of some metals which are known for their ability to form a vast array of tetracarboxylato complexes, namely chromium, copper, molybdenum, and rhodium, and have found that these novel compounds display some interesting structural and chemical properties.

The second subject of this dissertation is much more contemporary. Although compounds containing multiple bonds between metal atoms have been known since 1964, the

first triply-bonded divanadium compound was not synthesized until 1992, and only two additional compounds of this type have been made in the intervening ten years. In order to extend this chemistry, several additional compounds containing a triply bonded V_2^{4+} core have recently been characterized. In our study of these compounds, we have discovered the first example of a stable paddlewheel-type compound with a M_2^{3+} core.

ACKNOWLEDGMENTS

First and foremost I would like to acknowledge Professor F. A. Cotton. It has been an honor to know a man of such transparent brilliance and élan. Not only has he taught me about chemistry, but he has also taught me to never procrastinate and to apply reason to all things.

I would like to warmly thank Professor Carlos Murillo for helping me obtain my PhD. Without his thoughtful and erudite advice, I would have accomplished little.

Thanks to Dr. Lee Daniels for his cheerful tutoring in all aspects of X-ray crystallography, and to Dr. Xiaoping Wang for gracefully filling Lee's big shoes.

Dr. Hongcai Zhou and Dr. Marina Petrukhina showed me great kindness when I first joined the laboratory. Their unselfishness and patience while teaching me how to work in the lab is greatly appreciated.

The help of Beverly Moore has been indispensable in navigating the waters of journal editors and University administrators.

Finally, I would like to thank all of my coworkers for putting up with me: Panos Angaridis, John Berry, Evgeny Dikarev, Jim Donahue, Chris Fewox, Jiande Gu, Santi Herrero, Penglin Huang, Sergei Igbrahimov, Steve Jeffery, Peng Lei, Chun Lin, Chun Yuan Liu, Tongbu Lu, Barbara Modec, Paul Schooler, Salah Stiriba, Daren Timmons, Chad Wilkinson, and Rongmin Yu.

Cheers!

TABLE OF CONTENTS

LIST OF FIGURES

FIGURE Page

LIST OF TABLES

TABLE Page

CHAPTER I

INTRODUCTION

Since the recognition of the quadruple bond in $Re_2Cl_8^{2-}$, nearly 40 years ago,[1] the chemistry of metal-metal bonded species has grown at such a rapid pace that there are now thousands of such compounds that have been studied and characterized.[2] There is generally good understanding of the bonding and electronic structures,[3] and some of these compounds have many important applications in catalysis[4] and medicine[5] and some are potent reducing agents that can be used in synthesis.[6]

The most important structural motif thus far is the "paddlewheel" complex where two metal atoms are embraced by four bridging ligands, such as carboxylates, amidates, amidinates and others, as represented in Figure 1. Many transition elements form compounds with this structural motif and axial ligands, X, may or may not be present. Bonding interactions between the metal atoms arise from *d* orbital overlap, and bond orders can vary from 0 to 4, with oxidation states for isolated M_2^{n+} units from $n = 4$ to 7.

An important question concerning complexes of the type $M_2L_4{\cdot}X_n$ (where $n = 0$ to 2) is the extent to which the M–M distances are influenced by the identity of M, the nature of L, and the presence of X. It is for compounds of chromium that this question is most acute, since Cr–Cr

---

This dissertation follows the style and format of *Inorganic Chemistry*.

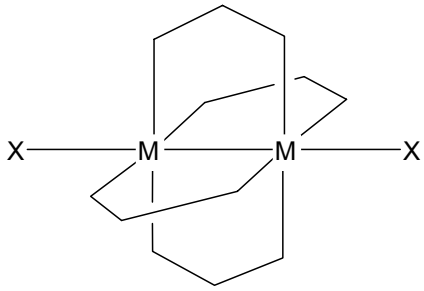

Figure 1. A schematic drawing of the paddlewheel structural motif.

distances range from 1.83 Å to 2.69 Å depending on L, X, and *n*, all within the common structural motif of the paddlewheel arrangement of the four L ligands. This extraordinary variation has provoked many theoretical studies[7] as well as extensive experimental explorations.[2] Two important observations have been made. The first is that Cr–Cr bond distances become shorter with the increased basicity of the bridging ligand. Secondly, Cr–Cr bond distances increase as the basicity of the axial ligands increases. For example, all compounds with Cr–Cr bonds under 2.00 Å are devoid of axial ligands, while axial ligation always occurs in molecules with Cr–Cr bonds over 2.00 Å. Furthermore, in the case of the carboxylates, the Cr–Cr bonds are all longer than 2.3 Å, and all possess axial ligation. Thus it is unclear whether the length of the Cr–Cr bonds in the carboxylato complexes can be attributed mainly to the presence of axial ligation or to the poor donor properties of the carboxylato ligands.

While chromium may provide the most dramatic setting for this problem due to the enormous sensitivity of the Cr–Cr bond, this question of the influence of axial ligands is not unique to dichromium systems. Our understanding of the factors impacting metal-metal bond distances has been limited by the fact that unsolvated, discrete $M_2(O_2CR)_4$ complexes are

virtually unknown for *all* transition metals. In most cases, the absence of exogenous axial ligands causes the metal atoms to satisfy their coordination sphere by accepting electron density from the carboxyl oxygen atom of an adjacent molecule, creating a chain as depicted in Figure 2. Thus, crystallization from a non-donor solvent is a necessary, but not sufficient method of obtaining crystals of unsolvated $M_2(O_2CR)_4$ compounds.

The first four chapters of this dissertation describe how we have solved the problem of creating metal carboxylates without axial ligation for M = Cr, Cu, Mo, and Rh. We have found that the resulting deprivation of any kind of axial ligation generates a unique situation in which the dimetal core compensates in often surprising ways. These four systems are particularly interesting in that their carboxylates are among the first examples in the study of metal-metal bonded compounds that were structurally characterized.

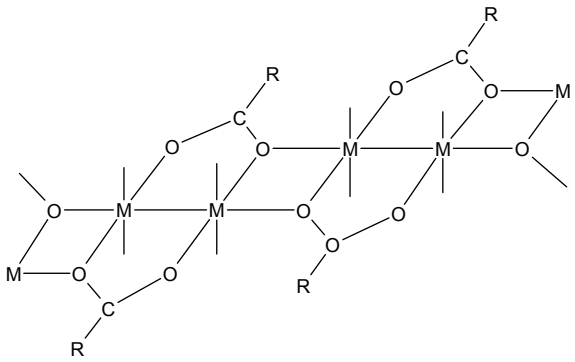

Figure 2. Self-association of $M_2(O_2CR)_4$ units in the absence of a donor solvent.

The latter portion of this dissertation treats a rather underdeveloped subject in the chemistry of metal-metal bonds. Although it has been more than 30 years since the quadruply-bonded $Cr_2(O_2CCH_3)_4$ compound was crystallographically characterized,[8] it was not until 1992 that the first triply-bonded V_2^{4+} core was reported in $V_2(DTolF)_4$, where DTolF is the anion of *N*,*N*'-di-*p*-tolylformamidine.[9] In the subsequent decade, only two other compounds of V_2^{4+} have been described, $V_2(DCyF)_4$[10] and $V_2(hpp)_4$[11], where DCyF is the anion of *N*,*N*'-dicyclohexylformamidine and hpp is the anion of 1,3,4,6,7,8-hexahydro-2*H*-pyrimido[1,2*a*]pyrimidine. Both of these compounds are similar to the first one, and very little has been learned about their properties. Thus the general impression has arisen that the chemistry of multiply-bonded divanadium compounds is quite limited. We have found, on the contrary, that several additional divanadium compounds can be made, including one with an unprecedented V_2^{3+} core. Six new divanadium compounds will be presented in this dissertation, along with their structural, electrochemical and spectroscopic characterization.

CHAPTER II

A CHROMIUM CARBOXYLATE WITH NO AXIAL LIGATION[1]

More than 155 years ago, Peligot[12] reported the synthesis of "$CrC_4H_4O_5$" which we now know to be $Cr_2(O_2CCH_3)_4(H_2O)_2$, with the structure represented in Figure 1. Over the intervening years many other studies of $Cr_2(O_2CR)_4L_2$ compounds, with an enormous variety of R and L have been published.[2] A few compounds that did not incorporate ligands, L, were also reported. While it had been shown[13] in 1953 that $Cr_2(O_2CCH_3)_4(H_2O)_2$ is isomorphous to a stoichiometrically analogous copper compound, the first metrically correct structure[14] was not published until 1971, where it was shown that the Cr–Cr distance is 2.362(1) Å. A very large number of $Cr_2(O_2CR)_4L_2$ structures have since been determined,[2] not one of which has a distance shorter than 2.29 Å, but many of which have longer distances, up to *ca*. 2.6 Å.

In 1977 the first structure of a $Cr_2(O_2CR)_4$ compound containing no exogenous ligands, the acetate, was reported, but this did not give information about the unligated molecule because the crystal contains infinite chains in which each $Cr_2(O_2CCH_3)_4$ molecule functions as an axial ligand to its neighbors,[14] as shown in Figure 2. Prior to the work reported here, no $Cr_2(O_2CR)_4$ compound has been obtained as a crystalline solid containing discrete molecules that have no axial ligation, either by exogenous ligands or by self-association.

---

[1]Reprinted in part with permission from Cotton, F. A.; Hillard, E. A.; Murillo, C. A.; Zhou, H.-C. "After 155 Years, A Crystalline Chromium Carboxylate with a Supershort Cr–Cr Bond." *J. Am. Chem. Soc.* **2000**, *122*, 416-417. Copyright 2000, American Chemical Society.

To obtain such a compound proved difficult. The simplest idea might seem to be to design a carboxylate ligand capable of preventing any exogenous ligand from reaching the axial positions. A little reflection will show that this requires considerable molecular engineering in view of how far away from the axial site one must begin to build a structure capable of blocking both axial sites, and the ability of even large substituents to get out of the way by rotation about C–C single bonds. Also, the presence of a heavily substituted, rigid R group might result in a molecule that either could not be made because of too much internal crowding, or might be too insoluble to permit the growth of crystals.

A more subtle approach was adopted here. The chosen carboxylate was sufficiently bulky to prevent the self-association depicted in Figure 2, while at the same time of such a nature as to ensure solubility in a non-coordinating solvent. In this way crystals were grown that could not have any exogenous axial ligands, simply because none are available, and self-association is sterically impossible. This approach also has the advantage that exogenous ligands (especially small ones such as CH_3CN) can be deliberately introduced so that their effect on the Cr–Cr distance in the very same molecule could be determined. The carboxylate that has been found to serve the purpose, 2,4,6-triisopropyl benzoate (TiPB), is shown in Figure 3.

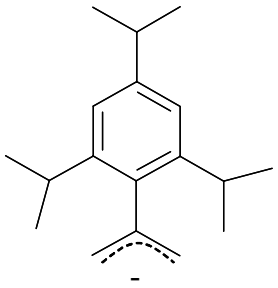

Figure 3. The anion of 2,4,6-triisopropyl benzoic acid, TiPB.

EXPERIMENTAL

General Considerations. All syntheses and manipulations were carried out in an inert atmosphere utilizing standard Schlenk and drybox techniques. All reagents and solvents were obtained commercially: 2,4,6-triisopropyl benzoic acid was purchased from Lancaster Research Chemicals and sublimed prior to use. Chromocene was purchased from Strem Chemicals. Acetonitrile was dried over calcium hydride, hexanes and toluene over Na/K alloy, and these solvents were freshly distilled under N_2 prior to use.

Physical Measurements. Elemental analyses were performed by Canadian Microanalytical Service, Ltd., Delta, British Columbia. ^{1}H NMR spectra were recorded on a Unity Plus 300 NMR spectrometer, with chemical shifts (δ) referenced to CH_2Cl_2. UV/vis spectra were recorded on a Cary 17D spectrophotometer. The IR spectrum was collected on a Perkin-Elmer 16PC FT-IR spectrophotometer using a KBr pellet.

Preparation of $Cr_2(TiPB)_4$, 1. Compound **1** was prepared by stirring a solution of $CrCp_2$ (0.187 g, 1.03 mmol) and 2,4,6-triisopropylbenzoic acid (0.496 g, 2.00 mmol) in toluene (10 mL) at reflux temperature for 12 h. The red solution obtained was then layered with hexanes. Large block-shaped, orange-red crystals grew after 2 weeks. Yield (crude product): 0.420 g (77.0 %). ^{1}H NMR (CD_2Cl_2) δ 7.003 (s, 8 H, aromatic), 3.152 (br, 8 H, *o*-isopropyl), 2.866 (septet, 6.6 Hz, 4 H, *p*-isopropyl), 1.087-1.266 (m, 72 H, methyl). IR (KBr, cm^{-1}) 1606m, 1570m, 1535s, 1462s, 1423vs, 1401vs, 1361m, 1320m, 1299w, 1261m, 1160m, 1104s, 1022m, 941w, 876m, 859w, 814s, 769w, 736w, 640s, 559w, 509s, 565w. UV/vis (CH_2Cl_2, nm) 453, 423. Mass spectroscopy (FAB$^+$, *m*/*z*) 1093, $[Cr_2(O_2CAr)_4]^+$. Anal. Calcd for $C_{64}H_{92}O_8Cr_2$: C, 70.31; H, 8.48. Found: C, 68.94; H, 8.42.

Preparation of $Cr_2(TiPB)_4(NCMe)_2$, 2. Compound **2** was prepared by layering a solution of **1** in CH_2Cl_2 with NCMe. Upon diffusion the solution color changed from yellow to pink. Large block-shaped red crystals of **2**·1.5CH_2Cl_2 were obtained in 2 days.

Preparation of $Cr_2(O_2CCH_3)_4(NCMe)_2$, 3. Compound **3** was prepared by dissolving $Cr_2(O_2CCH_3)_4$ powder in hot NCMe. The saturated red solution was then allowed to stand in a freezer at -20 °C for 2 days, giving block-shaped red crystals of **3**·2NCMe.

CRYSTALLOGRAPHIC STUDIES

Single crystals of **1**, **2**·1.5CH_2Cl_2, and **3**·2NCMe were attached to glass fibers with a small amount of silicon grease and mounted on the Bruker SMART CCD diffractometer. Cell parameters were determined using the program SMART.[15] Data reduction and integration were performed with the software program SAINTPLUS,[16] while an absorption correction was applied using the program SADABS.[17] Crystal and space group symmetries for all compounds were determined using the XPREP program.[18]

For all compounds, the coordinates of some or all of the non-hydrogen atoms were found via direct methods using the structure solution program in the SHELXTL package.[19] The positions of the remaining non-hydrogen atoms were located by use of a combination of least-squares refinement and difference Fourier maps in the SHELXL-93 program.[20] Non-hydrogen atoms were refined with anisotropic displacement parameters, except for disordered portions of the structures, (isopropyl groups in **2**·1.5CH_2Cl_2). The hydrogen atoms were included in the structure factor calculations at idealized positions. Cell parameters and refinement results for **1**, **2**·1.5CH_2Cl_2, and **3** ·2NCMe are summarized in Table 1, 2, and 3, respectively; selected bond

distances and angles for **1**, **2**·1.5CH_2Cl_2, and **3**·2NCMe, are summarized in Table 4, 5, and 6, respectively.

RESULTS AND DISCUSSION

Structural Considerations. The reaction between the parent acid of triisopropylbenzoate and $CrCp_2$ in toluene at reflux temperature readily gives $Cr_2(TiPB)_4$, **1**. It was crystallized from a toluene solution of **1** layered with hexanes. The crystal structure of **1** (Figure 4) shows a typical paddlewheel arrangement of the bridging ligands; no axial coordination of any kind has been found within the molecule or in the lattice. The Cr–Cr distance is 1.9662(5) Å.

This result affords total confirmation of previous ones for $Cr_2(O_2CCH_3)_4$ (by vapor electron diffraction)[21] where a Cr–Cr bond length of 1.97 Å, has been reported. This is extremely important since it has been suggested[7d] that the Cr–Cr distance obtained by gas phase electron diffraction is "questionable."

The bond lengths in both carboxylates, 1.97 Å, are only 0.03 Å longer than that in one compound with amidate ligands.[22] In general,[2] Cr–Cr distances in compounds with various N,N and N,O type bridging ligands (and no axial coordination) are in the range 1.84-1.94 Å, and thus they are only 0.13-0.03 Å shorter than in the carboxylates. The extreme sensitivity of $Cr_2(O_2CR)_4$ molecules to the addition of axial ligands has been demonstrated here by the structures of $Cr_2(TiPB)_4(NCMe)_2$ (Figure 5), **2**, and $Cr_2(O_2CCH_3)_4(NCMe)_2$ (Figure 6), **3**, in which the Cr–Cr distances are 2.3892(2) and 2.395(1) Å, respectively. These relationships may be compared with some contrary theoretical predictions to be discussed below.

Table 1. Crystal Data and Structure Refinement for **1**

Empirical formula	$C_{64}H_{92}Cr_2O_8$
Formula weight	1093.38
Space group	$P\bar{1}$
Unit cell dimensions	a = 9.7448(6) Å α = 70.8990(10)° b = 11.7879(7) Å β = 70.6910(10)° c = 14.652(1) Å γ = 76.1150(10)°
Volume	1484.5(2) Å³
Z	1
Density (calculated)	1.223 g/cm³
Crystal size	0.62 x 0.56 x 0.21 mm
Absorption coefficient	0.419 mm^{-1}
Data collection instrument	Bruker Smart CCD
Wavelength	0.71073 Å
Orientation reflections, number, range (θ)	7614, 2.339 - 28.66
Temperature	110(2) K
Scan method	ω scans
Theta range for data collection	1.53 to 28.71°
Reflections collected	26200
Independent reflections	6989 [R(int) = 0.0433]
Data / restraints / parameters	6989 / 0 / 510
Refinement method	Full-matrix least-squares on F^2
Final R indices [$I > 2\sigma(I)$]	$R1^a$ = 0.059, $wR2^b$ = 0.152
R indices (all data)	$R1^a$ = 0.065, $wR2^b$ = 0.160
Goodness-of-fit on F^2	1.135
Largest shift/esd, final cycle	0.085
Largest peak, final cycle	2.21(11) e/Å³

[a] $R1 = \sum||F_o| - |F_c||/\sum|F_o|$.
[b] $wR2 = [\sum[w(F_o^2-F_c^2)^2]/\sum[w(F_o^2)^2]]^{1/2}$, $w = 1/[\sigma^2(F_o^2) + (aP)^2 + bP]$, where $P = [\max(F_o^2 \text{ or } 0) + 2(F_c^2)]/3$.

Table 2. Crystal data and structure refinement for **2**·1.5CH_2Cl_2

Empirical formula	$C_{69.50}H_{101}Cl_3Cr_2N_2O_8$
Formula weight	1302.87
Space group	$P\bar{1}$
Unit cell dimensions	a = 14.445(2) Å α = 65.918(2)° b = 16.618(2) Å β = 74.912(2)° c = 17.529(2) Å γ = 82.713(3)°
Volume	3708.1(9) Å³
Z	2
Density (calculated)	1.167 g/cm³
Crystal size	0.46 x 0.41 x 0.39 mm
Absorption coefficient	0.451 mm^{-1}
Data collection instrument	Bruker SMART area detector
Wavelength	0.71073 Å
Orientation reflections, number, range (θ)	8188, 2.48 - 27.29
Temperature	213(2) K
Scan method	ω scans
Theta range for data collection	1.46 to 22.50°
Reflections collected	15829
Independent reflections	9653 [R(int) = 0.0231]
Data / restraints / parameters	9638 / 23 / 698
Refinement method	Full-matrix least-squares on F^2
Final R indices [$I > 2\sigma(I)$]	$R1^a$ = 0.091, $wR2^b$ = 0.266
R indices (all data)	$R1^a$ = 0.119, $wR2^b$ = 0.302
Goodness-of-fit on F^2	1.039
Largest shift/esd, final cycle	-0.080
Largest peak, final cycle	0.61(10) e/Å³

[a] $R1 = \sum||F_o| - |F_c||/\sum|F_o|$.
[b] $wR2 = [\sum[w(F_o^2-F_c^2)^2]/\sum[w(F_o^2)^2]]^{1/2}$, $w = 1/[\sigma^2(F_o^2) + (aP)^2 + bP]$, where $P = [\max(F_o^2 \text{ or } 0) + 2(F_c^2)]/3$.

Table 3. Crystal data and structure refinement for **3** ·2NCMe

Empirical formula	$C_{16}H_{24}Cr_2N_4O_8$
Formula weight	504.39
Space group	$P2_1/n$
Unit cell dimensions	a = 10.701(2) Å α = 90˚ b = 10.206(2) Å β = 101.978(4)˚ c = 10.912(2) Å γ = 90˚
Volume	1165.8(4) Å³
Z	2
Density (calculated)	1.437 g/cm³
Crystal size	0.36 x 0.28 x 0.26 mm
Absorption coefficient	0.977 mm^{-1}
Data collection instrument	Bruker SMART area detector
Wavelength	0.71073 Å
Orientation reflections, number, range (θ)	4632, 2.43 - 28.32
Temperature	213(2) K
Scan method	ω scans
Theta range for data collection	2.43 to 28.47˚
Reflections collected	7053
Independent reflections	2710 [R(int) = 0.0464]
Data / restraints / parameters	2708 / 0 / 143
Refinement method	Full-matrix least-squares on F^2
Final R indices [$I > 2\sigma(I)$]	$R1^a$ = 0.053, $wR2^b$ = 0.146
R indices (all data)	$R1^a$ = 0.069, $wR2^b$ = 0.169
Goodness-of-fit on F^2	1.096
Largest shift/esd, final cycle	0.008
Largest peak, final cycle	1.07(9) e/Å³

[a] $R1 = \sum||F_o| - |F_c||/\sum|F_o|$.
[b] $wR2 = [\sum[w(F_o^2-F_c^2)^2]/\sum[w(F_o^2)^2]]^{½}$, $w = 1/[\sigma^2(F_o^2) + (aP)^2 + bP]$, where $P = [\max(F_o^2 \text{ or } 0) + 2(F_c^2)]/3$.

Table 4. Selected Bond Lengths [Å] and Angles [˚] for **1**[a]

Cr–CrA[b]	1.9662(5)
Cr–O(1)	1.9779(12)
Cr–O(2)	1.9994(12)
Cr–O(3)	1.9897(12)
Cr–O(4)	1.9820(12)
CrA–Cr–O(1)	94.69(4)
CrA–Cr–O(2)	92.53(4)
CrA–Cr–O(3)	93.38(4)
CrA–Cr–O(4)	93.38(4)
cis - O–Cr–O	89.79[5]
trans - O–Cr–O	172.66[5]

[a] Square brackets refer to average values; parentheses refer to unique values.
[b] Symmetry transformations used to generate equivalent atoms: A 1-x+2,-y+1,-z+1.

Table 5. Selected Bond Lengths [Å] and Angles [˚] for **2**·1.5CH_2Cl_2[a]

Cr(2)-Cr(1)	2.3893(13)	O(101)-Cr(1)-Cr(2)	87.34(12)
Cr(1)-O(101)	2.028(4)	O(201)-Cr(1)-Cr(2)	87.28(11)
Cr(1)-O(201)	2.002(4)	O(301)-Cr(1)-Cr(2)	87.22(11)
Cr(1)-O(301)	2.021(4)	O(401)-Cr(1)-Cr(2)	87.25(11)
Cr(1)-O(401)	2.006(4)	O(102)-Cr(2)-Cr(1)	86.96(11)
Cr(2)-O(102)	2.025(4)	O(202)-Cr(2)-Cr(1)	87.14(11)
Cr(2)-O(202)	2.011(4)	O(302)-Cr(2)-Cr(1)	87.20(11)
Cr(2)-O(302)	2.017(4)	O(402)-Cr(2)-Cr(1)	86.88(11)
Cr(2)-O(402)	2.020(4)	*cis* - O–Cr(1)–O	89.9[2]
Cr(1)-N(501)	2.325(6)	*trans* - O–Cr(1)–O	174.2[2]
Cr(2)-N(601)	2.326(6)	*cis* - O–Cr(1)–O	89.9[2]
		trans - O–Cr(1)–O	173.8[2]
		N(501)-Cr(1)-Cr(2)	176.1(2)
		N(601)-Cr(2)-Cr(1)	177.1(2)

[a] Square brackets refer to average values; parentheses refer to unique values.

Table 6. Selected Bond Lengths [Å] and Angles [˚] for **3**·2NCMe[a]

Cr(1)-Cr(1A)[b]	2.3950(11)
Cr(1)-O(11A)	2.015(2)
Cr(1)-O(12)	2.010(3)
Cr(1)-O(21A)	2.013(3)
Cr(1)-O(22)	2.015(3)
Cr(1)-N(31)	2.326(3)
O(11A)-Cr(1)-Cr(1A)	88.17(8)
O(12)-Cr(1)-Cr(1A)	87.00(8)
O(21A)-Cr(1)-Cr(1A)	87.22(8)
O(22)-Cr(1)-Cr(1A)	88.04(8)
cis - O–Cr–O	89.9[1]
trans - O–Cr–O	175.2[1]
N(31)-Cr(1)-Cr(1A)	178.78(9)

[a] Square brackets refer to average values; parentheses refer to unique values.
[b] Symmetry transformations used to generate equivalent atoms: A -x,-y,-z.

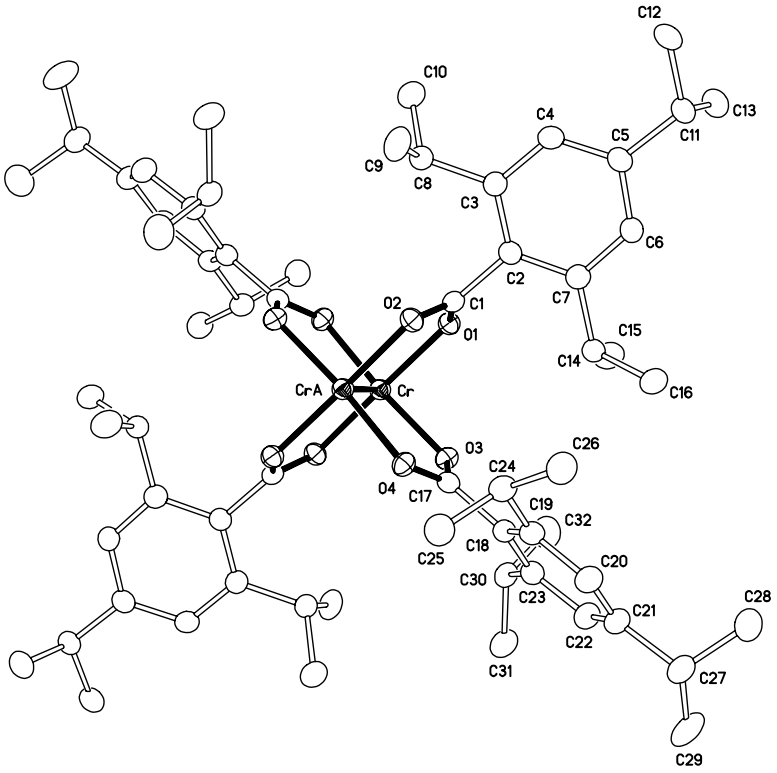

Figure 4. Thermal ellipsoid plot of $Cr_2(TiPB)_4$, **1**. Thermal ellipsoids are shown at the 50% probability level; hydrogen atoms have been omitted for clarity.

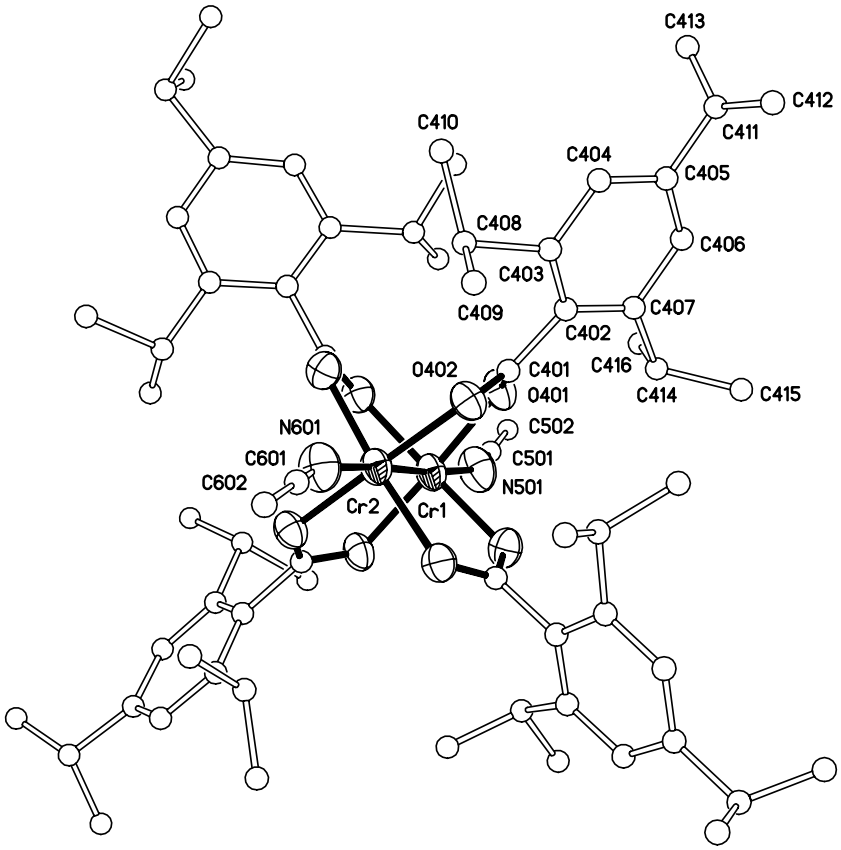

Figure 5. Thermal ellipsoid plot of $Cr_2(TiPB)_4(NCMe)_4$ in **2**·$1.5CH_2Cl_2$. Thermal ellipsoids are shown at the 50% probability level; carbon atoms for the core atoms are given on an arbitrary scale, and hydrogen atoms have been omitted for clarity. Only one of the two orientations of the disordered molecule is shown.

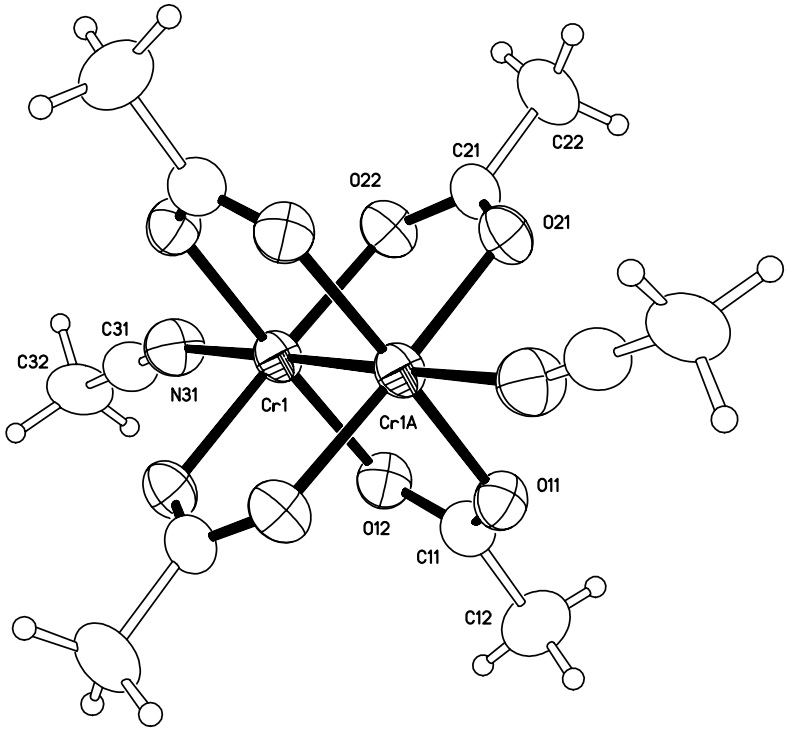

Figure 6. Thermal ellipsoid plot of $Cr_2(O_2CCH_3)_4(NCMe)_2$ in **3**·2NCMe. Thermal ellipsoids are shown at 50% probability level; hydrogen atoms are shown at an arbitrary scale.

Theoretical Considerations. There have been several theoretical studies addressing the nature of Cr≣Cr bonds, but only those[7c-f] dealing directly with the question of how the bond length is affected by the bridging and axial ligands will be discussed here. As a result of these calculations, there arose a consensus that while axial ligands played an important role, the bridging ligands were also of major importance. This view was stated as follows: (1) "the effect of bridging ligands is at least as important as the observed influence of axial coordination ...."[7e] This conclusion was drawn from the results of *ab initio* calculations on $Cr_2(NHCHO)_4$ and $Cr_2(O_2CH)_4$ which gave Cr–Cr bond distances of 1.92 Å and 2.53 Å, respectively. Similarly, for the formato species, other calculations[7c] gave a prediction of 2.4 Å for the Cr–Cr bond length. Still another theoretical study[7f] led to the conclusion "that the nature of the bridging ligand strongly affects the electronic structure of the quadruple bond" and that there should be "a bond shortening of 0.48 Å when the formato ligands are replaced by amino iminato ligands." In still another study[7d] it was proposed that the Cr–Cr distance in tetracarboxylate compounds, $Cr_2(O_2CR)_4$, would be in the range of 2.05-2.10 Å and that, as already noted, the experimental value of 1.97 Å for gaseous $Cr_2(O_2CCH_3)_4$ is "questionable."

Clearly, all of these dichromium molecules, and especially the $Cr_2(O_2CR)_4$ molecules have so far defied successful theoretical treatment. Now we have structural results that cannot possibly be considered questionable, and they show that while the introduction of axial coordination can make a huge change (ca. 0.4 Å) in the Cr–Cr distance, a change from an N,N or N,O bridging ligand to an O,O bridging ligands causes a much smaller change, viz., 0.13 Å at most.

The question of how a chromium-to-chromium quadruple bond is influenced by its surrounding ligands is important because (a) no other bond known in chemistry shows anywhere near as great sensivity to such influences, and (b) in several cases Cr≣Cr bonds are shorter than any other known bond relative to the size of the atoms making it up.[23]

The great advantage of having this crystalline form of a compound with unligated $Cr_2(O_2CR)_4$ molecules is that other important measurements can now be made which cannot be made on the vapor of $Cr_2(O_2CCH_3)_4$. One of these is an electron density mapping using low-temperature crystallography, and the polarized visible absorption spectrum, which will be particularly convenient in this case because all Cr–Cr units are parallel throughout the crystal.

CHAPTER III

A COPPER CARBOXYLATE WITH A NOVEL TRIMERIC GEOMETRY[2]

The chemistry of copper(II) complexes with various carboxylates has been very broadly researched with numerous studies on magnetic properties of the tetracarboxylate bridged compounds having two axial ligands L, $Cu_2(O_2CR)_4L_2$, Figure 7a.[24] These studies have been focused on the factors influencing the magnitude of the intramolecular magnetic exchange interaction which occurs between the two Cu^{II} ions in these type of compounds. Several crystal structures have been reported for $Cu_2(O_2CR)_4$ without any exogenous ligands, which were found to have a well-known chain structure built on the long Cu-O axial contacts in the solid state, Figure 7b.[25] For these non-adduct copper(II) carboxylates, relatively few studies have been reported on the magneto-structural correlations.[26]

Coordination flexibility of copper atoms, combined with the electronic and steric diversity of R groups in carboxylate anions O_2CR^-, still leads to novel and interesting results in such an 'old-fashioned' chemistry as copper carboxylates. For example, a remarkable copper(II) trifluoroacetate, $Cu_2(O_2CCF_3)_4$ was recently prepared, which was shown to have a unique chain motif in the crystalline form, different from any other carboxylates (Figure 7c).[27] It is therefore important to mention, that prior to this work, only one Cu^{II} carboxylate compound has been isolated in the solid state containing discrete hexanuclear molecules in which phenoxyacetate

---

[2]Reprinted in part with permission from Clérac, R.; Cotton, F. A.; Dunbar, K. R.; Hillard, E. A.; Murillo, C. A.; Petrukhina, M. A.; Smucker, B. W. "Crystal Structure and Magnetic Behavior of $Cu_3(O_2C_{16}H_{23})_6 \cdot 1.2C_6H_{12}$. An Unexpected Structure and an Example of Spin Frustration" *C. R. Acad. Sci., Ser. 2* **2001**, *4*, 315. Copyright 2001, Elsevier.

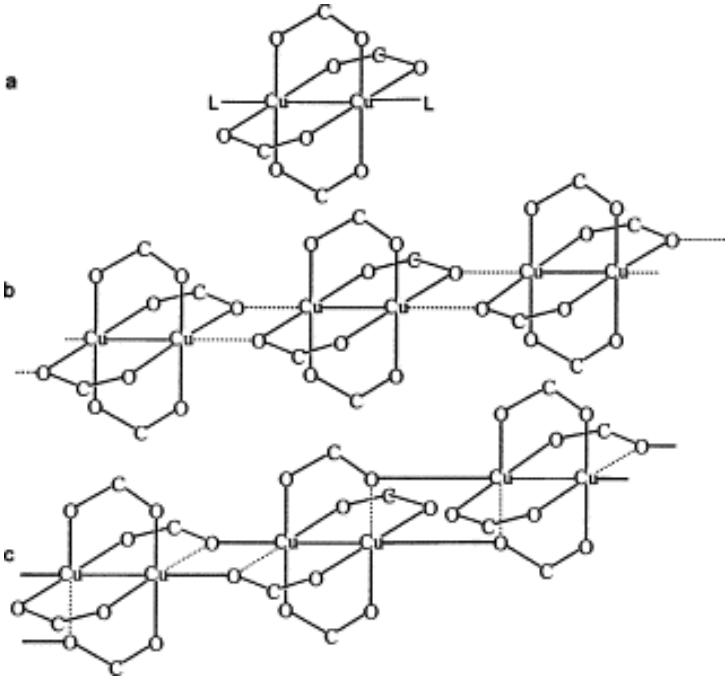

Figure 7. Previously known dicopper(II) tetracarboxylate structures. **a.** With two axial ligands. **b.** The usual chain structure for unligated molecules. **c.** The chain structure found only in $Cu_2(O_2CCF_3)_4$.

groups form both syn-syn and syn-anti bridges.[28] In the latter the Cu atoms together formed a compressed trigonal antiprism with six long edges (Cu-Cu 5.65 Å) bordering the equilateral triangular faces and six shorter edges (Cu-Cu 3.53 Å).

As a part of our studies on the interaction of the 2,4,6-triisopropylbenzoate (TiPB) ligand with the first row transition metals,[29] we have extended our research to the Cu^{II} -TiPB system. The TiPB ligand was already shown to be sufficiently bulky to successfully prevent self-association in the Cr^{II} case resulting in a dinuclear compound $Cr_2(TiPB)_4$ with a supershort Cr-Cr bond. Therefore, we believed that TiPB would be the best candidate to attempt the isolation of the discrete Cu^{II} carboxylate that has no axial ligation, either by exogenous ligands or by self-association.

EXPERIMENTAL

General Considerations. All manipulations were performed under nitrogen atmosphere using standard Schlenk techniques. The starting materials 2,4,6-triisopropylbenzoic acid was purchased from Lancaster Research Chemicals and $CuCO_3 \cdot Cu(OH)_2$ was purchased from Aldrich; these were used as received. Ethanol was dried over magnesium, acetone over potassium carbonate, and cyclohexanes over Na/K alloy. Elemental analyses were performed by Canadian Microanalytical Services, Ltd. The IR spectrum was collected on a Perkin-Elmer 16PC FT-IR spectrophotometer using a KBr pellet.

Preparation of $Cu_3(TiPB)_6$, 4. In a typical reaction, 50 mL ethanol was added to a mixture of 0.884 g (4 mmol) $CuCO_3$ and 0.993 g (4 mmol) 2,4,6-triisopropyl benzoic acid. The suspension was brought to reflux for 3 to 10 days; the yield of the heterogeneous reaction is a function of reflux time. After refluxing, the suspension was cooled and filtered over Celite to afford a blue-green solution. The solvent was removed under vaccuum, and the residue was heated to 100º C to sublime remaining HTiBP. The heat also removes axially ligated ethanol, as evidenced by the change in color of the solid from blue-green to dark green. The solid was then dissolved in 10 mL cyclohexane, the volume of the solution was reduced by one third, and stored at 10º C. Very dark green blocks appeared after one week. Yield (solid): 0.40 g, 36 % for 10 day reflux. Anal. calc. for $Cu_3(TiPB)_6 \cdot 1.2\ C_6H_{12}$: C, 69.80; H, 8.67. Found: C, 69.51; H, 8.64. IR (KBr, cm^{-1}) 1590vs, 1570s, 1560s, 1522m, 1509s, 1460s, 1413vs, 1382m, 1361m, 1344w, 1321m, 1304w, 1261m, 1242w, 1193w, 1171w, 1158m, 1109m, 1072m, 1054w, 1016m, 947w, 922w, 876m, 858w, 806m, 762m, 670w, 658w, 640m, 561w, 497m, and 458m.

Preparation of $Cu_2(TiPB)_4(C_2H_5OH)_2$, 5. A sample of $Cu_3(TiPB)_6$ was dissolved in ethanol to afford a concentrated blue-green solution. The solution was placed in the refrigerator and blue blocks grew after one week. Alternatively, slow evaporation of the filtrate from the reaction of $CuCO_3 \cdot CuOH$ and TiPBH in ethanol also affords blue blocks. Anal**.** calc. for $Cu_2(TiPB)_4(C_2H_5OH)_2 \cdot C_2H_5OH$: C, 67.17: H, 8.86. Found: C, 66.18; H, 8.69. $Cu_2(TiPB)_4(acetone)_2$ (**6**) was prepared similarly.

CRYSTALLOGRAPHIC STUDIES

The X-ray studies of **4** ·1.2C_6H_{12} and **6**·0.5acetone were carried out on a Nonius FAST diffractometer with an area detector using Mo-Kα radiation at 213(2) K. For **4**·1.2C_6H_{12} fifty reflections were used in cell indexing and 250 reflections in cell refinement ($15° < 2\theta < 42°$). A total of 2436 independent reflections in the range $4.5° < 2\theta < 45°$ were collected, 2075 with $I > 2\sigma(I)$. For **6**·0.5acetone fifty reflections were used in cell indexing and 248 reflections in cell refinement ($15° < 2\theta < 45.1°$). A total of 9597 independent reflections in the range $4.52° < 2\theta < 55.12°$ were collected, 7329 with $I > 2\sigma(I)$. Data were corrected for Lorentz and polarization effects using the MADNES program.[30] Reflections profiles were fitted and values of F^2 and $\sigma(F^2)$ for each reflection were obtained by the program PROCOR.[31] Systematic absences in the data uniquely determined the space group for **4**·1.2C_6H_{12} to be trigonal $P\bar{3}1c$ (*No*. 163).

The X-ray study for **5**·CH_3CH_2OH was carried out on a Bruker SMART diffractometer with an area detector using Mo-Kα radiation at 213(2) K. A total of 6928 reflections were used in cell refinement ($4.404 < 2\theta < 44.06°$). A total of 13689 independent reflections in the range $3.30° < 2\theta < 50.16°$ were collected, 7069 with $I > 2\sigma(I)$. Data were corrected for Lorentz and polarization effects using the program SAINTPLUS.[16] Absorption corrections were applied using SADABS.[17]

The coordinates of copper atoms were found in direct-method *E* maps using the structure solution program SHELXTL.[19] The positions of the remaining atoms were located by use of a combination of least-squares refinement and difference Fourier maps in the SHELXL-93 program.[20] In **4**·1.2C_6H_{12} ,the isopropyl groups of the ligand were found to be disordered over two different rotational orientations, and two molecules of disordered cyclohexane with partial occupancies were located in the structure. In **5**·CH_3CH_2OH and **6**·0.5acetone, the isopropyl

groups, one of the axial solvent molecules and one of the interstitial solvent molecules were also disordered.

For all structures, hydrogen atoms were included in the structure factor calculations at idealized positions. Anisotropic displacement parameters were assigned to all non-hydrogen atoms, except the in the disordered portions of the structure. All calculations were performed on a DEC Alpha running VMS. Crystal and structure refinement data are summarized in Tables 7-9 and selected bond distances and angles are listed in Tables 10-12.

RESULTS AND DISCUSSION

Synthesis and Structure. A standard literature procedure has been used to prepare $Cu_3(TiPB)_6$ (**4**).[32] The reflux reaction of the heterogeneous mixture containing the parent 2,4,6-triisopropylbenzoic acid and insoluble basic copper carbonate, $CuCO_3{\cdot}Cu(OH)_2$, in ethanol slowly afforded a blue-green solution. Several blue crystals of the composition $Cu_2(TiPB)_4(EtOH)_2{\cdot}C_2H_5OH$ (**5**$\cdot C_2H_5OH$) have been isolated directly from the reaction mixture upon cooling to room temperature. Evaporation of the solvent after removal of the unreacted copper carbonate from the blue solution resulted in a blue-green residue. After heating the solid under vacuum to sublime remaining HTiPB and ethanol, the dark green solid was dissolved in cyclohexane and the solution was placed in the refrigerator for a week, affording green crystals of **4**$\cdot 1.2C_6H_{12}$ in moderate yield. After dissolving these crystals in ethanol, followed by keeping the ethanol solution in the freezer for a few days, characteristic blue crystals of **5**$\cdot C_2H_5OH$

Table 7. Crystal Data and Structure Refinement for **4**·1.2C_6H_{12}

Empirical formula	$C_{103.27}H_{152.54}Cu_3O_{12}$
Formula weight	1776.65
Space group	$P\bar{3}1c$
Unit cell dimensions	a = 18.1331(6) Å α = 90˚ b = 18.1331(6) Å β = 90˚ c = 19.4989(6) Å γ = 120˚
Volume	5552.5(3) Å³
Z	2
Density (calculated)	1.063 g/cm³
Crystal size	0.30 x 0.20 x 0.15 mm
Absorption coefficient	0.620 mm^{-1}
Data collection instrument	Nonius FAST area detector
Wavelength	0.71073 Å
Orientation reflections, number, range (θ)	250, 7.50 - 20.8
Temperature	213(2) K
Scan method	ω scans
Theta range for data collection	2.25 to 22.48˚
Reflections collected	25697
Independent reflections	2436 [R(int) = 0.0815]
Data / restraints / parameters	2435 / 11 / 178
Refinement method	Full-matrix least-squares on F^2
Final R indices [$I > 2\sigma(I)$]	$R1^a$ = 0.075, $wR2^b$ = 0.205
R indices (all data)	$R1^a$ = 0.086, $wR2^b$ = 0.219
Goodness-of-fit on F^2	1.151
Largest shift/esd, final cycle	0.052
Largest peak, final cycle	0.73(9) e/Å³

[a] $R1 = \sum||F_o| - |F_c||/\sum|F_o|$.
[b] $wR2 = [\sum[w(F_o^2-F_c^2)^2]/\sum[w(F_o^2)^2]]^{½}$, $w = 1/[\sigma^2(F_o^2) + (aP)^2 + bP]$, where $P = [\max(F_o^2 \text{ or } 0) + 2(F_c^2)]/3$.

Table 8. Crystal Data and Structure Refinement for **5**·C_2H_5OH

Empirical formula	$C_{70}H_{110}Cu_2O_{11}$
Formula weight	1254.66
Space group	$P2_1/c$
Unit cell dimensions	a = 16.688(1) Å α = 90˚ b = 23.000(2) Å β = 105.526(1)˚ c = 20.966(2) Å γ = 90˚
Volume	7753(1) Å³
Z	4
Density (calculated)	1.075 g/cm³
Crystal size	0.43 x 0.36 x 0.18
Absorption coefficient	0.598 mm^{-1}
Data collection instrument	Bruker SMART area detector
Wavelength	0.71073 Å
Orientation reflections, number, range (θ)	6928, 2.202 - 22.028
Temperature	213(2) K
Scan method	ω scans
Theta range for data collection	1.65 to 25.08˚
Reflections collected	40642
Independent reflections	13694 [R(int) = 0.0915]
Data / restraints / parameters	13689 / 42 / 653
Refinement method	Full-matrix least-squares on F^2
Final R indices [$I > 2\sigma(I)$]	$R1^a$ = 0.105, $wR2^b$ = 0.277
R indices (all data)	$R1^a$ = 0.177, $wR2^b$ = 0.352
Goodness-of-fit on F^2	1.019
Largest shift/esd, final cycle	-0.041
Largest peak, final cycle	1.05(11) e/Å³

[a] $R1 = \sum||F_o| - |F_c||/\sum|F_o|$.
[b] $wR2 = [\sum[w(F_o^2-F_c^2)^2]/\sum[w(F_o^2)^2]]^{½}$, $w = 1/[\sigma^2(F_o^2) + (aP)^2 + bP]$, where $P = [\max(F_o^2 \text{ or } 0) + 2(F_c^2)]/3$.

Table 9. Crystal Data and Structure Refinement for **6**·0.5acetone

Empirical formula	$C_{71.50}H_{107}Cu_2O_{10.50}$
Formula weight	1261.65
Space group	$P\bar{1}$
Unit cell dimensions	a = 14.727(2) Å α = 65.388(14)° b = 16.314(2) Å β = 79.223(5)° c = 17.4722(13) Å γ = 87.872(8)°
Volume	3745.4(7) Å³
Z	2
Density (calculated)	1.119 g/cm³
Crystal size	0.20 x 0.15 x 0.12
Absorption coefficient	0.619 mm^{-1}
Data collection instrument	Nonius FAST area detector
Wavelength	0.71073 Å
Orientation reflections, number, range (θ)	248, 7.50 - 20.8
Temperature	213(2) K
Scan method	ω scans
Theta range for data collection	2.26 to 22.56°.
Reflections collected	24538
Independent reflections	9597 [R(int) = 0.0890]
Data / restraints / parameters	9583 / 18 / 743
Refinement method	Full-matrix least-squares on F^2
Final R indices [$I > 2\sigma(I)$]	$R1^a$ = 0.087, $wR2^b$ = 0.211
R indices (all data)	$R1^a$ = 0.116, $wR2^b$ = 0.239
Goodness-of-fit on F^2	1.076
Largest shift/esd, final cycle	0.000
Largest peak, final cycle	0.74(9) e/Å³

[a] $R1 = \sum||F_o| - |F_c||/\sum|F_o|$.
[b] $wR2 = [\sum[w(F_o^2-F_c^2)^2]/\sum[w(F_o^2)^2]]^{1/2}$, $w = 1/[\sigma^2(F_o^2) + (aP)^2 + bP]$, where $P = [\max(F_o^2 \text{ or } 0) + 2(F_c^2)]/3$.

Table 10. Selected Bond Lengths [Å] and Angles [˚] for **4**·1.2C_6H_{12}

Cu(1)–O(2)	1.891(3)
Cu(1)–O(1)	1.948(3)
O(2A)–Cu(1)–O(2)[a]	175.0(2)
O(2A)–Cu(1)–O(1)	93.8(1)
O(2)–Cu(1)–O(1)	87.1(1)
O(1)–Cu(1)–O(1A)	159.8(2)

[a] Symmetry transformations used to generate equivalent atoms: A x, x-y, -z+3/2.

Table 11. Bond Lengths [Å] and Angles [˚] for **5**·C_2H_5OH

Cu(1)–O(3)	1.941(6)
Cu(1)–O(1)	1.964(6)
Cu(1)–O(4)	1.981(5)
Cu(1)–O(2)	1.987(5)
Cu(1)–O(9)	2.146(6)
Cu(1)–Cu(2)	2.5617(13)
Cu(2)–O(7)	1.965(7)
Cu(2)–O(5)	1.966(7)
Cu(2)–O(6)	1.968(5)
Cu(2)–O(8)	1.978(5)
Cu(2)–O(10)	2.164(12)
Cu(2)–O(10X)	2.197(13)

Table 12. Bond Lengths [Å] and Angles [˚] for **6**·0.5acetone

Cu(1)–Cu(2)	2.574(1)
Cu(1)–O(1)	1.979(5)
Cu(1)–O(3)	1.968(5)
Cu(1)–O(5)	1.966(5)
Cu(1)–O(7)	1.967(5)
Cu(2)–O(2)	1.958(5)
Cu(2)–O(4)	1.947(5)
Cu(2)–O(6)	1.941(4)
Cu(2)–O(8)	1.967(5)
Cu(1)–O(9)	2.222(6)
Cu(2)–O(10)	2.199(5)

reappeared. Both the distinctive color change and the results of elemental analyses were indicative of the reversible transformations from the bis-adduct to the unligated complex and back. The compound $Cu_2(TiPB)_4(acetone)_2$ (**6**) has also been made. The identities of compounds **4**, **5**, and **6** were confirmed by the crystal structure determinations, shown in Figures 8, 9, and 10, respectively.

The crystal structure of **4**·$1.2C_6H_{12}$ consists of the discrete molecule $Cu_3(O_2C_{16}H_{23})_6$ having a triangular arrangement of the Cu^{II} atoms with a 3-fold axis passing through the center of the equilateral triangle. Two disordered cyclohexane molecules with partial occupancies have been located in the asymmetric unit giving a total of 1.2 molecules of solvent per Cu_3 moiety. Each pair of copper atoms in the Cu_3 unit is bridged by two TiPB carboxylate ligands in the *syn-syn* mode. This structure is without any precedent in the chemistry of copper carboxylates, although close analogues found in palladium systems, $Pd_3(O_2CR)_6$.[33]

The copper(II) centers in **4** are in a square planar environment of four oxygen atoms with the two equatorial Cu-O distances being slightly different, 1.891(3) and 1.948(3) Å. The O(1)-Cu-O(1) and O(2)-Cu-O(2) angles are 159.8(2) and 175.0(2)°, respectively, while O(1)-Cu-O(2) angles are averaged to 90.4[1]°. The Cu···Cu distances, 3.131(3) Å, are longer than might be expected for Cu-Cu bonds. Similarly, in all $Pd_3(O_2CR)_6$ molecules, the Pd···Pd distances range from 3.10 to 3.25 Å, greatly exceeding the usual length for Pd–Pd bonds and underscored the absence of bonded interactions.[34]

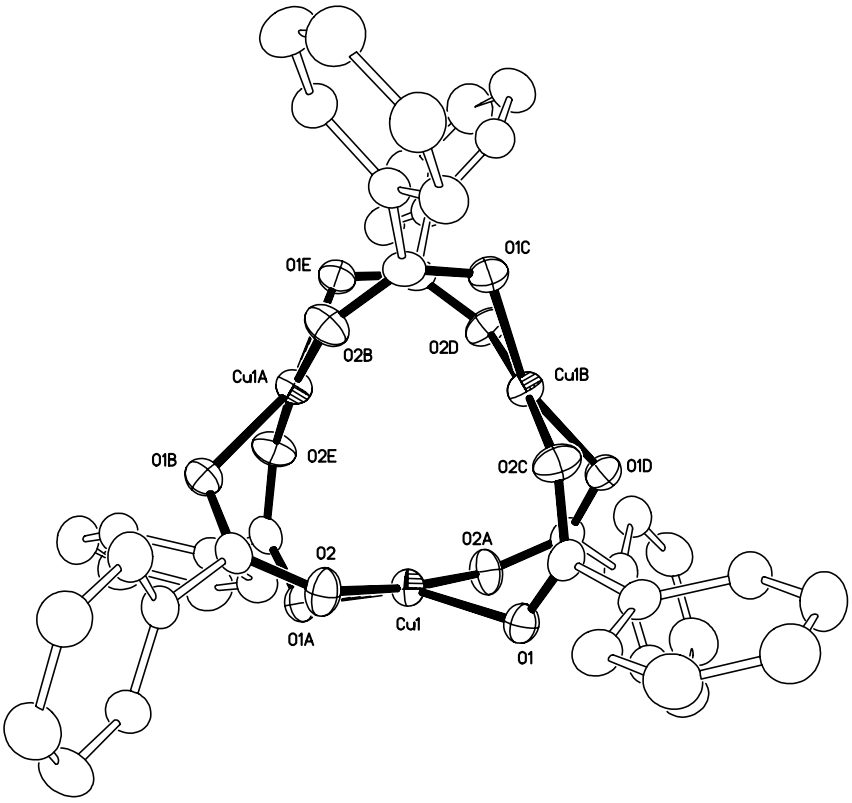

Figure 8. Thermal ellipsoid plot of $Cu_3(TiPB)_6$ in **4**·$1.2C_6H_{12}$. Thermal ellipsoids are shown at the 30% probability level. Isopropyl groups, hydrogen atoms, and interstitial solvent have been omitted for clarity.

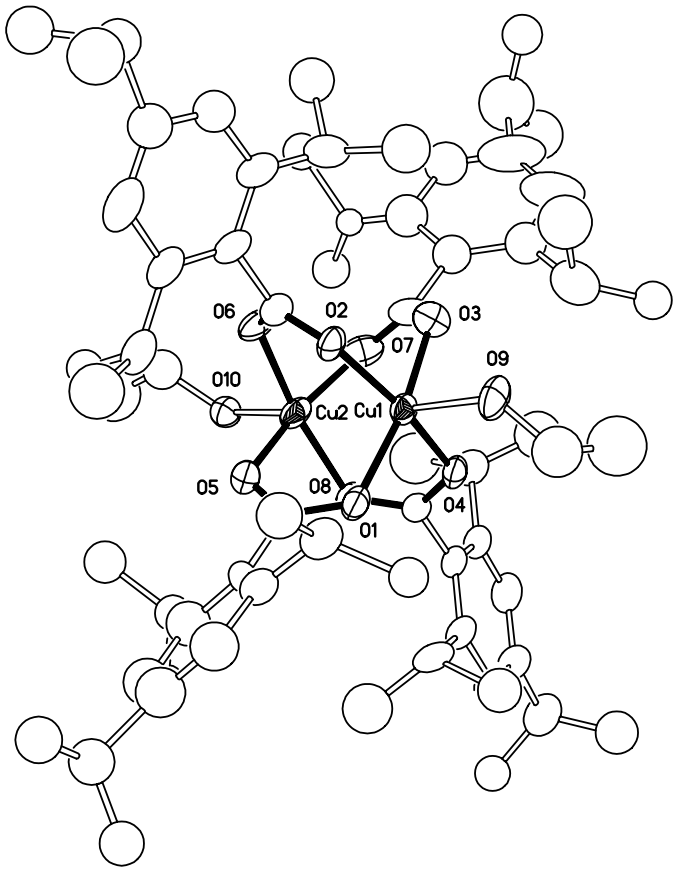

Figure 9. Thermal ellipsoid plot of $Cu_2(TiPB)_4(CH_3CH_2OH)_2$ in **5**·CH_3CH_2OH. Thermal ellipsoids are shown at the 30% probability level; hydrogen atoms have been omitted for clarity. Only one orientation of the disordered phenyl rings shown.

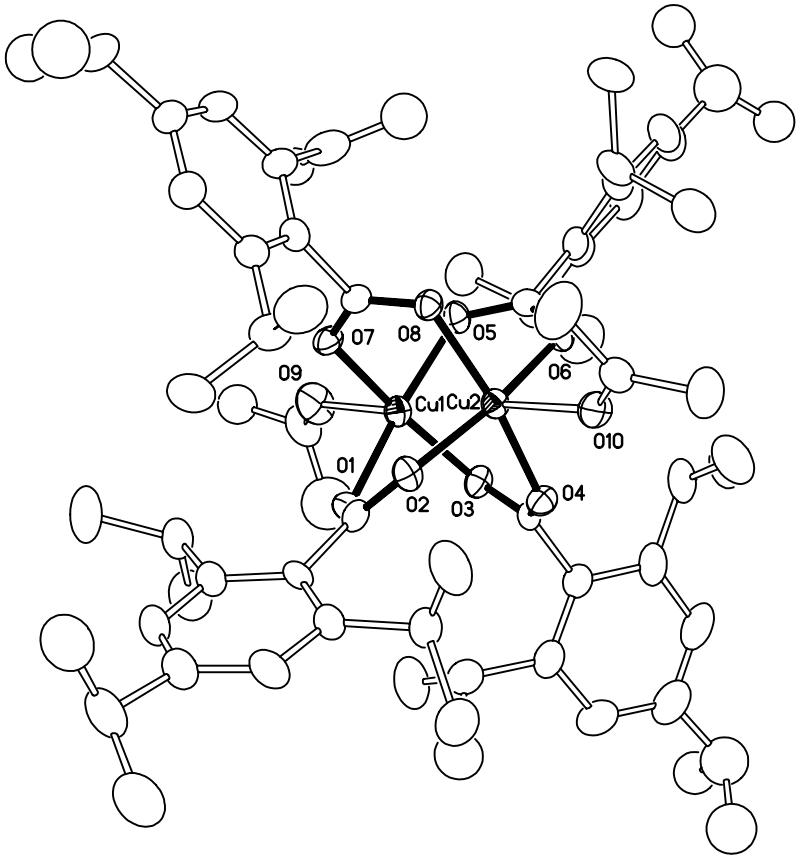

Figure 10. Thermal ellipsoid plot of $Cu_2(TiPB)_4(acetone)_2$ in **6**·0.5acetone. Thermal ellipsoids are shown at the 30% probability level; hydrogen atoms have been omitted for clarity. Only one orientation of the disordered isopropyl groups is shown.

CHAPTER IV

TETRACARBOXYLATO DIMOLYBDENUM CATIONS[3]

Among the thousands of M_2^{n+} compounds[2] the most numerous are those of Mo_2^{4+}. The earliest of the Mo_2^{4+} compounds to have been reported[35] and then structurally characterized[36] were those of the paddlewheel tetracarboxylato type, $Mo_2(O_2CR)_4$. These were also among the earliest M_2^{n+} compounds to be subjected to rigorous molecular orbital calculations,[37] detailed electronic spectroscopic,[38] and photoelectron spectroscopic[39] study. It is, therefore, surprising to note how little is known about their redox chemistry.[40] Even more surprising is the fact that although the limited electrochemical data show that reversible (or at least quasireversible) oxidation to $Mo_2(O_2CR)_4^+$ ions occurs at potentials well below +1.0 V,[41] no such species has ever been structurally characterized over the approximately 40 year period since the $Mo_2(O_2CR)_4$ compounds were discovered.

We now report that the gap has been filled by the preparation of $[Mo_2(TiPB)_4]PF_6 \cdot 2CH_2Cl_2$, **7**$\cdot 2CH_2Cl_2$, and $[Mo_2(TiPB)_4]BF_4 \cdot 2CH_2Cl_2$, **8**$\cdot 2CH_2Cl_2$, where TiPB is 2,4,6-triisopropylphenyl carboxylate, and their detailed structural and physical characterization. For comparison, we also report on the parent compound $Mo_2(TiPB)_4$, **9,** and the structure of the pivalato cation in $[Mo_2(O_2CC_4H_9)_4]PF_6$, **10**.

---

[3]Reprinted in part with permission from Cotton, F. A.; Daniels, L. M.; Hillard, E. A.; Murillo, C. A. "Filling a Void: Synthesis and Characterization of Tetracarboxylato Dimolybdenum Cations" *Inorg. Chem.*, *41*, 1639. Copyright 2002, American Chemical Society.

EXPERIMENTAL

General Considerations. All manipulations were carried out in an inert atmosphere utilizing standard Schlenk and drybox techniques. All reagents and solvents were obtained commercially. Anhydrous dichlorobenzene was purchased from Aldrich Chemical Company in Sure-Seal bottles. Dichloromethane was dried over P_2O_5, hexanes and toluene over Na/K alloy, and these solvents were freshly distilled under N_2 prior to use.

Physical Measurements. Elemental analyses were performed by Canadian Microanalytical Service, Ltd., Delta, British Columbia. ^{1}H NMR spectra were recorded on a Unity Plus 300 NMR spectrometer, with chemical shifts (δ) referenced to CH_2Cl_2. The cyclic voltammograms were recorded on a BAS 100 electrochemical analyzer in 0.1 M $Bu^n_4NPF_6$ solutions with Pt working and auxiliary electrodes and a Ag/AgCl reference electrode; scan rates were 100 mV s^{-1} in all cases. The EPR spectra were recorded on a Bruker ESP300 spectrometer. The magnetic susceptibility measurements were recorded on a Quantum Design SQUID MPMS-XL magnetometer. UV/vis spectra were recorded on a Cary 17D spectrophotometer.

Preparation of $[Mo_2(TiPB)_4]PF_6$, 7. $Mo_2(TiPB)_4$ (300 mg, 0.254 mmol) and $NOPF_6$ (45.0 mg, 0.257 mmol) were each combined with 20 mL CH_2Cl_2. The yellow solution was transferred to a flask containing an $NOPF_6$ suspension, quickly affording a purple solution that stirred for 2 h. The mixture was filtered over Celite to remove any unreacted $NOPF_6$, and concentrated to about 10 mL. Red needles of **7**·$2CH_2Cl_2$ suitable for X-ray structural analysis were grown after 24 h from the slow diffusion of hexanes into the filtrate. The yield was 0.060 g, (52%). After elimination of interstitial solvent molecules under vacuum: Anal. for $C_{64}H_{92}Mo_2O_8PF_6$, Calcd. (Found): C, 57.97 (57.51); H, 6.99 (6.84). IR (KBr): 2964, 2931, 2870,

2373, 2345, 1700, 1687, 1655, 1638, 1605, 1561, 1543, 1460, 1403, 1320, 1284, 1262, 1156, 1107, 1087 cm^{-1}.

Preparation of $[Mo_2(TiPB)_4]BF_4$, 8. The corresponding BF_4 salt of $Mo_2(TiPB)_4$ was prepared similarly, in comparable yield. After elimination of interstitial solvent molecules: Anal. for $C_{64}H_{92}Mo_2O_8BF_4$, Calcd. (Found): C, 60.62 (60.02); H, 7.31 (7.25). IR (KBr): 2963, 2930, 2870, 2373, 2345, 1701, 1686, 1655, 1637, 1605, 1562, 1544, 1460, 1403, 1320, 1292, 1261, 1194, 1156, 1108, 1089, 1052 cm^{-1}.

Preparation of $Mo_2(TiPB)_4$, 9. A mixture of $Mo(CO)_6$ (2.640 g, 10.00 mmol) and HTiPB (4.977 g, 20.04 mmol) in 25 mL *o*-dichlorobenzene was refluxed under N_2 for four days. Upon cooling, copious yellow solid was afforded, which was filtered and recrystallized by slow diffusion of hexanes into a hot, saturated toluene solution. The yield, before recrystallization, was essentially quantitative. Crystals suitable for X-ray crystallography were prepared by diffusion of hexanes into a saturated toluene solution of the product. Anal. for $C_{64}H_{92}Mo_2O_8$, Calcd. (Found): C, 65.08 (64.62); H, 7.85 (7.94).^{1}H NMR δ (ppm, in CD_2Cl_2): 7.131 (s, 8 H, aromatic), 3.363 (septet, 8 H, *o*-isopropyl), 2.933 (septet, 4 H, *p*-isopropyl), 1.274 (d, 24 H, methyl), 1.177 (d, 48 H, methyl). IR (KBr): 2960, 2933, 2870, 2374, 2345, 1698, 1605, 1564, 1484, 1464, 1411, 1387, 1360, 1318, 1297, 1259, 1242, 1195, 1158, 1105, 1071, 1054 cm^{-1}.

$[Mo_2(O_2CC_4H_9)_4]PF_6$, 10. $Mo_2(O_2CC_4H_9)_4$, (200 mg, 0.335 mmol), prepared from a literature procedure,[42] and $AgPF_6$ (85.0 mg, 0.335 mmol) were dissolved in 20 and 5 mL CH_2Cl_2, respectively. Upon addition of the molybdenum solution to the flask containing the $AgPF_6$ solution, a green solution and black precipitate (Ag) quickly formed. The mixture was stirred for 1 h, then filtered over Celite. A few green blocks of **10** suitable for X-ray structural analysis were grown after 24 h from the slow diffusion of hexanes into the filtrate. Besides the few crystals, copious yellow and brown solids precipitated out of solution.

CRYSTALLOGRAPHIC STUDIES

Single crystals of **7**·2CH_2Cl_2, **8**·2CH_2Cl_2, and **10** were attached to glass fibers with a small amount of silicon grease and mounted on the Bruker SMART system for data collection using Mo Kα radiation at 213(2) K. Single-crystal X-ray work on **9** was performed on a Nonius FAST diffractometer utilizing the program MADNES[30] with Mo Kα radiation at 213(2) K. Cell parameters were obtained from an autoindexing routine. For **7**·2CH_2Cl_2, cell parameters were refined with 3118 reflections within a 2θ range of 4.324-51.07°. For **8**·2CH_2Cl_2, cell parameters were refined with 5034 reflections within a 2θ range of 4.554-54.975°. For **9**, cell parameters were refined with 250 reflections within a 2θ range of 18.2-41.6°. For **10,** cell parameters were refined with 6400 reflections within a 2θ range of 4.684-54.98°

For all compounds, the coordinates of some or all of the non-hydrogen atoms were found via direct methods using the structure solution program SHELXS.[43] The positions of the remaining non-hydrogen atoms were located by use of a combination of least-squares refinement and difference Fourier maps in the SHELXL-93 program.[20] Non-hydrogen atoms were refined with anisotropic displacement parameters, except for disordered portions of the structures, (isopropyl groups in **7**·2CH_2Cl_2, fluorine atoms in **8**·2CH_2Cl_2, phenyl rings and isopropyl groups in **9**, and *t*-butyl groups in **10**). The hydrogen atoms were included in the structure factor calculations at idealized positions. Cell parameters and refinement results for all compounds are summarized in Tables 13-16. Selected bond distances and angles are given in Tables 17.

Table 13. Crystal Data and Structure Refinement for **7**·2CH_2Cl_2

Empirical formula	$C_{66}H_{96}Cl_4F_6Mo_2O_8P$
Formula weight	1496.08
Space group	$P2_1/n$
Unit cell dimensions	a = 9.4884(6) Å α = 90˚ b = 18.757(1) Å β = 98.319(2)˚ c = 20.428(1) Å γ = 90˚
Volume	3597.4(4) Å³
Z	2
Density (calculated)	1.381 g/cm³
Crystal size	0.20 x 0.13 x 0.10 mm
Absorption coefficient	0.584 mm^{-1}
Data collection instrument	Bruker SMART area detector
Wavelength	0.71073 Å
Orientation reflections, number, range (θ)	3118, 2.162 - 25.535
Temperature	213(2) K
Scan method	ω scans
Theta range for data collection	2.02 to 27.53˚
Reflections collected	22866
Independent reflections	8244 [R(int) = 0.0779]
Data / restraints / parameters	6750 / 78 / 394
Refinement method	Full-matrix least-squares on F^2
Final R indices [$I > 2\sigma(I)$]	$R1^a$ = 0.055, $wR2^b$ = 0.110
R indices (all data)	$R1^a$ = 0.135, $wR2^b$ = 0.142
Goodness-of-fit on F^2	0.944
Largest shift/esd, final cycle	0.016
Largest peak, final cycle	1.24(11) e/Å³

[a] $R1 = \sum||F_o| - |F_c||/\sum|F_o|$.
[b] $wR2 = [\sum[w(F_o^2-F_c^2)^2]/\sum[w(F_o^2)^2]]^{½}$, $w = 1/[\sigma^2(F_o^2) + (aP)^2 + bP]$, where $P = [\max(F_o^2 \text{ or } 0) + 2(F_c^2)]/3$.

Table 14. Crystal Data and Structure Refinement for **8**·$2CH_2Cl_2$

Empirical formula	$C_{66}H_{96}BCl_4F_4Mo_2O_8$
Formula weight	1437.92
Space group	$P2_1/n$
Unit cell dimensions	a = 9.2621(7) Å α = 90° b = 18.755(2) Å β = 98.210(2)° c = 20.510(2) Å γ = 90°
Volume	3526.3(4) Å³
Z	2
Density (calculated)	1.354 g/cm³
Crystal size	0.210 x 0.121 x 0.100 mm
Absorption coefficient	0.567 mm^{-1}
Data collection instrument	Bruker SMART area detector
Wavelength	0.71073 Å
Orientation reflections, number, range (θ)	5034, 2.28 - 27.49
Temperature	213(2) K
Scan method	ω scans
Theta range for data collection	2.01 to 24.00°
Reflections collected	17073
Independent reflections	5538 [R(int) = 0.0444]
Data / restraints / parameters	5538 / 1 / 382
Refinement method	Full-matrix least-squares on F²
Final R indices [$I > 2\sigma(I)$]	$R1^a$ = 0.037, $wR2^b$ = 0.073
R indices (all data)	$R1^a$ = 0.071, $wR2^b$ = 0.081
Goodness-of-fit on F^2	1.054
Largest shift/esd, final cycle	0.029
Largest peak, final cycle	0.56(7) e/Å³

[a] $R1 = \sum||F_o| - |F_c||/\sum|F_o|$.
[b] $wR2 = [\sum[w(F_o^2-F_c^2)^2]/\sum[w(F_o^2)^2]]^{½}$, $w = 1/[\sigma^2(F_o^2) + (aP)^2 + bP]$, where $P = [\max(F_o^2 \text{ or } 0) + 2(F_c^2)]/3$.

Table 15. Crystal Data and Structure Refinement for **9**

Empirical formula	$C_{64}H_{92}Mo_2O_8$
Formula weight	1181.26
Space group	$P\bar{1}$
Unit cell dimensions	a = 9.709(6) Å α = 100.01(4)° b = 12.035(8) Å β = 107.95(3)° c = 14.574(6) Å γ = 103.36(6)°
Volume	1520.0(15) Å³
Z	1
Density (calculated)	1.290 g/cm³
Crystal size	0.3 x 0.25 x 0.2 mm
Absorption coefficient	0.464 mm^{-1}
Data collection instrument	Nonius FAST
Wavelength	0.71073 Å
Orientation reflections, number, range (θ)	250, 9.1 - 20.8
Temperature	213(2) K
Scan method	ω scans
Theta range for data collection	2.26 to 23.29°.
Reflections collected	7961
Independent reflections	3996 [R(int) = 0.0745]
Data / restraints / parameters	3986 / 36 / 295
Refinement method	Full-matrix least-squares on F^2
Final R indices [$I > 2\sigma(I)$]	$R1^a$ = 0.062, $wR2^b$ = 0.156
R indices (all data)	$R1^a$ = 0.069, $wR2^b$ = 0.171
Goodness-of-fit on F^2	1.087
Largest shift/esd, final cycle	-0.012
Largest peak, final cycle	1.42(13) e/Å³

[a] $R1 = \sum||F_o| - |F_c||/\sum|F_o|$.
[b] $wR2 = [\sum[w(F_o^2-F_c^2)^2]/\sum[w(F_o^2)^2]]^{1/2}$, $w = 1/[\sigma^2(F_o^2) + (aP)^2 + bP]$, where $P = [\max(F_o^2 \text{ or } 0) + 2(F_c^2)]/3$.

Table 16. Crystal Data and Structure Refinement for **10**

Empirical formula	$C_{20}H_{36}F_6Mo_2O_8P$
Formula weight	741.34
Space group	*C*2/*c*
Unit cell dimensions	a = 16.764(4) Å α = 90˚ b = 10.454(2) Å β = 115.351(3)˚ c = 19.246(4) Å γ = 90˚
Volume	3048.1(11) Å³
Z	4
Density (calculated)	1.615 g/cm³
Crystal size	0.429 x 0.197 x 0.175 mm
Absorption coefficient	0.949 mm^{-1}
Data collection instrument	Bruker SMART area detector
Wavelength	0.71073 Å
Orientation reflections, number, range (θ)	6400, 2.342 - 27.488
Temperature	213(2) K
Scan method	ω scans
Theta range for data collection	2.37 to 27.51˚
Reflections collected	9279
Independent reflections	3486 [*R*(int) = 0.0181]
Data / restraints / parameters	3486 / 18 / 191
Refinement method	Full-matrix least-squares on F^2
Final *R* indices [$I > 2\sigma(I)$]	$R1^a$ = 0.028, $wR2^b$ = 0.072
R indices (all data)	$R1^a$ = 0.033, $wR2^b$ = 0.076
Goodness-of-fit on F^2	1.094
Largest shift/esd, final cycle	-0.003
Largest peak, final cycle	0.67(6) e/Å³

[a] $R1 = \sum||F_o| - |F_c||/\sum|F_o|$.
[b] $wR2 = [\sum[w(F_o^2-F_c^2)^2]/\sum[w(F_o^2)^2]]^{½}$, $w = 1/[\sigma^2(F_o^2) + (aP)^2 + bP]$, where $P = [\max(F_o^2 \text{ or } 0) + 2(F_c^2)]/3$.

Table 17. Selected Bond Lengths [Å] and Angles [˚] for $[Mo_2(O_2CR)_4]^{0/+}$ Complexes[a]

	7·2CH$_2$Cl$_2$	**8·2CH$_2$Cl$_2$**	**9**	**10**
Mo(1)–Mo(1a)[b]	2.1364(8)	2.1441(5)	2.076(1)	2.1512(5)
Mo(1)–O(1)	2.074(3)	2.071(2)	2.084(4)	2.079(2)
Mo(1)–O(2)	2.066(3)	2.070(1)	2.113(4)	2.080(2)
Mo(1)–O(3)	2.063(3)	2.065(2)	2.084(4)	2.073(2)
Mo(1)–O(4)	2.062(3)	2.065(1)	2.088(4)	2.077(2)
Mo(1)–Mo(1)–O(1)	91.70(9)	91.54(5)	92.8(1)	91.31(5)
Mo(1a)–Mo(1)–O(2)	91.67(8)	91.64(4)	90.9(1)	91.04(5)
Mo(1a)–Mo(1)–O(3)	90.6(1)	90.71(5)	91.4(1)	91.25(5)
Mo(1a)–Mo(1)–O(4)	90.57(9)	90.61(5)	92.0(1)	91.04(5)
cis-O–Mo(1)–O	90.0[1]	89.98[6]	89.9[2]	89.98[8]
trans-O–Mo(1)–O	176.7[1]	176.96[6]	176.1[1]	177.67[6]

[a] Square brackets refer to average values; parentheses refer to unique values.
[b] Mo(1) and Mo(1a) are related by an inversion center in all compounds.

In **8**·2CH_2Cl_2, the BF_4^- group resides on the inversion center half-way between the dinuclear Mo centers, located directly in line with the axial positions. The anion was modeled as a rigid tetrahedron, and further refinement followed by examination of difference Fourier maps revealed at least two other orientations in addition to the disorder imposed by the site symmetry. Therefore three BF_4^- units were included at the site as rigid tetrahedra in which the B–F bonds were allowed to shrink or expand. The B atoms were not constrained to remain exactly on the inversion center. The sum of the occupancies was constrained to equal full occupancy for the site, and one common isotropic displacement factor was refined for all F atoms and another for all B atoms. The final occupancies for the three orientations converged to 36.57(2), 31.06(2), and 32.37(2)%.

RESULTS AND DISCUSSION

Synthetic Considerations. Compounds **7**, **8**, and **9** were synthesized by the following reactions:

$$Mo_2(TiPB)_4 + NOPF_6 \xrightarrow{CH_2Cl_2} [Mo_2(TiPB)_4]PF_6 + NO \quad (1)$$

$$Mo_2(TiPB)_4 + NOBF_4 \xrightarrow{CH_2Cl_2} [Mo_2(TiPB)_4]BF_4 + NO \quad (2)$$

$$2Mo(CO)_6 + 4HTiPB \xrightarrow{\Delta,\ o\text{-}Cl_2C_6H_4} Mo_2(TiPB)_4 + 12CO + 2H_2 \quad (3)$$

The neutral, quadruply bonded $Mo_2(TiPB)_4$ was obtained in excellent yield by the classical route. It displays a brilliant canary yellow color typical of other $Mo_2(O_2CR)_4$ compounds. However, it is slightly more air sensitive than $Mo_2(O_2CCH_3)_4$, and the crystals turn greenish brown after several hours of exposure to the atmosphere. It is far more soluble in hexanes, toluene, ether, and dichloromethane than $Mo_2(O_2CCH_3)_4$ or $Mo_2(O_2CC_4H_9)_4$. This increased solubility makes recrystallization difficult, and crystals can be obtained only when a highly saturated solution of hot toluene is layered with hexanes. The solubility of the compound even in hexanes reduces the yields for the crystalline material; the extreme solubility of the compound in dichloromethane precludes crystallization from this solvent.

The paramagnetic cationic species, $[Mo_2(TiPB)_4]PF_6$ is deep red, while the BF_4 salt is somewhat more orange in color. These complexes are quite soluble and stable in dichloromethane, but completely insoluble in hexanes, thus contributing to the ease of preparation and crystallization. These solids are moderately air stable, and decompose after about an hour in air, when they turn from red to brown. However, solutions of these complexes are extremely air-sensitive, and lose all color within a couple of minutes in air. This process has also been observed *via* UV/vis spectroscopy, where all transitions in the visible range disappear after air exposure.

Structural Considerations. In **9**, the four carboxylato groups bridge the quadruply bonded Mo_2^{4+} unit, giving the typical paddlewheel arrangement shown in Figure 11. The Mo–Mo distance of 2.076(1) Å is marginally shorter by *ca* 0.02 Å than that of most of the previously reported quadruply bonded $Mo_2(O_2CR)_4$ compounds[1] and the structure is similar to that of the chromium analog.[29]

For the oxidized species, shown in Figures 12 and 13, the structure of the cation is generally similar, but the Mo–Mo separation, 2.1364(8) Å in **7** and 2.1441(5) Å in **8**, is

significantly greater than that of the unoxidized starting material, (2.076(1) Å). Thus, removal of one electron, which reduces the Mo–Mo bond order to 3.5, increases the distance by about 0.06-0.07 Å relative to that in the parent compound. The magnitude of the change in going from the $\sigma^2\pi^4\delta^2$ to the $\sigma^2\pi^4\delta$ configuration is typical for such a change, as may be seen by comparison with those for the pairs, $Mo_2(SO_4)_4^{4-}$,[44] and $Mo_2(SO_4)_4^{3-}$,[45] with Mo–Mo distances of 2.110(2) and 2.164(2) Å, respectively, and for $Mo_2(hpp)_4$[46] and $[Mo_2(hpp)_4]^+$,[47] (where hpp is the anion of 1,3,4,6,7,8-hexahydro-2H-pyrimido[1,2-a]pyrimidine), where the bond distances are 2.067(1) and 2.127 Å, respectively. However, the change in the Mo–Mo distances is significantly smaller upon oxidation of $Mo_2[\mu\text{-}\eta\text{-}(NPh)_2CNHPh]_4$, being only 2.0839(9)[48] to 2.1194(12),[49] (0.0355 Å). Furthermore, the increase in charge on the Mo_2 core from the loss of one electron causes the Mo–O bonds in the cations to contract by *ca* 0.025 Å relative to the neutral parent compound.

Electrochemistry. The one-electron electrochemical oxidation (Mo_2^{4+}/Mo_2^{5+}) of **9** in dichloromethane, acetonitrile, and ethanol exhibits values for $E_{1/2}$ of +0.621, +0.448, and +0.462 V (*vs* Ag/AgCl), respectively. A representative cyclic voltammogram is depicted in Figure 14. While the trend is the same as that reported for solutions of $Mo_2(butyrate)_4$,[50] ($E_{1/2}$ values of +0.45, +0.30, and +0.39 V *vs* SCE), the $E_{1/2}$ values are higher for **9** in all cases, when the difference in referencing procedures is taken into account. The cyclic voltammogram of $Mo_2(O_2CCH_3)_4$ in methanol is similar to that of compound **9**, with $E_{1/2}$ = +0.24 V *vs* Ag/AgCl,[51] while measurements on solutions of $Mo_2(pivalate)_4$ in acetonitrile and THF have $E_{1/2}$ values of +0.38 V *vs* SCE[52] and +0.86 V *vs* Ag wire,[53] respectively. These results contrast with those reported for $Mo_2(aspirinate)_4$,[51] where an irreversible one-electron oxidation wave was observed. It is surprising that all of the noted compounds are more easily oxidized than **9**, yet no structures of the cations have been reported.

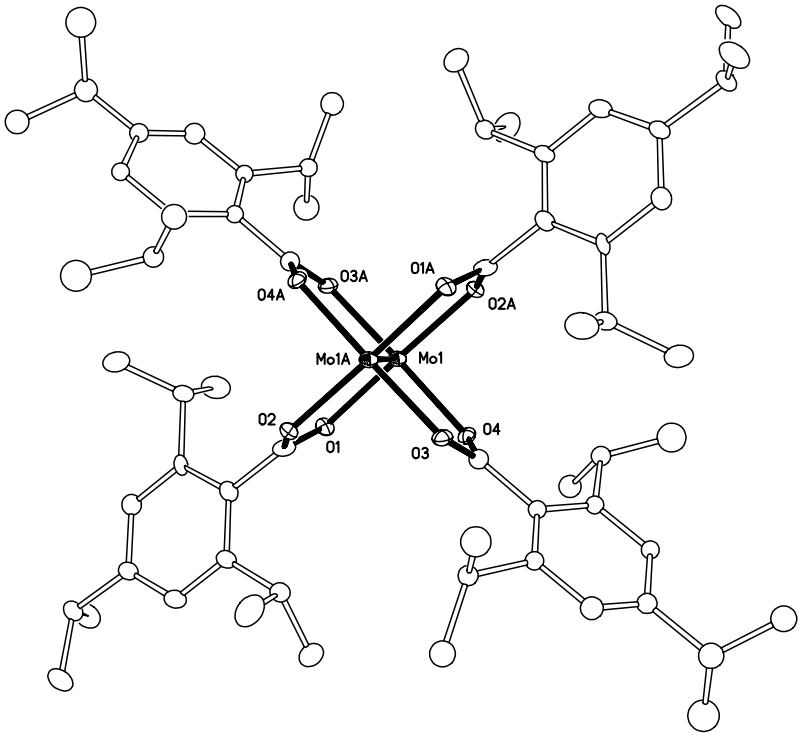

Figure 11. Thermal ellipsoid plot of $Mo_2(TiPB)_4$, **9**. Probability ellipsoids are shown at the 30% level. Hydrogen atoms and disordered phenyl and isopropyl groups of minor occupancy have been omitted for clarity.

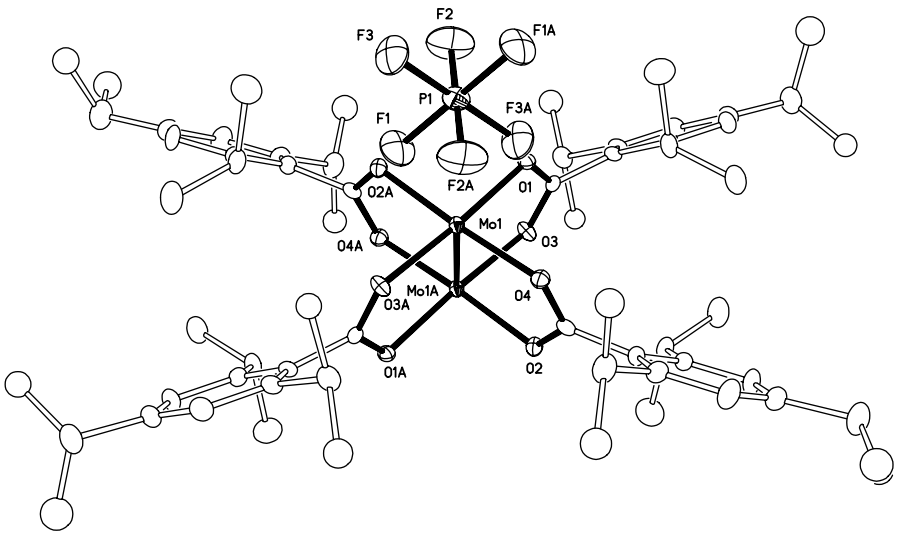

Figure 12. Thermal ellipsoid plot of $[Mo_2(TiPB)_4]PF_6$ in **7**·$2CH_2Cl_2$. Probability ellipsoids are shown at the 30% level. Hydrogen atoms, solvent of crystallization, disordered isopropyl groups and disordered fluorine atoms of minor occupancy have been omitted for clarity.

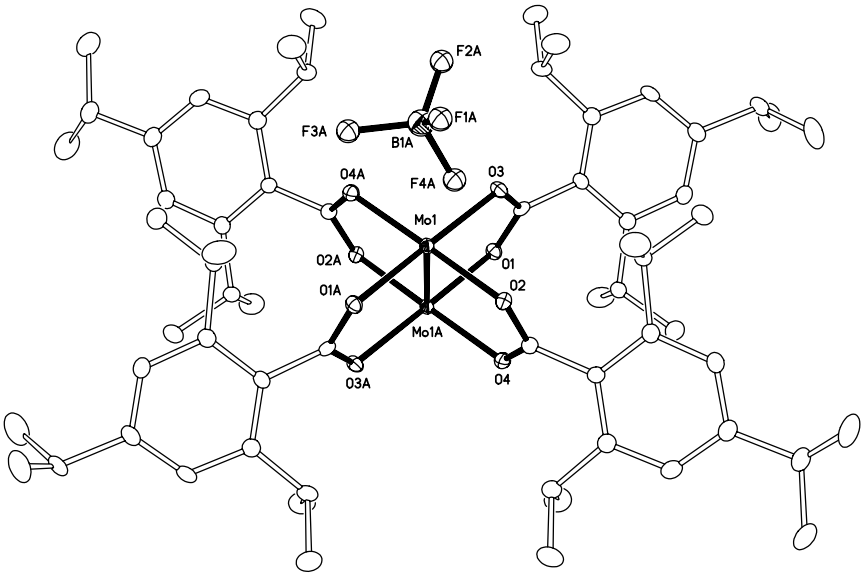

Figure 13. Thermal ellipsoid plot of $[Mo_2(TiPB)_4]BF_4$ in **8**·$2CH_2Cl_2$. Probability ellipsoids are shown at the 30% level. Hydrogen atoms, solvent of crystallization and disordered tetrafluoroborate anion have been omitted for clarity.

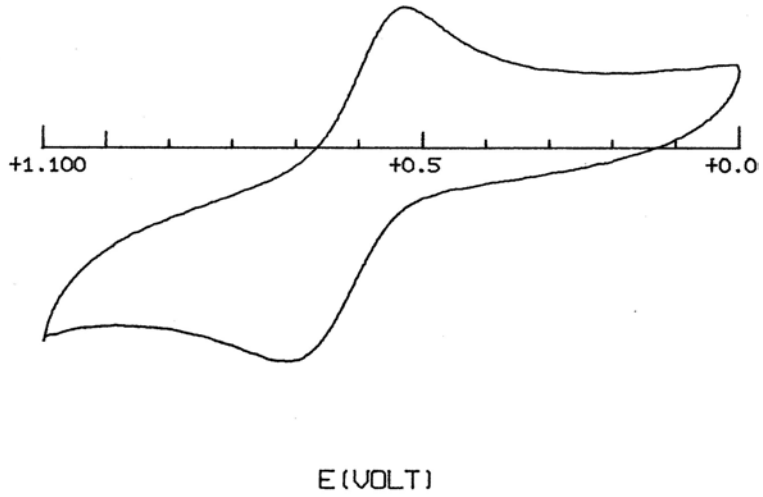

Figure 14. Cyclic voltammogram of **9** in dichloromethane.

To determine the reason for this gap in the literature, we sought to chemically oxidize another dimolybdenum carboxylate. We chose the pivalato derivative, $Mo_2(O_2CC_4H_9)_4$, due to its favorable solubility in dichloromethane and the presence of an electrochemically reversible oxidation wave ($\Delta E^0(CH_2Cl_2)$ = 0.133 V), from which we determined $E_{1/2}(CH_2Cl_2)$ = 0.522 (*vs* Ag/AgCl). Although crystalline samples of **7**·2CH_2Cl_2 and **8**·2CH_2Cl_2 were obtained in moderate yield, according to equations (1) and (2), we found that a similar oxidation of Mo_2(pivalate)$_4$ provides green crystals of **10** only as a very minor product. Copious yellow and brown solids settle out of the dichloromethane solution when carefully layered with hexanes. Furthermore, these crystals are significantly less stable than those of **7**·2CH_2Cl_2 and **8**·2CH_2Cl_2, and lose crystallinity within a couple of days. After a great deal of effort, a crystal structure was obtained, Figure 15, with a Mo–Mo distance of 2.1512(5) Å, 0.063 Å longer than that in the parent compound.[54] Unfortunately, the low yield made bulk measurements impractical. It is also worth mentioning that the tetrabutyrato dimolybdenum cation has also been isolated.[50] However, electrochemical experiments indicated that the cation was unstable, with a lifetime on the order of 1 minute. Very likely the reason for the increased stability of the Mo_2^{5+} unit, when surrounded by the bulkier 2,4,6-triisopropylbenzoate anions, as compared to the less bulky pivalate or butyrate groups, is the capacity of the former to isolate the radical dimetal unit more effectively from the surrounding environment. This ability to tune the region of stability might be potentially useful for the exploitation of such units as one-electron oxidants for organic substrates. This is an area of great current interest[55] and where further work might prove rewarding.

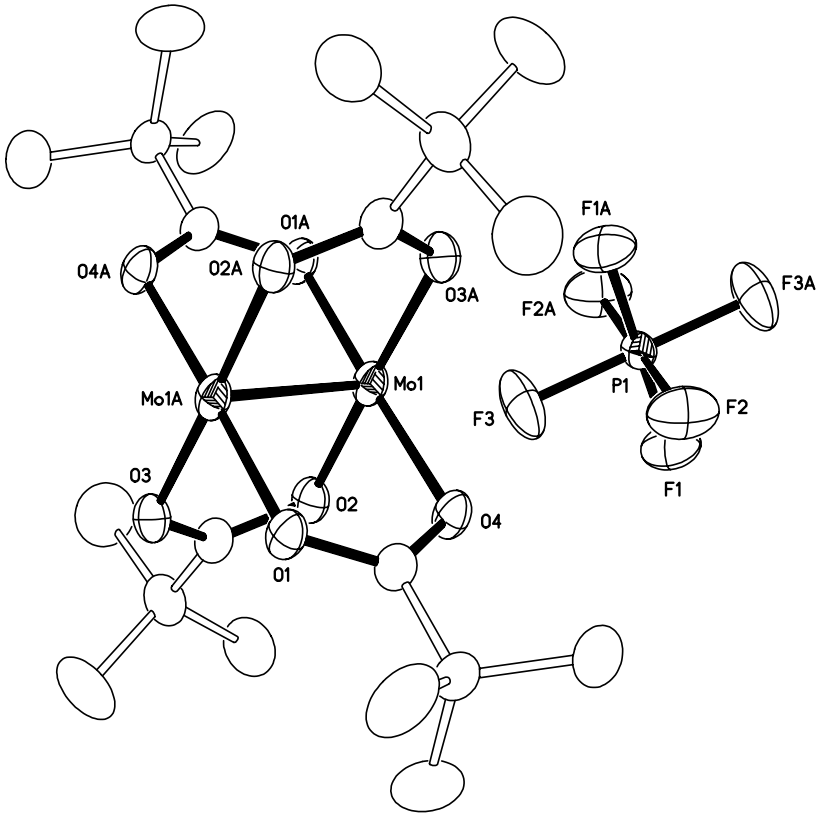

Figure 15. Thermal ellipsoid plot of $[Mo_2(O_2CMe_3)_4]PF_6$, **10**. Probability ellipsoids are shown at the 30% level. Hydrogen atoms and disordered *t*-butyl groups of minor occupancy have been omitted for clarity.

EPR Spectroscopy. The X-band (microwave frequency 9.42 GHz) EPR spectra of **7** and **8** in frozen dichloromethane at 70 K are consistent with a doublet ground state with both $g_{//}$ and $g_{\perp}$ having the same value of 1.936. The spectra are similar to that reported for $[Mo_2(O_2CC_3H_7)_4]^+$, with $g_{//} = g_{\perp} = 1.941$,[50] and each may be interpreted in terms of the spin Hamiltonian (Equation 4), with $S = 1/2$ and including species with nuclear spin states $I^1 + I^2 = J =$ 0, 5/2, and 5 with a natural abundance of 56%, 37.7%, and 6.3%, respectively.[56] We were not able to directly observe the eleven-line pattern arising from the $J = 5$ isotopomer, likely due to poor instrument resolution. It should be pointed out that this small component is also not discernable in the simulation, although it has been added to our model at the appropriate natural abundance. The spin Hamiltonian parameters for **7** and **8** are listed in the caption to Figure 16, and are very similar to those reported for $Mo_2(O_2CC_3H_7)_4$.[50]

$$H = m\left[g_{||}H_zS_z + g_{\perp}(H_xS_x + H_yS_y)\right] + A_{||}S_z(I^1z + I^2z) + A_{\perp}\left[S_x(I^1x + I^2x) + S_y(I^1y + I^2y)\right] \qquad (4)$$

It may be noted that for the $[Mo_2(HPO_4)_4]^{3-}$ ion the $g_{//}$ and $g_{\perp}$ were distinguishable (1.894, 1866), but only barely.[57]

The clear evidence of an unpaired electron from EPR spectroscopy provoked us to further investigate the magnetic properties of the cation, $[Mo_2(TiPB)_4]^+$. Molar magnetic susceptibility measurements were carried out on crystalline samples of **8** using a SQUID magnetometer at 1000 Gauss in the temperature range 300 to 2 K. The data for **8** were corrected for diamagnetic contribution by measuring the magnetic susceptibility of the neutral parent compound, (-0.0010 emu mol^{-1}). Compound **8** displays a linear $1/\chi$ plot, Figure 17, with the *x*-intercept very near zero (1.286 K), and a slope of 0.3474, as expected for a Curie paramagnet

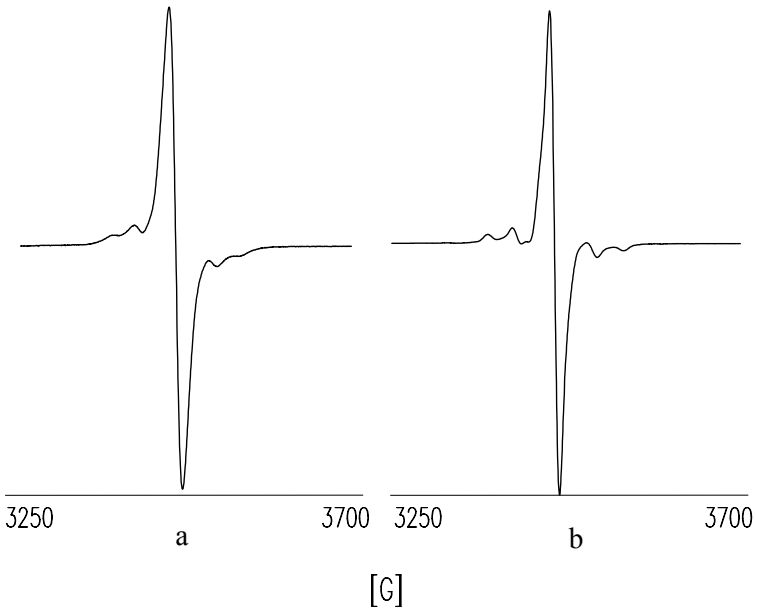

Figure 16. Electron paramagnetic resonance spectrum of **7** (a) and **8** (b). Dichloromethane glass; $g_{\parallel} = g_{\perp} = 1.936$, $A_{\parallel} = 35.60 \times 10^{-4}$ cm^{-1}, and $A_{\perp} = 18.20 \times 10^{-4}$ cm^{-1}.

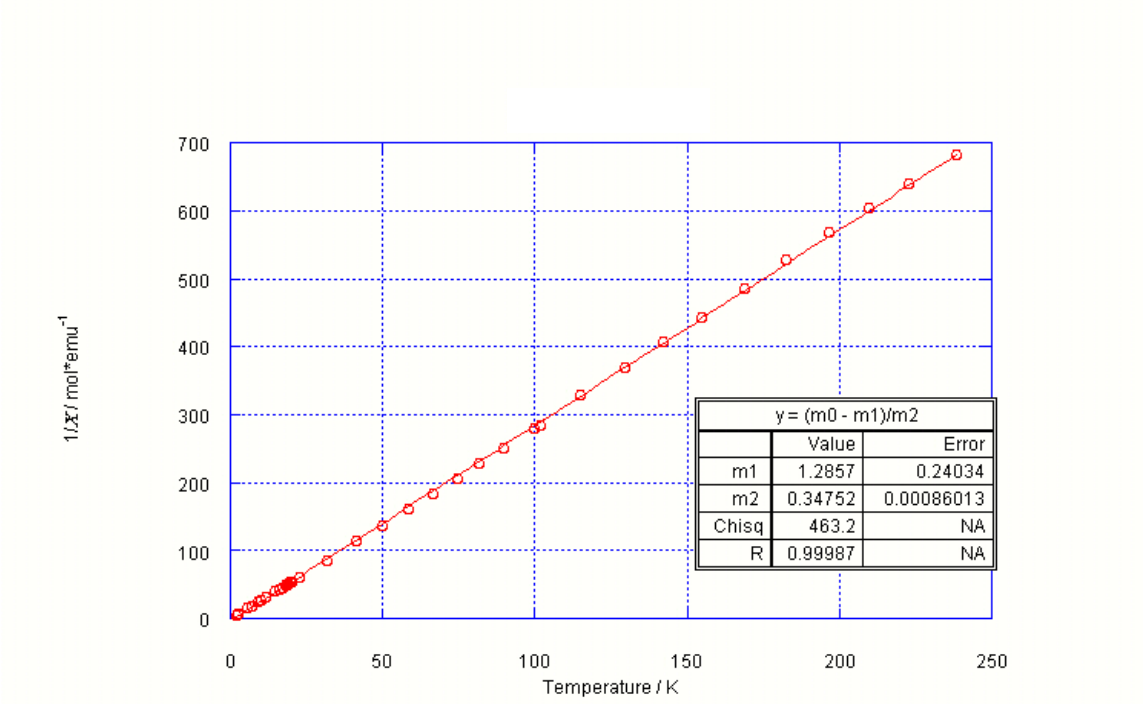

Figure 17. Magnetic susceptibility plot for **8**.

with $S = 1/2$. From equation 5, g was calculated to be 1.93, in rough agreement with the value extracted from the EPR data.

$$C = \frac{1}{8} g^2 (S(S+1)) \tag{5}$$

Visible Spectroscopy. The room temperature electronic spectrum for **7** shows three peaks: 550 nm (ϵ = 4700 $M^{-1}cm^{-1}$), 365 nm (ϵ = 8400 $M^{-1}cm^{-1}$), and 290 nm (ϵ = 10900 $M^{-1}cm^{-1}$). The spectrum for **8** is quite similar, with peaks at 530 (ϵ = 4400 $M^{-1}cm^{-1}$), 365 (ϵ = 8880 $M^{-1}cm^{-1}$), and 290 nm (ϵ = 11100 $M^{-1}cm^{-1}$). Compound **9** exhibits a poorly resolved shoulder at *ca* 390 nm (ϵ = 13800 $M^{-1}cm^{-1}$), a peak at 350 nm (ϵ = 22000 $M^{-1}cm^{-1}$) and a shoulder at 295 nm (ϵ = 11400 $M^{-1}cm^{-1}$). While the $\delta \rightarrow \delta^*$ transition in $Mo_2(O_2CCR)_4$ complexes typically occurs at ca. 440 nm,[2] this region of the spectrum is obscured by what is a large, broad, presumably charge transfer band at 350 nm. It is tempting, albeit speculative, to assign the shoulder at *ca* 390 nm to the $\delta \rightarrow \delta^*$ transition for two reasons. First, in light of the observation that axial ligands tend to lengthen the Mo–Mo bond, one expects the $\delta \rightarrow \delta^*$ transition to be at higher energy for the non-axially ligated compound **9**. Second, if we assign the lowest energy peak in **7** and **8** to the $\delta \rightarrow \delta^*$ transition, the difference in transition energy between the one-electron and two-electron systems is *ca* 7300 cm^{-1}, a fair approximation of the exchange energy of quadruply bonded molybdenum compounds.[58] The large molar absorptivity coefficient of the putative $\delta \rightarrow \delta^*$ transition may be explained by significant mixing with the proximal, intense CT transition.

The blue shift of the CT band in **9** from the 428 nm peak[59] exhibited by $Mo_2(O_2CC_6H_5)_4$ has been attributed to the twisting of the phenyl rings out of the CO_2 plane in the case of $Mo_2(O_2C(2,4,6\text{-}Me_3C_6H_2))_4$.[60] Likewise, in the centrosymmetric **9**, one phenyl blade is twisted 68°, while the other is twisted 34°from the carboxylate plane, thus disrupting the ligand conjugation and destabilizing the acceptor molecular orbital for a MLCT transition.

Concluding Remarks. The first examples of dimolybdenum tetracarboxylato cations have been structurally characterized in $[Mo_2(TiPB)_4]PF_6$, $[Mo_2(TiPB)_4]BF_4$, and $[Mo_2(O_2CC_4H_9)_4]PF_6$. The crystal structures, EPR spectra, and electronic spectra all indicate that the lone electron resides in a metal-based δ orbital. While other $[Mo_2(O_2CR)_4]^+$ complexes have been accessed via reversible oxidation waves in solution, the 2,4,6-triisopropylphenyl carboxylato complexes exhibit far superior stability, and the three compounds whose structures are described here are the first and only ones that have been isolated and characterized fully.

CHAPTER V

DIRHODIUM TETRACARBOXYLATES[4]

One of the most remarkable and important new classes of homogeneous catalysts,[4] which has been developed in recent years (and which is still growing in scope),[4b,c] is based on dirhodium tetracarboxylates and similar paddlewheel species with bridging ligands that are stereoelectronic equivalents of a carboxyl group (e.g., amidato anions). The first such catalysts to be employed were the acetate, $Rh_2(O_2CCH_3)_4(H_2O)_2$ and other $Rh_2(O_2CR)_4L_2$ compounds.[61] The acetate itself, the first compound of the entire class of Rh_2^{4+} compounds, was reported in 1962,[62] although the simplest member of the class, the tetraformate, had been reported, but incorrectly formulated, a little earlier.[63] As first reported, the structure, as depicted in Figure 1, was somewhat imprecise though qualitatively correct; an accurate structure was published in 1970.[64]

Their role as catalysts is far from the only reason for wide interest in compounds of the general type $Rh_2L^{br}_4$ (where L^{br} is any η^2–μ_2 ligand). Other important features of their chemistry relate to their potential as therapeutic agents,[5] their interactions with DNA and nucleosides,[5f,g] their utility in forming supramolecular structures[65] and the exceptional ability of $Rh_2(O_2CCF_3)_4$ to function as a powerful difunctional Lewis acid.[66]

---

[4] Reprinted in part with permission from Cotton, F. A.; Hillard, E. A.; Murillo, C. A. "The First Dirhodium Tetracarboxylate Molecule without Axial Ligation: New Insight into the Electronic Structures of Molecules with Importance in Catalysis and other Reactions" *J. Am. Chem. Soc.* **2002**, *41*, 1639. Copyright 2002, American Chemical Society and Cotton, F. A.; Hillard, E. A.; Liu, C. Y.; Murillo, C. A.; Wang, W.; Wang, X. "Steps on the Way to the First Dirhodium Tetracarboxylate with no Axial Ligation: Synthetic Lessons and a Plethora of $Rh_2(O_2CR)_4L_{2-n}$ Compounds, n = 0, 1, 2" *Inorg. Chim. Acta*, **2002**, *337*, 233. Copyright 2002, Elsevier.

A key factor in stabilizing $Rh_2(O_2CR)_4L_2$ compounds is the formation of a Rh–Rh single bond, and this bond length is generally in the range 2.34-2.41 Å; mononuclear rhodium(II) compounds are almost unknown.[67]

The work reported here, which provides important new data bearing on the question of electronic structure, begins with the solution of a synthetic problem. In *all* previously known $Rh_2(O_2CR)_4$ compounds, there has been axial ligation. Even two structurally characterized compounds, $Rh_2(O_2CC_3H_7)_4$ and $Rh_2(O_2CCF_3)_4$, whose formulas do not have exogenous ligands, have structures in which the molecules form infinite chains[68,69] in such a way that each molecule has its axial sites occupied by oxygen atoms from its neighbors, as shown in Figure 2. This means that all theoretical work bearing on how axial ligation affects the electronic structure of an $Rh_2(O_2CR)_4$ molecule has been untested by experiment.

For many years, the problem of isolating a paddlewheel compound, $M_2(O_2CR)_4$, with no axial ligands, especially when the metal is Cr or Rh, for which the $M_2(O_2CR)_4$ compounds have a very strong affinity for axial ligands, remained unsolved for several reasons. (1) Merely driving the solvent off of a crystalline $M_2(O_2CR)_4L$ or $M_2(O_2CR)_4L_2$ compound leaves an amorphous product from which structural information cannot be obtained. (2) It is impractical to design and synthesize a compound with an R group capable of blocking the axial positions completely. An R group that might be able to accomplish this would tend to be so bulky as to make the compound nonvolatile and to create a severe solubility problem in any solvent that is not able to be an axial ligand. (3) Solubility or volatility alone do not, of course, suffice because, as noted, these give crystals in which the molecules form self-ligating chains.

A workable strategy for overcoming these difficulties was found several years ago and applied successfully to give the first example of a crystalline $Cr_2(O_2CR)_4$ compound that was totally lacking in axial ligation.[29] That strategy was to employ an R group that meets two

requirements:[70] (1) It can block the formation of chains of the type depicted in Figure 2, even though the axial positions are still accessible to many ligands. (2) This R group renders the $M_2(O_2CR)_4$ compound soluble in one or more non-coordinating solvents from which crystals may be grown. In the case of $Cr_2(O_2CR)_4$, we used the R group 2,4,6-triisopropylphenyl. This choice has the added practical advantage that the needed acid, TiPBH, is commercially available at relatively low cost. We have now applied our strategy to what we believe is the second most difficult case, namely, $Rh_2(TiPB)_4$. The route to the target molecule was not straightforward and many unsuccessful efforts were made in a process that yielded a plethora of axially coordinated dirhodium tetracarboxylates. Here, we summarize the syntheses and structures of these molecules.

EXPERIMENTAL

General Considerations. All reactions were carried out under an atmosphere of dry nitrogen using standard Schlenk techniques, although starting materials were often handled in air. Dirhodium tetraacetate and $Rh_2(O_2CCF_3)_4$ were synthesized by literature procedures.[71,72] Anhydrous $Rh_2(O_2CCF_3)_4$ was stirred in acetonitrile for 30 min and dried under vacuum to produce $Rh_2(O_2CCF_3)_4(CH_3CN)_2$. Triisopropylbenzoic acid (TiPBH) was purchased from Lancaster Synthesis, Inc. Toluene was dried over Na/K alloy, acetonitrile over calcium hydride, ethanol over magnesium metal, acetone over potassium carbonate, and decane and *o*-xylene over molecular sieves. All solvents were freshly distilled under N_2 prior to use, except for decane and *o*-xylene, which were degassed by bubbling N_2. In the cases of compounds **11**, **16** and **18**, crystallizations were carried out by slow concentration of solutions in a vial enclosed within a Schlenk tube containing mineral oil or rubber septa fragments. In this way an inert atmosphere

could be attained while solvent from the solutions was transferred by evaporation to the material inside the Schlenk tube. Thermogravimetric analysis was performed on an Instrument Specialist TGA 1000. Electronic spectra were recorded on a Cary 17D spectrophotometer. NMR spectra were recorded on a Varian Unity 300 spectrometer.

General to most syntheses are the following considerations, 1) A stream of dry nitrogen was blown over the refluxing reaction mixtures, so that byproducts (acetic or trifluoroacetic acid) were distilled out of the reaction flask. The solvents also were distilled until there was only a small amount (*ca* 1 ml) remaining. The remaining solvent was then pumped off at room temperature. 2) After the removal of all solvent, any excess TiPBH was removed by vacuum sublimation.

Preparation of $[Rh_2(TiPB)_2(O_2CCF_3)_2(TiPBH)]_2 \cdot C_6H_{14}$, $11 \cdot C_6H_{14}$. The compounds $Rh_2(O_2CF_3)_4$ (30 mg, 0.046 mmol) and TiPBH (91 mg, 0.37 mmol) were combined in 6 ml of toluene. The green solution was refluxed at 120 ºC while trifluoroacetic acid distilled away under a flow of nitrogen. After 4 h the temperature was raised to 130 ºC and the toluene distilled until about 3 ml remained. The remaining toluene was pumped off, leaving a blue-green solid. Excess TiPBH was removed by vacuum sublimation at 105–110 ºC for 1 h. The remaining solid was extracted with 3 ml of hexanes, and slow evaporation of this solution yielded green blocks after 24 h.

Preparation of $Rh_2(TiPB)_3(O_2CCF_3)(TiPBH)_2$, 12. The compounds $Rh_2(O_2CCF_3)_4$ (30 mg, 0.046 mmol) and TiPBH (91 mg, 0.37 mmol) were combined in 10 ml of decane. The blue-green solution was stirred at 130 ºC for 4 h. Solvent was then removed under vacuum and TiPBH was removed by vacuum sublimation at 110 ºC for 2 h, yielding a blue solid. The solid was extracted with 6 ml of hexanes and slow evaporation of this solution yielded both blue and

green crystals. Only the structure of the blue plates was determined as the green crystals were not suitable for X-ray diffraction.

Preparation of $[Rh_2(TiPB)_2(O_2CCF_3)_2(C_6H_5CH_3)]_2 \cdot 2C_6H_5CH_3$, $13 \cdot 2C_6H_5CH_3$ The lithium salt of TiPB was prepared by adding 1 equiv of BuLi in hexanes to TiPBH in a THF solution. $Rh_2(O_2CCF_3)_4$ (82.3 mg, 0.125 mmol) and TiPBLi (0.127 g, 0.500 mmol) were combined in 20 ml of toluene. The green solution was refluxed for 12 h, yielding a dark yellow precipitate. The suspension was filtered through Celite and the filtrate was concentrated to about 2 ml. The solution was placed in a freezer at −10 °C and pale green plates grew after one day.

Preparation of $[Rh_2(TiPB)_2(O_2CCF_3)_2(acetone)]_2$, 14 and $Rh_2(TiPB)_2(O_2CCF_3)_2(acetone)_2$, 15. The compounds $Rh_2(O_2CCF_3)_4(CH_3CN)_2$ (50 mg, 0.068 mmol) and TiPBH (0.168 g, 0.676 mmol) were combined in 10 ml of toluene. The fuchsia solution was refluxed for 3 h. The color quickly turned green, and the solution was concentrated by distillation to about 1 ml. The remaining solvent was removed under vacuum and the TiPBH was sublimed at 120 ºC, leaving a light green solid. As the solid proved only sparingly soluble in hexanes, it was dissolved in 10 ml of acetone, affording a deep blue-green solution. Removal of solvent under vacuum afforded a dark blue solid, which was dissolved in hexanes. The solution was concentrated to 5 ml and placed in the freezer. After one night two types of crystals had formed: light green plates and very dark blocks. The plate-like crystals corresponded to **14** and the dark block crystals to **15**.

Preparation of $Rh_2(TiPB)_4(TiPBH)_2 \cdot 0.5C_6H_{14}$, $16 \cdot 0.5C_6H_{14}$. The compound $Rh_2(O_2CCF_3)_4(CH_3CN)_2$ and excess TiPBH were combined in 7 ml of decane. The solution was refluxed for 2 h, after which a distillation apparatus was attached. The solution was concentrated to about 2 ml by distillation over the course of two days. All solvent was evaporated under vacuum, yielding a blue solid. Excess TiPBH was sublimed at 150 ºC, and the solid turned

green. It was dissolved in 6 ml of warm hexanes and filtered through Celite. Slow evaporation yielded blue-green blocks after several days.

Preparation of $Rh_2(TiPB)_4(acetone)_2$·0.90acetone, 17·0.90acetone. Method A: Several crystals of $Rh_2(TiPB)_4(TiPBH)_2$ ·$0.5C_6H_{14}$, **16**·$0.5C_6H_{14}$, were dissolved in acetone, in which they are moderately soluble. The blue solution was filtered through Celite, concentrated to 3 ml, and placed in the freezer. Blue-green rhomboidal crystals appeared after 24 h.

Method B: Sodium ethoxide, (0.17 g, 2.5 mmol), was dissolved in 30 ml of ethanol and TiPBH (0.55 g, 2.2 mmol) was added. Once the TiPBH had dissolved, $RhCl_3$·$3H_2O$ (0.15 g, 0.55 mmol) was added, affording an orange-brown suspension. The mixture was refluxed for 18 h, yielding a green solution as well as a deposit of rhodium metal. The suspension was filtered through Celite, and the solvent removed under vacuum. The blue-green solid was extracted with 20 ml of chloroform, dried under vacuum and redissolved in 30 ml of acetone. The solution was concentrated to *ca* 5 ml and placed in a freezer at −10 °C. After 12 h, a crop of blue-green rhomboidal crystals had grown. Anal. for $C_{70}H_{104}Rh_2O_{10}$, Calcd. (Found): C, 64.11 (64.11); H, 7.99 (7.70). ^{1}H NMR δ (ppm, in benzene-d_6): 7.037 (s, 8 H, aromatic), 3.306 (septet, 8 H, *o*-C*H*$(CH_3)_2$), 2.683 (septet, 4 H, *p*-C*H*$(CH_3)_2$), 1.832 (s, 12 H, acetone methyl), 1.211 (d, 48 H, *o*-CH(C*H*$_3)_2$), 1.139 (d, 24 H, *p*-CH(C*H*$_3)_2$). IR (KBr): 3455, 2963, 2871, 1693, 1604, 1573, 1553, 1460, 1401, 1319, 1261, 1236, 1159, 1105, 1020, 944, 877, 811, 749, 650, 558, 506, 460 cm^{-1}.

Preparation of $Rh_2(TiPB)_4(H_2O)(C_6H_5CH_3)$, 18. Several crystals of $Rh_2(TiPB)_4(acetone)_2$·0.90(acetone), **17**·0.90 acetone, were dissolved in toluene. The solution was heated to 60 ºC and vacuum distilled, until the solution was concentrated to about 1 ml. Slow evaporation of the solution yielded green plates after 2 weeks. As water had not been purposely added to the reaction, it is assumed to have entered adventitiously.

Preparation of $Rh_2(TiPB)_4$, 19. Method A: Several crystals of $Rh_2(TiPB)_4(acetone)_2$·0.90acetone, **17**·0.90acetone, from the preparation given in Method A of **17**·0.90 acetone were placed under vacuum at 130 ºC. Over the course of about 4 h, they changed from blue-green to green to yellow-green. The yellow-green solid was dissolved in hexanes (in which it is sparingly soluble) and filtered through Celite. The hexanes were evaporated under a slow stream of nitrogen, yielding a mixture of green and yellow crystals. The structure presented here is that of a yellow crystal.

Method B: Several $Rh_2(TiPB)_4(acetone)_2$·0.90acetone crystals from the preparation given in Method B of **17**·0.90acetone were placed under vacuum at 130 ºC. Over the course of about 4 h, they changed from blue-green to green to yellow-green. The yellowish solid was dissolved in hexanes and filtered through Celite. The hexanes were evaporated under a stream of nitrogen, yielding yellow crystals. Anal. for $C_{64}H_{92}Rh_2O_8$, Calcd. (Found): C, 64.31 (63.94); H, 7.76 (7.51). ^{1}H NMR δ (ppm, in CD_2Cl_2): 6.911 (s, 8 H, aromatic), 2.847 (m, 12 H, -C*H*$(CH_3)_2$), 1.202 (d, 24 H, *p*-CH(C*H*$_3)_2$), 1.043 (d, 48 H, *o*-CH(C*H*$_3)_2$). IR (KBr): 3429, 2963, 2871, 1609, 1569, 1551, 1460, 1401, 1318, 1261, 1157, 1102, 1023, 944, 874, 808, 750, 652, 564, 509, 466 cm^{-1}.

CRYSTALLOGRAPHIC STUDIES

Single crystals of compounds **11**·C_6H_{14} - **19** were obtained as described above. Each crystal was mounted on a glass fiber with silicone grease and transferred to a goniometer. In subsequent experiments, the crystal was cooled under a stream of nitrogen at -60 °C. Data for **16**·0.5C_6H_{14} were collected on a Bruker Nonius FAST diffractometer utilizing the program MADNES.[30] Cell parameters were obtained from an autoindexing routine and refined with 250 reflections within the 2θ range of 18.1 - 41.6°. The cell dimensions and Laue symmetry were confirmed with axial photographs. A combination of 0.2° ω- and ϕ- scans were performed at four different settings to collect a nominal hemisphere of data. The data were corrected for Lorentz and polarization effects and processed using an ellipsoid-mask fitting program PROCOR.[31] Data for **11**·C_6H_{14} - **15**, **17**·0.90acetone - **19** were collected with a Bruker SMART 1000 CCD area detector system using 0.3° ω-scans at 0°, 90° and 180° in ϕ. Cell parameters were determined using the program SMART.[15] Data reduction and integration were performed with the software package SAINTPLUS.[16] while an absorption correction was applied using the program SADABS.[17] Crystal and space group symmetries for all compounds were determined using XPREP program.[18] For all compounds, the positions of some or all of the non-hydrogen atoms were found by direct methods using the solution program SHELXS.[43] The position of the remaining non-hydrogen atoms were located by use of a combination of least-squares refinement and difference Fourier maps in the SHELXL-93[19] or SHELXL-97[73] program. Non-hydrogen atoms were refined with anisotropic displacement parameters except for disordered portions found in structures of **11**·C_6H_{14} - **14**, and **15**·C_6H_{14} - **19**. The hydrogen atoms were included in the

structure factor calculations at idealized positions. Crystal data and refinement results for all compounds are listed in Tables 18-26. Selected bond distances and angles are listed in Table 27.

RESULTS AND DISCUSSION

Structural Considerations. All the structures of **11**·C_6H_{14} - **19** are of the paddlewheel type, and all but $Rh_2(TiPB)_4$ (**19**) have axial ligation either by exogenous solvent molecules or by self-association to create a dimeric structure. Thermal ellipsoid plots of all compounds are presented in Figures 18 to 26. The compounds with axial ligation at each end, where one of the axial ligands is an oxygen atom from an adjacent rhodium molecule have Rh–Rh bond distances ranging from 2.358[1] Å in $[Rh_2(TiPB)_2(O_2CCF_3)_2(TiPBH)]_2$ (**11**) to 2.3959(6) Å in $[Rh_2(TiPB)_2(O_2CCF_3)_2(C_6H_5CH_3)]_2$ (**13)**. Where both axial ligands are exogenous, the Rh–Rh bond distances range from 2.3638(5) Å in $Rh_2(TiPB)_4(H_2O)(C_6H_5CH_3)$ (**18**), to 2.4008(8) Å in $Rh_2(TiPB)_2(O_2CCF_3)_2(acetone)_2$ (**15**), significantly overlapping with the previous group.

Note that in compounds **11**, **13**, and **14**, association does occur because only two to three of the carboxylato groups are the bulky TiPB anions, while the others (which make the connection by sharing oxygen atoms) have only small R groups, viz., CH_3 or CF_3.

Table 18. Crystal Data and Structure Refinement for **11**·C_6H_{14}

Empirical formula	$C_{110}H_{154}F_{12}O_{20}Rh_4$
Formula weight	2435.97
Space group	$P\bar{1}$
Unit cell dimensions	a = 13.173(1) Å α = 101.762(2)° b = 14.302(1) Å β = 93.241(2)° c = 17.597(2) Å γ = 103.765(2)°
Volume	3133.2(5) Å³
Z	1
Density (calculated)	1.291 g/cm³
Crystal size	0.36 x 0.28 x 0.12 mm
Absorption coefficient	0.593 mm^{-1}
Data collection instrument	Bruker SMART area detector
Wavelength	0.71073 Å
Orientation reflections, number, range (θ)	5877, 2.152 - 27.53
Temperature	213(2) K
Scan method	ω scans
Theta range for data collection	1.60 to 25.00°
Reflections collected	16585
Independent reflections	10879 [R(int) = 0.0283]
Data / restraints / parameters	10879 / 15 / 682
Refinement method	Full-matrix least-squares on F^2
Final R indices [$I > 2\sigma(I)$]	$R1^a$ = 0.054, $wR2^b$ = 0.135
R indices (all data)	$R1^a$ = 0.092, $wR2^b$ = 0.148
Goodness-of-fit on F^2	1.041
Largest shift/esd, final cycle	0.034
Largest peak, final cycle	1.07(11) e/Å³

[a] $R1 = \sum||F_o| - |F_c||/\sum|F_o|$.
[b] $wR2 = [\sum[w(F_o^2-F_c^2)^2]/\sum[w(F_o^2)^2]]^{1/2}$, $w = 1/[\sigma^2(F_o^2) + (aP)^2 + bP]$, where $P = [\max(F_o^2 \text{ or } 0) + 2(F_c^2)]/3$.

Table 19. Crystal Data and Structure Refinement for **12**

Empirical formula	$C_{82}H_{117}F_3O_{12}Rh_2$
Formula weight	1557.58
Space group	$P\bar{1}$
Unit cell dimensions	a = 14.2912(12) Å α = 82.134(2)° b = 14.7538(13) Å β = 89.157(2)° c = 20.1020(17) Å γ = 88.435(2)°
Volume	4196.8(6) Å³
Z	2
Density (calculated)	1.233 g/cm³
Crystal size	0.45 x 0.40 x 0.09 mm
Absorption coefficient	0.455 mm^{-1}
Data collection instrument	Bruker SMART area detector
Wavelength	0.71073 Å
Orientation reflections, number, range (θ)	6101, 2.341 - 27.51
Temperature	213(2) K
Scan method	ω scans
Theta range for data collection	1.84 to 25.00°
Reflections collected	21803
Independent reflections	14486 [R(int) = 0.0285]
Data / restraints / parameters	14486 / 59 / 809
Refinement method	Full-matrix least-squares on F²
Final R indices [$I > 2\sigma(I)$]	$R1^a$ = 0.063, $wR2^b$ = 0.179
R indices (all data)	$R1^a$ = 0.085, $wR2^b$ = 0.190
Goodness-of-fit on F^2	1.044
Largest shift/esd, final cycle	0.038
Largest peak, final cycle	1.32(11) e/Å³

[a] $R1 = \sum||F_o| - |F_c||/\sum|F_o|$.
[b] $wR2 = [\sum[w(F_o^2-F_c^2)^2]/\sum[w(F_o^2)^2]]^{1/2}$, $w = 1/[\sigma^2(F_o^2) + (aP)^2 + bP]$, where $P = [\max(F_o^2 \text{ or } 0) + 2(F_c^2)]/3$.

Table 20. Crystal Data and Structure Refinement for **13**·$2C_6H_5CH_3$

Empirical formula	$C_{50}H_{62}F_6O_8Rh_2$
Formula weight	1110.82
Space group	$P2_1/n$
Unit cell dimensions	a = 17.6938(11) Å α = 90˚ b = 16.7759(10) Å β = 110.2860(10)˚ c = 18.4802(11) Å γ = 90˚
Volume	5145.2(5) Å³
Z	4
Density (calculated)	1.434 g/cm³
Crystal size	0.21 x 0.17 x 0.06 mm
Absorption coefficient	0.712 mm^{-1}
Data collection instrument	Bruker SMART area detector
Wavelength	0.71073 Å
Orientation reflections, number, range (θ)	6795, 2.314 - 27.092
Temperature	213(2) K
Scan method	ω scans
Theta range for data collection	1.73 to 25.00˚
Reflections collected	26596
Independent reflections	9049 [R(int) = 0.0428]
Data / restraints / parameters	9049 / 147 / 586
Refinement method	Full-matrix least-squares on F^2
Final R indices [$I > 2\sigma(I)$]	$R1^a$ = 0.053, $wR2^b$ = 0.126
R indices (all data)	$R1^a$ = 0.081, $wR2^b$ = 0.144
Goodness-of-fit on F^2	1.017
Largest shift/esd, final cycle	0.032
Largest peak, final cycle	1.88(11) e/Å

[a] $R1 = \sum||F_o| - |F_c||/\sum|F_o|$.
[b] $wR2 = [\sum[w(F_o^2-F_c^2)^2]/\sum[w(F_o^2)^2]]^{½}$, $w = 1/[\sigma^2(F_o^2) + (aP)^2 + bP]$, where $P = [\max(F_o^2 \text{ or } 0) + 2(F_c^2)]/3$.

Table 21. Crystal Data and Structure Refinement for **14**

Empirical formula	$C_{78}H_{104}F_{12}O_{18}Rh_4$
Formula weight	1969.26
Space group	$P\bar{1}$
Unit cell dimensions	a = 12.1209(6) Å α = 74.0320(10)° b = 17.2005(9) Å β = 79.0030(10)° c = 25.0450(13) Å γ = 89.5640(10)°
Volume	4922.3(4) Å³
Z	2
Density (calculated)	1.329 g/cm³
Crystal size	0.26 x 0.18 x 0.12 mm
Absorption coefficient	0.736 mm
Data collection instrument	Bruker SMART area detector
Wavelength	0.71073 Å
Orientation reflections, number, range (θ)	9249, 2.239 - 27.376
Temperature	213(2) K
Scan method	ω scans
Theta range for data collection	1.69 - 25.00
Reflections collected	29160
Independent reflections	17136 [R(int) = 0.0644]
Data / restraints / parameters	16177 / 189 / 997
Final R indices [$I > 2\sigma(I)$]	$R1^a$ = 0.0572, $wR2^b$ = 0.1688
R indices (all data)	$R1^a$ = 0.0990, $wR2^b$ = 0.2103
Goodness-of-fit on F^2	1.081
Largest shift/esd, final cycle	-0.024
Largest peak, final cycle	1.63(11) e/Å

[a] $R1 = \sum||F_o| - |F_c||/\sum|F_o|$.
[b] $wR2 = [\sum[w(F_o^2-F_c^2)^2]/\sum[w(F_o^2)^2]]^{1/2}$, $w = 1/[\sigma^2(F_o^2) + (aP)^2 + bP]$, where $P = [\max(F_o^2 \text{ or } 0) + 2(F_c^2)]/3$.

Table 22. Crystal Data and Structure Refinement for **15**

Empirical formula	$C_{42}H_{58}F_6O_{10}Rh_2$
Formula weight	1042.70
Space group	$I4_1/a$
Unit cell dimensions	a = 17.9478(11) Å α = 90˚ b = 17.9478(11) Å β = 90˚ c = 30.418(3) Å γ = 90˚
Volume	9798.4(12) Å³
Z	8
Density (calculated)	1.414 g/cm³
Crystal size	0.27 x 0.19 x 0.16 mm
Absorption coefficient	0.746 mm^{-1}
Data collection instrument	Bruker SMART area detector
Wavelength	0.71073 Å
Orientation reflections, number, range (θ)	6813, 2.307 - 26.797
Temperature	213(2) K
Scan method	ω scans
Theta range for data collection	2.09 to 25.00˚
Reflections collected	28534
Independent reflections	4328 [R(int) = 0.0851]
Data / restraints / parameters	3403 / 0 / 271
Refinement method	Full-matrix least-squares on F^2
Final R indices [$I > 2\sigma(I)$]	$R1^a$ = 0.045, $wR2^b$ = 0.104
R indices (all data)	$R1^a$ = 0.096, $wR2^b$ = 0.160
Goodness-of-fit on F^2	1.094
Largest shift/esd, final cycle	-0.001
Largest peak, final cycle	0.79(10) e/Å³

[a] $R1 = \sum||F_o| - |F_c||/\sum|F_o|$.
[b] $wR2 = [\sum[w(F_o^2-F_c^2)^2]/\sum[w(F_o^2)^2]]^{½}$, $w = 1/[\sigma^2(F_o^2) + (aP)^2 + bP]$, where $P = [\max(F_o^2 \text{ or } 0) + 2(F_c^2)]/3$.

Table 23. Crystal Data and Structure Refinement for **16**

Empirical formula	$C_{99}H_{146}O_{12}Rh_2$
Formula weight	1733.98
Space group	$P\bar{1}$
Unit cell dimensions	a = 14.7166(2) Å α = 66.4250(10)° b = 26.3248(15) Å β = 85.971(5)° c = 28.853(5) Å γ = 79.239(5)°
Volume	10064.7(18) Å³
Z	4
Density (calculated)	1.144 g/cm³
Absorption coefficient	0.382 mm^{-1}
Data collection instrument	Nonius FAST area detector
Wavelength	0.71073 Å
Orientation reflections, number, range (θ)	250, 9.1 - 20.9
Temperature	213(2) K
Scan method	ω scans
Theta range for data collection	1.91 to 25.00°
Reflections collected	60260
Independent reflections	31259 [R(int) = 0.0786]
Data / restraints / parameters	31259 / 16 / 1707
Refinement method	Full-matrix least-squares on F²
Final R indices [$I > 2\sigma(I)$]	$R1^a$ = 0.075, $wR2^b$ = 0.167
R indices (all data)	$R1^a$ = 0.108, $wR2^b$ = 0.189
Goodness-of-fit on F^2	1.033
Largest shift/esd, final cycle	0.007
Largest peak, final cycle	1.06(10) e/Å³

[a] $R1 = \sum||F_o| - |F_c||/\sum|F_o|$.
[b] $wR2 = [\sum[w(F_o^2-F_c^2)^2]/\sum[w(F_o^2)^2]]^{1/2}$, $w = 1/[\sigma^2(F_o^2) + (aP)^2 + bP]$, where $P = [\max(F_o^2 \text{ or } 0) + 2(F_c^2)]/3$.

Table 24. Crystal Data and Structure Refinement for **17**·0.90acetone

Empirical formula	$C_{72.67}H_{109.44}O_{10.90}Rh_2$
Formula weight	1363.32
Space group	$P\bar{1}$
Unit cell dimensions	a = 14.7760(12) Å α = 65.4570(10)° b = 16.4290(14) Å β = 78.709(2)° c = 17.4638(15) Å γ = 87.445(2)°
Volume	3778.5(6) Å³
Z	2
Density (calculated)	1.198 g/cm³
Crystal size	0.48 x 0.27 x 0.08 mm
Absorption coefficient	0.489 mm^{-1}
Data collection instrument	Bruker SMART area detector
Wavelength	0.71073 Å
Orientation reflections, number, range (θ)	5061, 2.395 - 27.4725
Temperature	213(2) K
Scan method	ω scans
Theta range for data collection	1.87 to 25.00°
Reflections collected	20051
Independent reflections	13143 [R(int) = 0.0183]
Data / restraints / parameters	13143 / 120 / 577
Refinement method	Full-matrix least-squares on F^2
Final R indices [$I > 2\sigma(I)$]	$R1^a$ = 0.052, $wR2^b$ = 0.134
R indices (all data)	$R1^a$ = 0.068, $wR2^b$ = 0.147
Goodness-of-fit on F^2	1.042
Largest shift/esd, final cycle	0.042
Largest peak, final cycle	0.92(9) e/Å³

[a] $R1 = \sum||F_o| - |F_c||/\sum|F_o|$.
[b] $wR2 = [\sum[w(F_o^2-F_c^2)^2]/\sum[w(F_o^2)^2]]^{1/2}$, $w = 1/[\sigma^2(F_o^2) + (aP)^2 + bP]$, where $P = [\max(F_o^2 \text{ or } 0) + 2(F_c^2)]/3$.

Table 25. Crystal Data and Structure Refinement for **18**

Empirical formula	$C_{71}H_{100}O_9Rh_2$
Formula weight	1303.33
Space group	$P2_1/n$
Unit cell dimensions	a = 10.9216(7) Å α = 90° b = 30.849(2) Å β = 91.9570(10)° c = 20.4951(13) Å γ = 90°
Volume	6901.3(8) Å³
Z	4
Density (calculated)	1.254 g/cm³
Crystal size	0.21 x 0.16 x 0.06 mm
Absorption coefficient	0.530 mm^{-1}
Data collection instrument	Bruker SMART area detector
Wavelength	0.71073 Å
Orientation reflections, number, range (θ)	9132, 2.1865 - 27.453
Temperature	213(2) K
Scan method	ω scans
Theta range for data collection	1.65 to 27.56°
Reflections collected	48701
Independent reflections	15788 [R(int) = 0.0633]
Data / restraints / parameters	15784 / 51 / 725
Refinement method	Full-matrix least-squares on F^2
Final R indices [$I > 2\sigma(I)$]	$R1^a$ = 0.057, $wR2^b$ = 0.110
R indices (all data)	$R1^a$ = 0.114, $wR2^b$ = 0.135
Goodness-of-fit on F^2	1.014
Largest shift/esd, final cycle	0.003
Largest peak, final cycle	1.10(10) e/Å³

[a] $R1 = \sum||F_o| - |F_c||/\sum|F_o|$.
[b] $wR2 = [\sum[w(F_o^2-F_c^2)^2]/\sum[w(F_o^2)^2]]^{1/2}$, $w = 1/[\sigma^2(F_o^2) + (aP)^2 + bP]$, where $P = [\max(F_o^2 \text{ or } 0) + 2(F_c^2)]/3$.

Table 26. Crystal Data and Structure Refinement for **19**

Empirical formula	$C_{64}H_{92}O_8Rh_2$
Formula weight	1195.20
Space group	$P2_1/n$
Unit cell dimensions	a = 13.6919(8) Å α = 90˚ b = 30.8320(19) Å β = 97.3500(10)˚ c = 15.1279(9) Å γ = 90˚
Volume	6333.7(7) Å³
Z	4
Density (calculated)	1.253 g/cm³
Crystal size	0.350 x 0.145 x 0.047 mm
Absorption coefficient	0.570 mm^{-1}
Data collection instrument	Bruker SMART area detector
Wavelength	0.71073 Å
Orientation reflections, number, range (θ)	5412, 2.247 - 27.46
Temperature	213(2) K
Scan method	ω scans
Theta range for data collection	1.64 to 27.50˚
Reflections collected	39947
Independent reflections	14415 [R(int) = 0.0391]
Data / restraints / parameters	14415 / 42 / 612
Refinement method	Full-matrix least-squares on F^2
Final R indices [$I > 2\sigma(I)$]	$R1^a$ = 0.050, $wR2^b$ = 0.103
R indices (all data)	$R1^a$ = 0.079, $wR2^b$ = 0.116
Goodness-of-fit on F^2	1.062
Largest shift/esd, final cycle	0.001
Largest peak, final cycle	1.07(9) e/Å³

[a] $R1 = \sum||F_o| - |F_c||/\sum|F_o|$.
[b] $wR2 = [\sum[w(F_o^2-F_c^2)^2]/\sum[w(F_o^2)^2]]^{½}$, $w = 1/[\sigma^2(F_o^2) + (aP)^2 + bP]$, where $P = [\max(F_o^2 \text{ or } 0) + 2(F_c^2)]/3$.

Table 27. Rh–Rh Bond Lengths [Å]

	Rh–Rh (Å)	**Rh–O_{eq} (Å), *avg.***	**Rh–L_{ax} (Å)**[a]
11·C_6H_{14}	2.3893(6)	2.035[4]	2.300[4]
12	2.3669(7)	2.038[5]	2.242[4]
13·2$C_6H_5CH_3$	2.3959(6)	2.037[4]	2.300(3)[b]
14	2.3916[8]	2.036[5]	2.297[6]
15	2.4008(8)	2.037[4]	2.268(4)
16·0.5C_6H_{14}	2.3674[7]	2.036[4]	2.285[4]
17·0.90acetone	2.3700(5)	2.037[3]	2.31[1]
18	2.3638(5)	2.041[3]	2.271(4)[c]
19	2.3499(4)	2.032[2]	---

[a] Square brackets refer to average values; parentheses refer to unique values.
[b] The value refers to intermolecular axial coordination. There is also a toluene molecule oriented in a η^2 fashion towards the free axial position of each subunit, which are related by an inversion center, at an average distance of 2.70 Å.
[c] The value refers to the axial water molecule. There is also a toluene molecule oriented in a η^2 fashion towards the other axial position at an average distance of 2.80 Å.

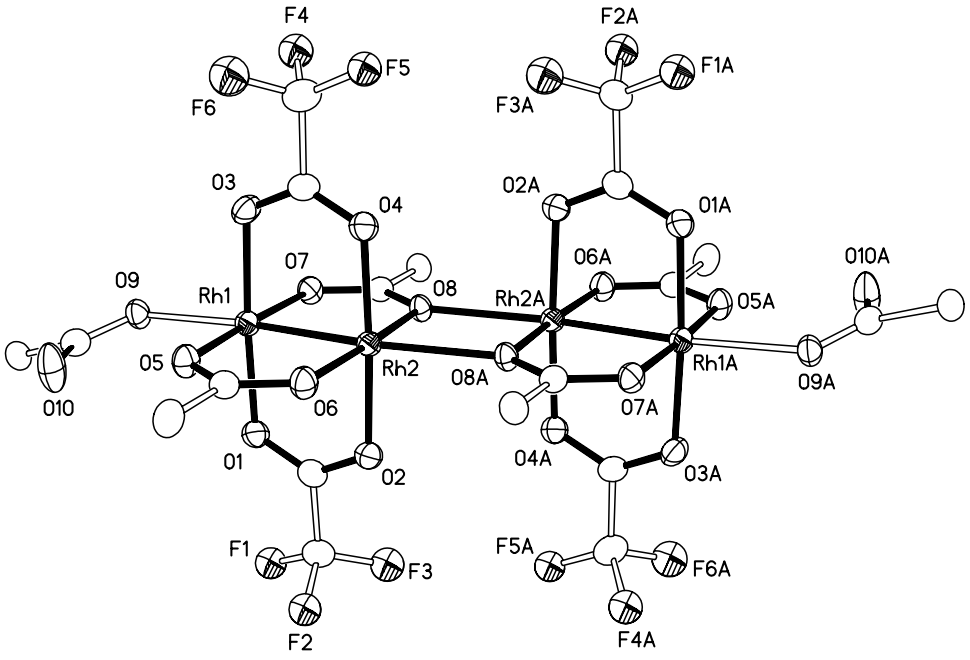

Figure 18. Thermal ellipsoid plot of $[Rh_2(O_2CCF_3)_2(TiPB)_2(TiPBH)]_2$ in **11**·C_6H_{14}. Thermal ellipsoids are shown at the 30% probability level; hydrogen atoms, isopropylphenyl rings and interstitial solvent molecules have been omitted for clarity. Only one orientation of the -CF_3 groups is shown.

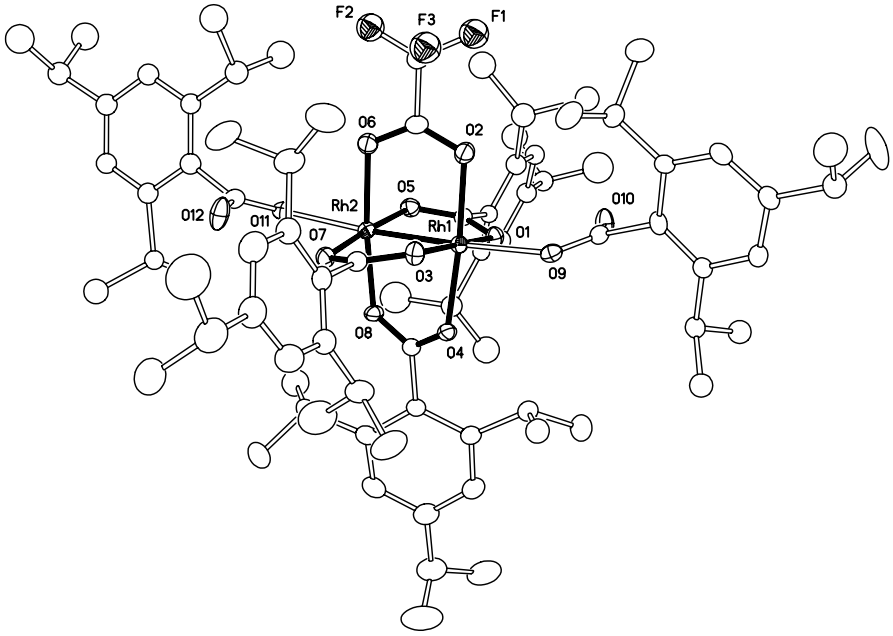

Figure 19. Thermal ellipsoid plot of $Rh_2(O_2CCF_3)(TiPB)_3(TiPBH)_2$, **12**. Thermal ellipsoids are shown at the 30% probability level; hydrogen atoms have been omitted for clarity. Only one orientation of disordered -CF_3 groups and phenyl rings is shown.

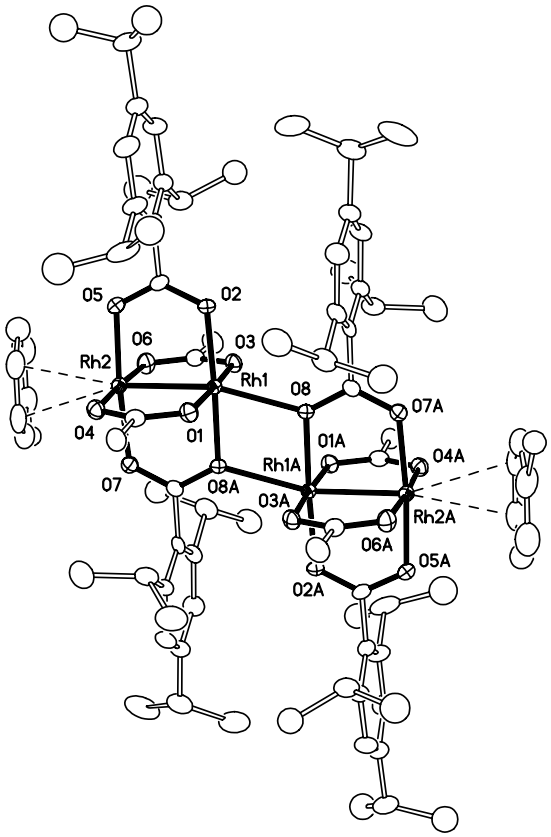

Figure 20. Thermal ellipsoid plot of $[Rh_2(O_2CCF_3)_2(TiPB)_2(toluene)]_2$ in **13**·$2C_6H_5CH_3$. Thermal ellipsoids are shown at the 30% probability level; hydrogen and fluorine atoms have been omitted for clarity.

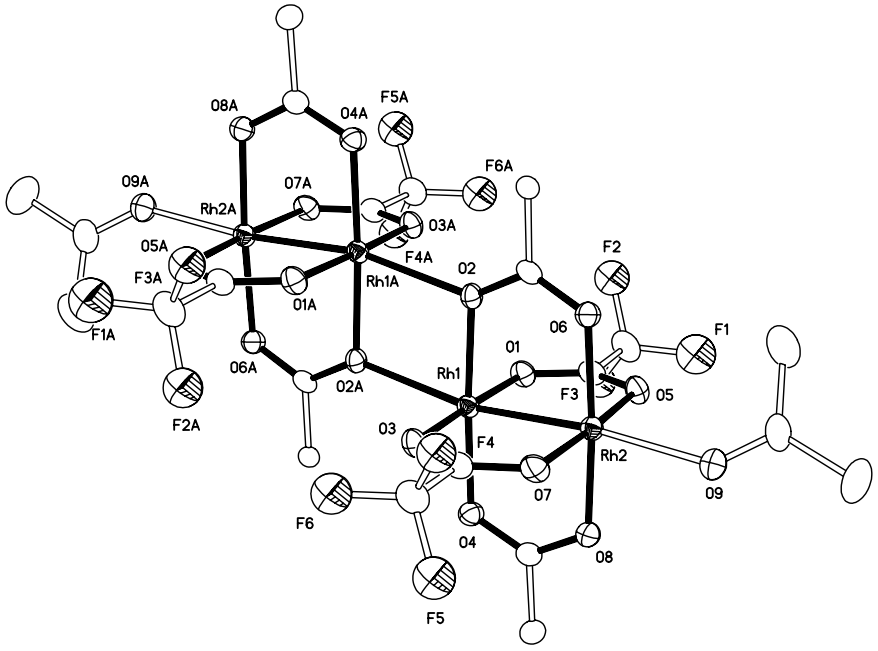

Figure 21. Thermal ellipsoid plot of $[Rh_2(O_2CCF_3)_2(TiPB)_2(acetone)]_2$, **14**. Thermal ellipsoids are shown at the 30% probability level; hydrogen atoms and isopropylphenyl groups have been omitted for clarity. Only one of the two independent molecules in the asymmetric unit is shown.

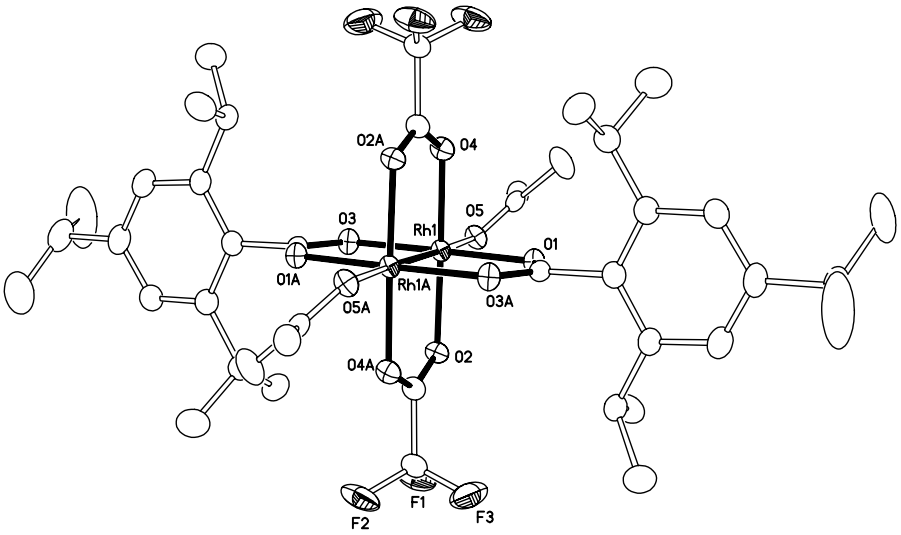

Figure 22. Thermal ellipsoid plot of $Rh_2(O_2CCF_3)_2(TiPB)_2(acetone)_2$, **15**. Thermal ellipsoids are shown at the 30% probability level; hydrogen atoms have been omitted for clarity.

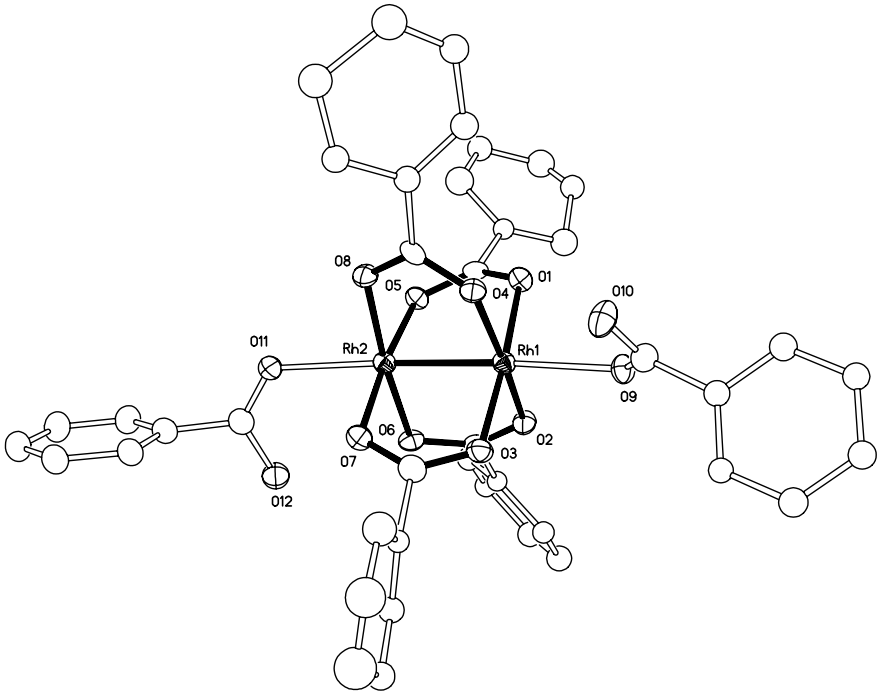

Figure 23. Thermal ellipsoid plot of $Rh_2(TiPB)_4(TiPBH)_2$, **16**. Thermal ellipsoids are shown at the 30% level; hydrogen atoms and isopropyl groups have been omitted for clarity. Only one orientation of the disordered rings is shown, and only one of the two independent molecules in the asymmetric unit is shown.

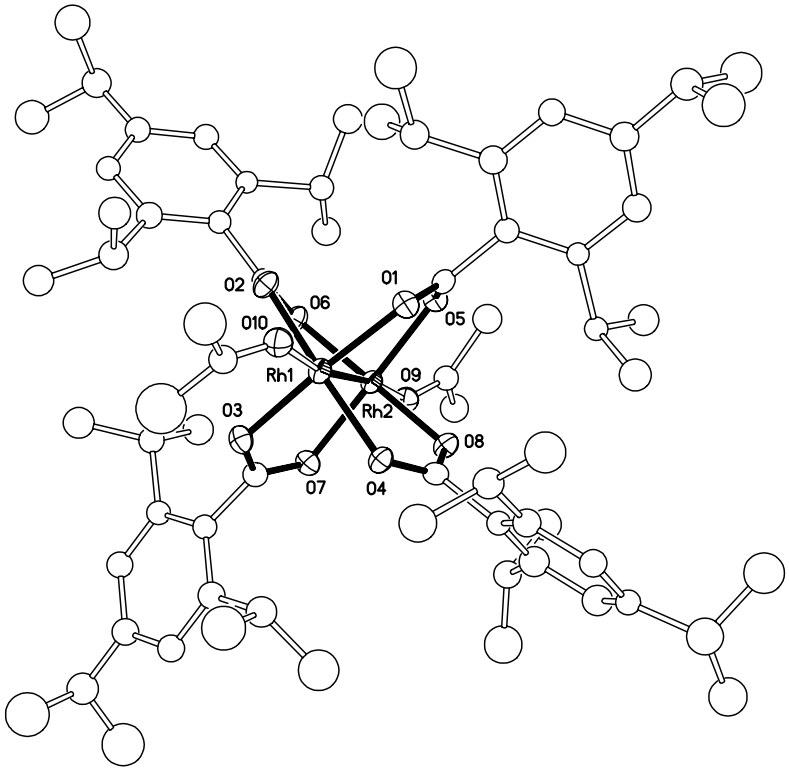

Figure 24. Thermal ellipsoid plot of $Rh_2(TiPB)_4(acetone)_2$ in **17**·0.90acetone. Thermal ellipsoids are shown at the 30% probability level; hydrogen atoms and interstitial solvent molecules have been omitted for clarity.

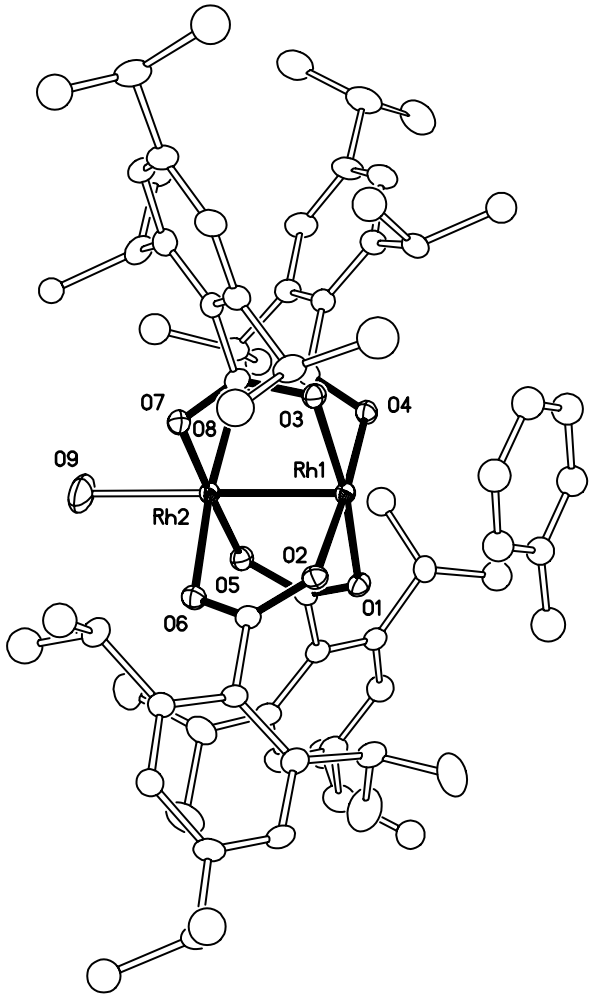

Figure 25. Thermal ellipsoid plot for $Rh_2(TiPB)_4(toluene)(H_2O)$, **18**. Thermal ellipsoids are shown at the 30% probability level; hydrogen atoms have been omitted for clarity.

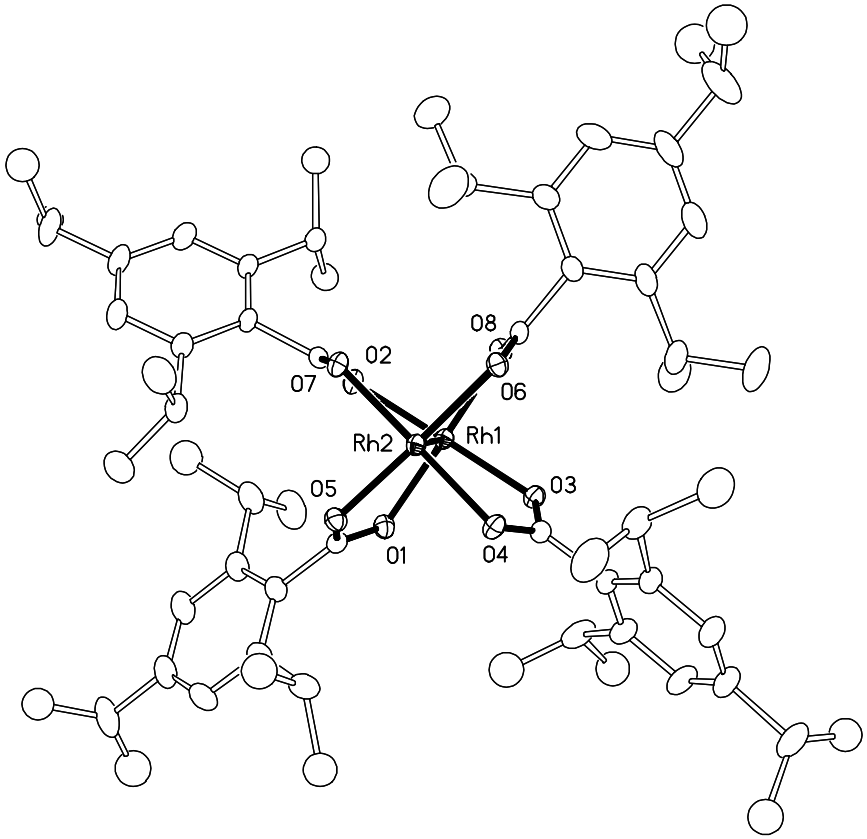

Figure 26. Thermal ellipsoid plot of $Rh_2(TiPB)_4$, **19**. Thermal ellipsoids are shown at the 30% probability level; hydrogen atoms have been omitted for clarity.

Synthetic Considerations. The most common preparation of rhodium(II) carboxylates begins with the synthesis of rhodium(II) acetate by combination of $RhCl_3 \cdot 3H_2O$ with a mixture of sodium acetate and acetic acid in refluxing ethanol. Although prolonged refluxing causes deposition of Rh metal, yields of the acetate have reached as high as 85%. Carboxylate exchange reactions with the acetate have then been used to yield a variety of $Rh_2(O_2CR)_4L_2$ molecules; typically a great excess of the acid of the target carboxylate is used as the solvent.[74] Our strategy deviated only in that we employed a variety of high-boiling solvents instead of a neat reaction, due to the high melting point of our ligand precursor, TiPBH (*ca* 185 °C). Most of our syntheses, followed this basic outline: 1) reflux the rhodium(II) precursor with TiPBH in a high boiling solvent, while distilling out the acid byproduct, 2) distill the remaining solvent, 3) sublime excess TiPBH, 4) extract solid, 5) crystallize material by evaporation or cooling.

We used two different Rh_2 precursors in our investigations: anhydrous $Rh_2(O_2CCF_3)_4$ and $Rh_2(O_2CCF_3)_4(CH_3CN)_2$, and applied a variety of reaction conditions. Given the variety of partially substituted paddlewheel structures that we have characterized, it becomes clear that 1) carboxylate exchange reactions are not straightforward for so bulky a substituent as TiPB, and 2) the starting materials with acetonitrile in the axial position outperformed the anhydrous $Rh_2(O_2CCF_3)_4$, by yielding more highly TiPB-substituted products under relatively milder conditions, and 3) a mixture of products reflecting various degrees of substitution was often observed.

The difficulty in preparing the fully TiPB-substituted product compared to other $Rh_2(O_2CR)_4$ compounds, where R is an alkyl or aryl group should not be terribly surprising. Studies indicate that substitution reactions of paddlewheel structures occur by initial coordination in the axial position by the incoming group, followed by dissociative ring opening of the leaving group, freeing an equatorial site for coordination by the incoming group.[75] When

the incoming group is very bulky, it is easy to imagine that steric crowding in the equatorial region would adversely affect the rate of the substitution. The resistance to substitution seemed to increase as the reaction progressed, thus accounting for the frequent isolation of only partially substituted compounds, in agreement with what has been previously noted for dirhodium carboxylates, namely, that acetate substitution is retarded with the increase in size of the incoming carboxylate group.[76] Another possible reason for the difficulty of substitution may be found in our choice of solvents; we chose to use nonpolar solvents with the idea that they would not act as axial ligands. However, the acetato anion intermediate appears to be less stabilized in nonpolar solvents than it would be in the more often used neat carboxylic acids.

The observed difference in lability between the starting materials, $Rh_2(O_2CR)_4$ and $Rh_2(O_2CR)_4L_2$ is probably also a matter of kinetics. The anhydrous $Rh_2(O_2CCF_3)_4$ is not a discrete molecule, but a one-dimensional polymer of the type depicted in Figure 2. Thus, the axial positions are well shielded by very bulky "ligands", which hinder the first step of the substitution process. The polymer is also insoluble in solvents which cannot act as axial ligands, and only becomes soluble at high temperature, presumably because the TiPBH (or in one case LiTiPB) molecules begin to slowly degrade the polymer by axial coordination. Thus, even when vigorous reaction conditions were employed, full substitution by TiPB was not attained (presumably due to oligomerization of the starting material) and this strategy was quickly abandoned. The rhodium precursors with acetonitrile in the axial position, however, are discrete molecules of the type depicted in Figure 1. Because acetonitrile is small and linear, the axial positions are not entirely blocked by these molecules, thus allowing a closer approach by the incoming acid.

Substitution of the acetato or trifluoroacetato groups by TiPB is only a first step. Even when substitution is complete, the axial positions are not shielded in any way. For example, in

the absence of any other potential axial ligand, the carboxylic acid itself (which is necessarily in excess) coordinates to the axial position to give **16**. The axial TiPBH was easily removed however, by dissolving the solid in a coordinating solvent such as acetone to give **17**. Thermogravimetric analysis shows the stepwise removal of the two coordinated acetone molecules at 130 and 230 °C, and when $Rh_2(TiPB)_4(acetone)_2$ was placed under vacuum at 130 °C a color change from blue-green to green to yellow-green was observed, presumably corresponding to the bis-, mono-, and non-axially ligated compounds, respectively. The amorphous $Rh_2(TiPB)_4$, **19**, was then recrystallized from hexanes, in which it is sparingly soluble; $Rh_2(TiPB)_4(TiPBH)_2$ is much more soluble in hexanes.

It has been found that when bulky incoming ligands are used in dirhodium carboxylate exchange reactions, mixtures of partially- and fully-substituted products are obtained even under vigorous conditions.[76] We have found that, in some cases, two distinctly different types of crystals were grown simultaneously out of the same reaction flask, (see preparation of **12**). Thus, the separation of similar molecules becomes a problem, and a cleaner reaction pathway was eventually pursued in the direct reaction of the sodium salt of TiPB with $RhCl_3{\cdot}3H_2O$ in boiling ethanol. Although the yield of **19** by this method was very low (15%) due to the copious deposition of rhodium metal, *only* the fully substituted product was obtained. The crystals grown from an acetone solution had the same unit cell and crystal structure as $Rh_2(TiPB)_4(acetone)_2{\cdot}0.90$acetone synthesized by the carboxylate exchange reaction.

Spectroscopy. A conspicuous feature of $Rh_2(O_2CR)_4L_2$ chemistry is that the various adducts exhibit a wide variety of colors depending on the nature of the axial ligand. It was noted as early as 1963 that the low energy band (around 600-700 nm) in the visible spectrum increases in energy with increasing donor strength of the axial ligand.[77] This property, and the presence of a Rh–Rh bond, has led to extensive study of the electronic structure of $Rh_2(O_2CR)_4L_2$

compounds, both by experimental and theoretical methods.[78] The earliest quantitative calculations, by Norman and Kolari, produced a $\sigma^2\pi^4\delta^2\pi^{*4}\delta^{*2}$ configuration for $Rh_2(O_2CH)_4$ and a $\pi^4\sigma^2\delta^2\pi^{*4}\delta^{*2}$ for $Rh_2(O_2CH)_4(H_2O)_2$, with a σ^* LUMO and a single bond in each case. The ordering of the bonding orbitals in the two compounds was attributed to the interaction of the symmetric and antisymmetric combinations of the two σ lone pair orbitals of the H_2O molecules with the Rh–Rh σ and σ^* orbitals, respectively, which destabilizes these orbitals relative to those of the anhydrous compound. This destabilization of the σ-bonding orbital corresponds to a slight weakening of the Rh–Rh bond, while the destabilization of the σ^* orbital results in a larger HOMO-LUMO gap, thus accounting for the spectrochemical behavior of the low energy peak in the visible spectrum. However, because *all* of the isolated $Rh_2(O_2CR)_4$ compounds have had axial ligands, there has been no experimental confirmation of the structural nor electronic theoretical predictions, although some spectroscopic data previously reported by Drago are entirely consistent with what we now believe.[79]

The electronic spectra of $Rh_2(O_2CR)_4L_2$ compounds exhibit two principal bands in the visible region; band A (around 17 000 cm^{-1}) has been assigned to the $\pi^*(Rh_2) \rightarrow \sigma^*(Rh_2)$ transition,[80] while the assignment of band B is still debatable, although it has been attributed to a $\pi(Rh-O) \rightarrow \sigma^*(Rh-O)$ transition. Band A is quite sensitive to the nature of the axial ligand, and this is what accounts for the variety of colors observed in $Rh_2(O_2CR)_4L_2$ compounds. The band maximum increases in energy with increasing donor strength, as the $\sigma^*(Rh_2)$ orbital is destabilized. The electronic spectra of $Rh_2(TiPB)_4$, $Rh_2(TiPB)_4(H_2O)_2$, and $Rh_2(TiPB)_4(acetone)_2$ are presented in Figure 27. The extremely low energy (760 nm) of band A for non-axially ligated $Rh_2(TiPB)_4$ is consistent with this interpretation of the electronic structure, first proposed by Dubicki and Martin and quantitatively described by Norman and Kolari.

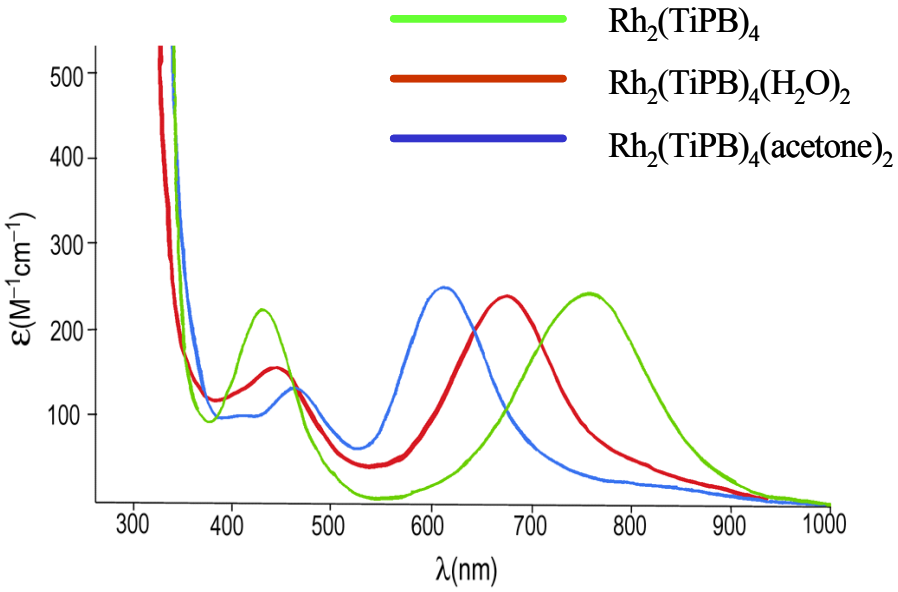

Figure 27. Electronic spectra of $Rh_2(TiPB)_4$ and its adducts in hexanes. For **19** λ(ϵ), nm($M^{-1}cm^{-1}$): 760(251). 430(225); for **19**·$2H_2O$: 670(250), 445(164); for **19**·2acetone: 610(255), 460(123).

Concluding Remarks. The variety of $Rh_2(O_2CR)_4$ compounds produced by carboxylate exchange reactions offers the opportunity to make several important observations. 1) The Rh–Rh distance is not very sensitive to the nature (or even the absence) of the axial ligand. 2) Carboxylate exchange reactions require more vigorous conditions as the acid becomes bulkier. 3) Dirhodium tetracarboxylate precursors with small molecules in the axial position are more reactive than anhydrous, polymeric forms. 4) The ligand TiPB does little to block the axial position, but the presence of four of them prevents intermolecular self-association of the dirhodium units. 5) The presence of only two TiPB ligands *trans* to each other does not prevent association. 6) The difficulty in substitution by a bulky ligand often does not allow the reaction to proceed cleanly, and direct reaction between $RhCl_3(H_2O)_3$ and NaTiPB may be a superior preparative method. 7) It appears that both bulkiness and solubilizing groups in the carboxylate ligands are necessary to the preparation of non-axially ligated $Rh_2(O_2CR)_4$ compounds that could be crystallized from non-coordinating solvents. 8) Results from electronic spectroscopy are consistent with the prevailing interpretation of the electronic structure of $Rh_2(O_2CR)_4L_2$ compounds, and an extremely low energy transition is observed when there are no axial interactions whatsoever.

CHAPTER VI

DIVANADIUM CHEMISTRY[5]

Although it was in 1964[1] that the quadruply-bonded Re_2^{6+} unit (in $Re_2Cl_8^{2-}$) was recognized and in 1965 that the existence of Tc_2^{5+} (in $Tc_2Cl_8^{3-}$) and Mo_2^{4+} (in $Mo_2(O_2CCH_3)_4$) were established,[81,36] it was not until 1992 that the first compound of the triply-bonded V_2^{4+} core ($V_2(DTolF)_4$) was reported.[82] In the meantime thousands of compounds containing metal-metal bonds have been synthesized and characterized, and have found applications in catalysis, medicine, and supramolecular chemistry. Nonetheless, in the 10 years since the report of $V_2(DTolF)_4$, the chemistry of the V_2^{4+} core has continued to be virtually ignored. Only two other compounds of V_2^{4+} have been described, $V_2(DCyF)_4$[83] and $V_2(hpp)_4$[84], where hpp is the anion of 1,3,4,6,7,8-hexahydro-2*H*-pyrimido[1,2*a*]pyrimidine. Both of these compounds are similar to the first one, and very little has been learned about the properties of these compounds (e.g., spectra, electrochemistry) and thus the general impression has arisen that the chemistry of multiply-bonded divanadium compounds would be quite limited. We present here a report of work which shows that this impression is incorrect. We have found that many other V_2^{4+} containing compounds can be made, and include in this report the characterization of $V_2(DPhF)_4$, **20**, $V_2(DAniF)_4$, **21**, $V_2(D^{Cl}PhF)_4$, **22**, $V_2(TPG)_4$, **23**, and $V_2(ap)_4$, **24**, the ligands of which are depicted in Figure 28.

---

[5]Reprinted in part with permission from Cotton, F. A.; Hillard, E. A.; Murillo, C. A. "A Highly Reduced V_2^{3+} Unit with a Metal-Metal Bond Order of 3.5" *J. Am. Chem. Soc.* **2003**, *in press.* Copyright 2000, American Chemical Society.

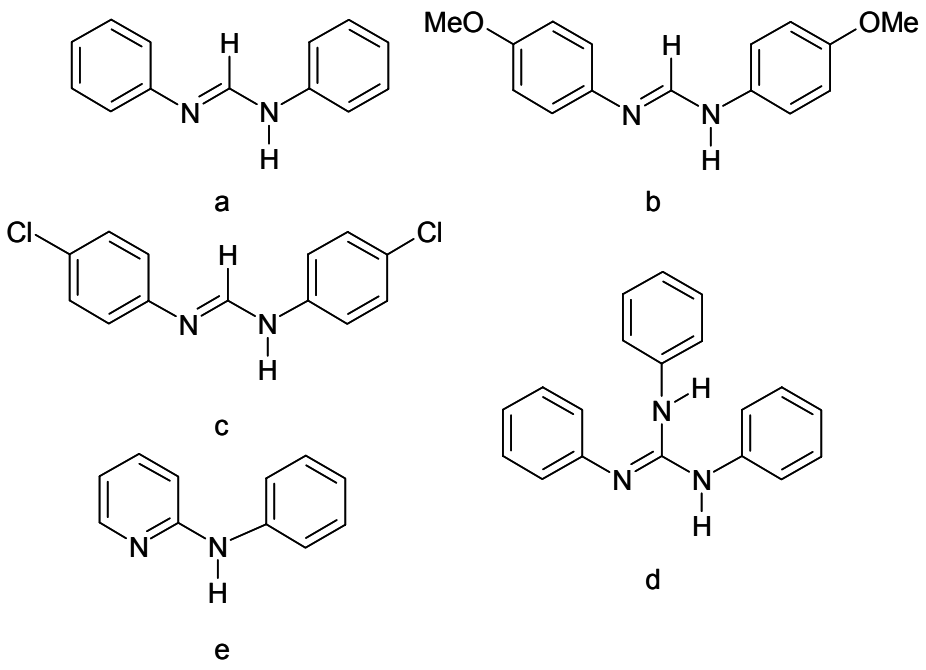

Figure 28. Ligands used to make divanadium compounds. (a) *N*, *N*'-diphenylformamidine, DPhF, (b) *N*, *N*'-di-*p*-anisylformamidine, DAniF, (c) *N*, *N*'-di-*p*-chloroformamidine, $D^{Cl}PhF$, (d) triphenylguanidine, TPG, (e) anilinopyridine, ap.

We have investigated the electrochemistry of these molecules and have been rewarded with the discovery of the first stable paddlewheel-type complex with an M_2^{3+} core in $[K(THF)_3]V_2(DPhF)_4$, **25**. Oxidation states for isolated M_2^{n+} units had been previously restricted to only three values, namely n = 4, 5, and 6, although the oxidation number 7 was recently discovered for M = Os[85] and Re[86] in complexes of the type $[M_2(hpp)_4Cl_2]PF_6$. Although higher oxidation numbers are not uncommon in transition metal chemistry, it has been thought that these would not favor metal-metal bond formation due to the known contraction experienced by the *d* orbitals as the positive charge increases. On the other hand, oxidation numbers of less than 2 are uncommon for transition metals in general, except in the case of the coinage metals or when non-innocent ligands, i.e., those with π-acceptors, are present.[67] We believe that, in this case, the stability of the V_2^{3+} core can be attributed to the V–V bond order of 3.5.

EXPERIMENTAL

General Considerations. All syntheses and sample manipulation were carried out under an atmosphere of dry and deoxygenated argon with standard Schlenk and drybox techniques. Solvents were distilled under nitrogen from Na/K-benzophenone. $VCl_3 \cdot 3THF$ was prepared according to the literature method[87] and stored at -10 °C prior to use, to prevent loss of THF. Di-*p*-anisylformamdine and Di-*p*-chlorophenylformamidine were prepared by a reported method.[88] Methyllithium (1.6 M in diethyl ether) was purchased from Acros Organics. Sodium triethylborohydride (1 M in THF), diphenylformamidine, triethylorthoformate, *p*-anisidine, *p*-chloroaniline, and 2-anilinopyridine were purchased from Aldrich Chemical Co. 1,2,3-triphenylguanidine was purchased from TCI America. Potassium graphite was prepared by

combining an equimolar amount of C_8 and K, and stirring under nitrogen at 130 °C until the solid turned bronze in color.

Physical Measurements. Elemental analyses were performed by Canadian Microanalytical Service, Ltd., Delta, British Columbia. ^{1}H NMR spectra were recorded on a Mercury 300 NMR spectrometer. The cyclic voltammograms were recorded on a BAS 100 electrochemical analyzer in 0.1 M $Bu^n_4NPF_6$ solutions with Pt working and auxiliary electrodes and a Ag/AgCl reference electrode; scan rates were 100 mV s^{-1} in all cases. The EPR spectra were recorded on a Bruker ESP300 9.458 GHz spectrometer. UV/vis spectra were recorded on a Shimadzu 2501-PC spectrophotometer.

Preparation of $V_2(NXN)_4$ Compounds 20-24. Compounds **20-24** were prepared by the method of Cotton and coworkers.[81] In a typical reaction, 0.40 g (1.07 mmol) of $VCl_3 \cdot 3THF$ was dissolved in 10 mL THF and reduced by the dropwise addition of one equivalent $NaEt_3BH$ at -78 °C. In a separate flask, two equivalents of the desired ligand were deprotonated with MeLi at -78 °C. Each solution was allowed to reach room temperature, by which time the respective reactions were essentially complete, and were then cooled again to -78 °C and combined by using a cannula. After stirring ½ to 1 h at room temperature, the THF was removed by vacuum evaporation and the residue was extracted with approximately 30 mL of toluene (benzene in the case of **23**) and filtered over Celite. X-ray quality crystals were grown by the slow diffusion of hexanes into the toluene or benzene solution.

NMR Spectroscopy. ^{1}H NMR: For **20**, (benzene-d_6, ppm): 5.953 (d, 16 H), 6.736 (m, 24 H), 10.007 (s, 4H); for **21**, ($CDCl_3$, ppm): 3.607 (s, 24 H), 5.803 (d, 16 H), 6.341 (d, 16 H), 10.017 (s, 4 H, methyne); for **22**, (benzene-d_6, ppm): 5.527 (d, 16 H), 6.667 (d, 16 H), 9.680 (s, 4 H).

Elemental Analyses. For **20**, anal. for $C_{52}H_{44}V_2N_8$, Calcd. (Found): C, 70.74 (70.92); H, 5.02 (5.18); N, 12.69 (12.64). For **21**, anal. for $C_{60}H_{60}V_2N_8O_8$, C, 64.17(63.84); H, 5.39 (5.76); N, 9.98 (8.99).

Electronic Spectroscopy. All spectra were obtained from THF solutions. For **20**: 464 (90, sh), 398 (1730); for **21**: 488 (300), 414 (539); for **23**: 588 (730); for **24**: 533 (950), 410.5 (2520).

Preparation of Compound 25. In a typical reaction, a solution of 60 mg (0.068 mmol) of $V_2(DPhF)_4$ in 15 mL THF was added via cannula into a suspension of 25 mg (0.185 mmol) KC_8 in 10 mL THF at -78 °C. The mixture was allowed to stir at -78 °C for 1 h, after which time the solution had turned from red to green. The solution was filtered over Celite and hexanes (10 mL) was added. The mixture was placed in the freezer at -10 °C. Black block-like crystals of **25** were obtained after 3 days.

CRYSTALLOGRAPHIC STUDIES

Single crystals of compounds **20**-**22** and **24** were obtained by the slow diffusion of hexanes into a toluene solution of the divanadium compound. For **23**, benzene was used instead of toluene. For **25**, a saturated THF/hexanes solution was cooled to -10 °C. Each crystal was mounted on a glass fiber with silicone grease and transferred to a goniometer. In all subsequent experiments, the crystal was cooled under a stream of nitrogen at -60 °C. Data were collected with a Bruker SMART 1000 CCD area detector system using 0.3° ω-scans at 0°, 90° and 180° in ϕ. Cell parameters were determined using the program SMART.[15] Data reduction and integration were performed with the software package SAINTPLUS.[16] while an absorption correction was

applied using the program SADABS.[17] Crystal and space group symmetries for all compounds were determined using the XPREP program.[18] For all compounds, the positions of some or all of the non-hydrogen atoms were found by direct methods using the solution program SHELXS.[43] The position of the remaining non-hydrogen atoms were located by use of a combination of least-squares refinement and difference Fourier maps in the SHELXL-93[20] or SHELXL-97 [73] program. Non-hydrogen atoms were refined with anisotropic displacement parameters. The hydrogen atoms were included in the structure factor calculations at idealized positions. Crystal data and refinement results for all compounds are listed in Tables 28-34. Selected bond distances and angles are listed in Tables 35-39.

RESULTS AND DISCUSSION

Five new compounds, along with the three previously known are listed in Table 40, where some additional information about each one is also presented. It will be noted that these are all similar in two respects. (1) Each one is a neutral paddlewheel molecule with four NXN^- bridging ligands. We have not yet succeeded in making any compounds with NXO^- or $OC(R)O^-$ ligands. It is not clear whether this is possible or not, but efforts to do so continue. (2) All compounds have been accurately characterized as to structure by single-crystal X-ray cyrstallography. The V–V distances are all within the relatively narrow range 1.93 Å to 1.99 Å. The longer bond distances correspond to the formamidinates, while the shorter ones belong to the guanidinate and aminopyridine. The V–V distances correlate fairly well with reduction potentials. The more negative reduction potentials belong to the molecules with the shorter bond

.

Table 28. Crystal Data and Structure Refinement for **20**

Empirical formula	$C_{60}H_{60}N_8O_8V_2$
Formula weight	1123.04
Space group	$P\bar{1}$
Unit cell dimensions	a = 10.2646(6) Å α = 80.2650(10)° b = 10.3332(6) Å β = 75.0710(10)° c = 13.9625(9) Å γ = 81.1600(10)°
Volume	1400.90(15) Å³
Z	1
Density (calculated)	1.331 g/cm³
Crystal size	0.61 x 0.42 x 0.32 mm
Absorption coefficient	0.396 mm^{-1}
Data collection instrument	Bruker SMART area detector
Wavelength	0.71073 Å
Orientation reflections, number, range (θ)	5433, 2.2575 - 27.5095
Temperature	193(2) K
Scan method	ω scans
Theta range for data collection	2.01 to 27.53°
Reflections collected	8883
Independent reflections	6190 [R(int) = 0.0138]
Data / restraints / parameters	6190 / 0 / 352
Refinement method	Full-matrix least-squares on F^2
Final R indices [I > 2σ(I)]	$R1^a$ = 0.040, $wR2^b$ = 0.104
R indices (all data)	$R1^a$ = 0.048, $wR2^b$ = 0.110
Goodness-of-fit on F^2	1.023
Largest shift/esd, final cycle	0.001
Largest peak, final cycle	0.40(5) e/Å³

[a] $R1 = \sum||F_o| - |F_c||/\sum|F_o|$.
[b] $wR2 = [\sum[w(F_o^2-F_c^2)^2]/\sum[w(F_o^2)^2]]^{1/2}$, $w = 1/[\sigma^2(F_o^2) + (aP)^2 + bP]$, where $P = [\max(F_o^2 \text{ or } 0) + 2(F_c^2)]/3$.

Table 29. Crystal Data and Structure Refinement for **21**

Empirical formula	$C_{52}H_{44}N_8V_2$
Formula weight	882.83
Space group	*P*2/*n*
Unit cell dimensions	a = 17.8740(14) Å α = 90˚ b = 10.3011(8) Å β = 102.156(2)˚ c = 24.4161(19) Å γ = 90˚
Volume	4394.7(6) Å³
Z	4
Density (calculated)	1.334 g/cm³
Crystal size	0.54 x 0.29 x 0.06 mm
Absorption coefficient	0.472 mm^{-1}
Data collection instrument	Bruker SMART area detector
Wavelength	0.71073 Å
Orientation reflections, number, range (θ)	6688, 2.26 - 25.02
Temperature	213(2) K
Scan method	ω scans
Theta range for data collection	1.98 to 25.04˚
Reflections collected	22241
Independent reflections	7761 [*R*(int) = 0.0554]
Data / restraints / parameters	7761 / 0 / 575
Refinement method	Full-matrix least-squares on F^2
Final *R* indices [I > 2σ(*I*)]	$R1^a$ = 0.057, $wR2^b$ = 0.136
R indices (all data)	$R1^a$ = 0.089, $wR2^b$ = 0.153
Goodness-of-fit on F^2	1.020
Largest shift/esd, final cycle	0.001
Largest peak, final cycle	1.21(8) e/Å³

[a] $R1 = \sum||F_o| - |F_c||/\sum|F_o|$.

[b] $wR2 = [\sum[w(F_o^2-F_c^2)^2]/\sum[w(F_o^2)^2]]^{1/2}$, $w = 1/[\sigma^2(F_o^2) + (aP)^2 + bP]$, where $P = [\max(F_o^2 \text{ or } 0) + 2(F_c^2)]/3$.

Table 30. Crystal Data and Structure Refinement for **22**

Empirical formula	$C_{52}H_{36}Cl_8N_8V_2$
Formula weight	1158.37
Space group	*Fddd*
Unit cell dimensions	a = 26.5959(17) Å α = 90˚ b = 27.2378(17) Å β = 90˚ c = 29.7981(19) Å γ = 90˚
Volume	21586(2) Å³
Z	16
Density (calculated)	1.426 g/cm³
Crystal size	0.28 x 0.24 x 0.23 mm
Absorption coefficient	0.786 mm^{-1}
Data collection instrument	Bruker SMART area detector
Wavelength	0.71073 Å
Orientation reflections, number, range (θ)	6873, 2.54 - 24.974
Temperature	213(2) K
Scan method	ω scans
Theta range for data collection	2.03 to 25.02˚
Reflections collected	27664
Independent reflections	4772 [R(int) = 0.0361]
Data / restraints / parameters	4772 / 0 / 318
Refinement method	Full-matrix least-squares on F^2
Final R indices [I > 2σ(I)]	$R1^a$ = 0.037, $wR2^b$ = 0.086
R indices (all data)	$R1^a$ = 0.060, $wR2^b$ = 0.100
Goodness-of-fit on F^2	1.026
Largest shift/esd, final cycle	0.001
Largest peak, final cycle	0.47(5) e/Å³

[a] $R1 = \sum||F_o| - |F_c||/\sum|F_o|$.
[b] $wR2 = [\sum[w(F_o^2-F_c^2)^2]/\sum[w(F_o^2)^2]]^{1/2}$, $w = 1/[\sigma^2(F_o^2) + (aP)^2 + bP]$, where $P = [\max(F_o^2 \text{ or } 0) + 2(F_c^2)]/3$.

Table 31. Crystal Data and Structure Refinement for **23**·4benzene

Empirical formula	$C_{100}H_{88}N_{12}V_2$
Formula weight	1559.70
Space group	$P\bar{1}$
Unit cell dimensions	a = 14.4048(13) Å α = 72.170(2)° b = 15.0819(13) Å β = 79.445(2)° c = 21.2103(18) Å γ = 69.961(2)°
Volume	4105.3(6) Å³
Z	2
Density (calculated)	1.262 g/cm³
Crystal size	0.34 x 0.15 x 0.10 mm
Absorption coefficient	0.285 mm^{-1}
Data collection instrument	Bruker SMART area detector
Wavelength	0.71073 Å
Orientation reflections, number, range (θ)	3571, 2.419 - 23.6375
Temperature	213(2) K
Scan method	ω scans
Theta range for data collection	1.51 to 25.09°
Reflections collected	21848
Independent reflections	14289 [R(int) = 0.0379]
Data / restraints / parameters	14289 / 0 / 1027
Refinement method	Full-matrix least-squares on F^2
Final R indices [I > 2σ(I)]	$R1^a$ = 0.055, $wR2^b$ = 0.106
R indices (all data)	$R1^a$ = 0.111, $wR2^b$ = 0.128
Goodness-of-fit on F^2	1.000
Largest shift/esd, final cycle	0.001
Largest peak, final cycle	0.42(6) e/Å³

[a] $R1 = \sum||F_o| - |F_c||/\sum|F_o|$.
[b] $wR2 = [\sum[w(F_o^2-F_c^2)^2]/\sum[w(F_o^2)^2]]^{1/2}$, $w = 1/[\sigma^2(F_o^2) + (aP)^2 + bP]$, where $P = [\max(F_o^2 \text{ or } 0) + 2(F_c^2)]/3$.

Table 32. Crystal Data and Structure Refinement for **24**

Empirical formula	$C_5 H_{48}N_8V_2$
Formula weight	934.90
Space group	$P\bar{1}$
Unit cell dimensions	a = 9.9082(10) Å α = 97.989(2)° b = 10.1633(10) Å β = 109.990(2)° c = 12.7609(13) Å γ = 101.325(2)°
Volume	1154.1(2) Å³
Z	1
Density (calculated)	1.345 g/cm³
Crystal size	0.75 x 0.38 x 0.37 mm
Absorption coefficient	0.453 mm^{-1}
Data collection instrument	Bruker SMART area detector
Wavelength	0.71073 Å
Orientation reflections, number, range (θ)	6277, 2.274 - 27.528
Temperature	213(2) K
Scan method	ω scans
Theta range for data collection	1.74 to 27.53°
Reflections collected	7930
Independent reflections	4987 [R(int) = 0.0128]
Data / restraints / parameters	4987 / 0 / 298
Refinement method	Full-matrix least-squares on F^2
Final R indices [I > 2σ(I)]	$R1^a$ = 0.030, $wR2^b$ = 0.085
R indices (all data)	$R1^a$ = 0.032, $wR2^b$ = 0.087
Goodness-of-fit on F^2	1.055
Largest shift/esd, final cycle	0.002
Largest peak, final cycle	0.31(5) e/Å³

[a] $R1 = \sum||F_o| - |F_c||/\sum|F_o|$.
[b] $wR2 = [\sum[w(F_o^2-F_c^2)^2]/\sum[w(F_o^2)^2]]^{1/2}$, $w = 1/[\sigma^2(F_o^2) + (aP)^2 + bP]$, where $P = [\max(F_o^2 \text{ or } 0) + 2(F_c^2)]/3$.

Table 33. Crystal Data and Structure Refinement for **25**

Empirical formula	$C_{64}H_{68}KN_8O_3V_2$
Formula weight	1138.24
Space group	$Pna2_1$
Unit cell dimensions	a = 20.2487(10) Å α = 90˚ b = 12.4492(6) Å β = 90˚ c = 22.9565(12) Å γ = 90˚
Volume	5786.9(5) Å³
Z	4
Density (calculated)	1.306 g/cm³
Crystal size	0.30 x 0.27 x 0.09 mm
Absorption coefficient	0.448 mm^{-1}
Data collection instrument	Bruker SMART area detector
Wavelength	0.71073 Å
Orientation reflections, number, range (θ)	5019, 2.593 - 21.5565
Temperature	213(2) K
Scan method	ω scans
Theta range for data collection	1.77 to 25.06˚
Reflections collected	29454
Independent reflections	10209 [R(int) = 0.0590]
Data / restraints / parameters	10209 / 1 / 703
Refinement method	Full-matrix least-squares on F^2
Final R indices [I > 2σ(I)]	$R1^a$ = 0.046, $wR2^b$ = 0.081
R indices (all data)	$R1^a$ = 0.081, $wR2^b$ = 0.095
Goodness-of-fit on F^2	1.022
Largest shift/esd, final cycle	0.001
Largest peak, final cycle	0.39(5) e/Å³

[a]R1 = $\sum||F_o| - |F_c||/\sum|F_o|$. [b]wR2 = $[\sum[w(F_o^2-F_c^2)^2]/\sum[w(F_o^2)^2]]^{½}$, w = $1/[\sigma^2(F_o^2) + (aP)^2 + bP]$, where P = $[\max(F_o^2 \text{ or } 0) + 2(F_c^2)]/3$.

Table 34. Bond Lengths [Å] and Angles [˚] for **20**[a]

V(1)-V(1A)[b]	1.9876(5)
V(1)-N(1)	2.082(2)
V(1)-N(2)	2.105(2)
V(1)-N(4A)	2.112(2)
V(1)-N(3)	2.125(2)
V(1A)-V(1)-N(1)	92.69(4)
V(1A)-V(1)-N(2)	94.29(4)
V(1A)-V(1)-N(3)	95.92(4)
V(1A)-V(1)-N(4A)	94.41(4)
cis - N–V–N	89.68[6]
trans - N–V–N	171.12[6]

[a] Square brackets refer to average values; parentheses refer to unique values.
[b] Symmetry transformations used to generate equivalent atoms: A -x+1,-y-1,-z+1.

Table 35. Bond Lengths [Å] and Angles [°] for **21**[a]

V(1)-V(1A)[b]	1.9788(10)
V(1)-N(1)	2.086(3)
V(1)-N(2)	2.117(3)
V(1)-N(3)	2.078(3)
V(1)-N(4)	2.122(3)
V(2)-V(2A)	1.9781(10)
V(2)-N(5)	2.094(3)
V(2)-N(6)	2.117(3)
V(2)-N(7)	2.078(3)
V(2)-N(8)	2.119(3)
V(1A)-V(1)-N(1)	96.86(7)
V(1A)-V(1)-N(2)	91.95(7)
V(1A)-V(1)-N(3)	96.28(7)
V(1A)-V(1)-N(4)	92.74(7)
V(2A)-V(2)-N(5)	96.53(7)
V(2A)-V(2)-N(6)	92.33(7)
V(2A)-V(2)-N(7)	96.05(7)
V(2A)-V(2)-N(8)	92.96(7)
cis - N–V(1)–N	89.7[1]
trans - N–V(1)–N	171.0[1]
cis - N–V(2)–N	89.7[1]
trans - N–V(2)–N	171.0[1]

[a] Square brackets refer to average values; parentheses refer to unique values.
[b] Symmetry transformations used to generate equivalent atoms: A -x+1/2,y,-z+3/2.

Table 36. Bond Lengths [Å] and Angles [°] for **22**[a]

V(1)-V(1A)[b]	1.9742(11)
V(1)-N(1)	2.118(2)
V(1)-N(2)	2.068(2)
V(2)-V(2A)	1.9820(12)
V(2)-N(3)	2.105(2)
V(2)-N(4)	2.121(2)
V(1A)-V(1)-N(1)	92.86(6)
V(1A)-V(1)-N(2)	95.56(6)
V(2A)-V(2)-N(3)	94.38(6)
V(2A)-V(2)-N(4)	94.45(6)
cis - N–V1–N	89.72[9]
trans - N–V1–N	171.6[1]
cis - N–V2–N	89.66[9]
trans - N–V2–N	171.2[1]

[a] Square brackets refer to average values; parentheses refer to unique values.
[b] Symmetry transformations used to generate equivalent atoms: A -x+1/4, -y+5/4, z.

Table 37. Bond Lengths [Å] and Angles [°] for **23**·4benzene[a]

V(1)-V(2)	1.9521(7)
V(1)-N(1)	2.103(2)
V(1)-N(4)	2.103(3)
V(1)-N(7)	2.101(2)
V(1)-N(10)	2.091(3)
V(2)-N(3)	2.077(3)
V(2)-N(6)	2.097(3)
V(2)-N(9)	2.089(3)
V(2)-N(12)	2.089(3)
V(2)-V(1)-N(1)	92.99(7)
V(1)-V(2)-N(3)	94.36(7)
V(2)-V(1)-N(4)	94.82(7)
V(1)-V(2)-N(6)	92.99(7)
V(2)-V(1)-N(7)	92.85(7)
V(1)-V(2)-N(9)	95.10(7)
V(2)-V(1)-N(10)	93.87(7)
V(1)-V(2)-N(12)	93.59(7)
cis - N–V(1)–N	89.8[1]
trans - N–V(1)–N	172.6[1]
cis - N–V(2)–N	89.7[1]
trans - N–V(2)–N	171.9[1]

[a] Square brackets refer to average values; parentheses refer to unique values.

Table 38. Bond Lengths [Å] and Angles [°] for **24**[a]

V(1)-V(1A)[b]	1.9425(4)
V(1)-N(1)	2.1555(11)
V(1)-N(2A)	2.0412(11)
V(1)-N(3)	2.1429(12)
V(1)-N(4)	2.0506(11)
V(1A)-V(1)-N(1)	95.63(3)
V(1A)-V(1)-N(2A)	93.81(3)
V(1A)-V(1)-N(3)	92.88(3)
V(1A)-V(1)-N(4)	95.63(3)
cis - N–V(1)–N	89.66[5]
trans - N–V(1)–N	168.37(4)

[a] Square brackets refer to average values; parentheses refer to unique values.
[b] Symmetry transformations used to generate equivalent atoms: A -x+1,-y+1,-z+1.

Table 39. Bond Lengths [Å] and Angles [°] for **25**[a]

V(1)-V(2)	1.9295(8)
V(1)-N(1)	2.110(3)
V(1)-N(2)	2.125(3)
V(1)-N(3)	2.153(3)
V(1)-N(4)	2.160(3)
V(2)-N(5)	2.141(3)
V(2)-N(6)	2.164(3)
V(2)-N(7)	2.155(3)
V(2)-N(8)	2.124(3)
V(1)-K(1)	3.9040(12)
N–K	3.124[3]
O–K	2.729[3]
V(2)-V(1)-N(1)	95.00(9)
V(2)-V(1)-N(2)	94.38(9)
V(2)-V(1)-N(3)	94.49(9)
V(2)-V(1)-N(4)	97.07(9)
V(1)-V(2)-N(5)	95.20(9)
V(1)-V(2)-N(6)	95.93(9)
V(1)-V(2)-N(7)	95.59(9)
V(1)-V(2)-N(8)	92.59(9)
cis - N–V(1)–N	89.5[1]
trans - N–V(1)–N	169.3[1]
cis - N–V(1)–N	89.6[1]
trans - N–V(1)–N	170.1[1]

[a] Square brackets refer to average values; parentheses refer to unique values.

Table 40. Compounds Containing the V_2^{4+} Core

Ligand	**V–V Bond Distance [Å]**	**Reduction Potential, V**
DTolF	1.978(2)	not reported
DCyF	1.968(2)	not reported
hpp	1.932(1)	not reported
DPhF	1.979(1)	-1.46
DAniF	1.9876(5)	-1.77
DClPhF	1.982(1) 1.974(1)	-1.23
TPG	1.9521(7)	-1.99
ap	1.9425(4)	-1.82

lengths, while the more accessible potentials correspond to those with the longer bond lengths. All bond distances are consistent with the assignment of a $\sigma^2\pi^4$ triple bond to each, and it is notable that the V–V bonds are the only known metal-metal bonds, other than the fully developed Cr–Cr quadruple bonds, that are shorter than 2.00 Å. In marked contrast to the Cr_2 quadruply bonded compounds, which very strongly bind axial ligands, the V–V compounds all crystallize without axial ligation.

Electrochemistry. We have for the first time investigated the electrochemistry of V_2^{4+} compounds, and have been rewarded by results leading to an important advance in the chemistry. The cyclic voltammagram for compound **20** is shown in Figure 29. While no reversible oxidation occurs, there is a reversible reduction - both observations being somewhat contrary to our expectations. The reduction product can be formally considered to provide an example of the rare oxidation state V^+ (known only in relatively exotic species such as $[V(C_5H_5)_2]^+$ and $[V(CO)_6]^+$). However, we considered it much more likely that the additional electron is introduced into the δ bonding orbital, where it is delocalized in a V_2^{3+} core which has an overall electron configuration of $\sigma^2\pi^4\delta^1$ and a metal-metal bond order of 3.5.

Each of the compounds, **20**-**24** exhibit a similar reduction wave, the potentials of which are listed in Table 40. There is a notable trend in reduction potential: as the bridging ligand becomes more basic, it becomes more difficult to add an additional electron to the valance, presumably δ-type, orbital, and thus the reaction potentials become more negative. A similar, but opposite, correlation between oxidation potentials and the ligand basicity of various formamidinate ligands has been shown in dinickel,[89] and dimolybdenum[90] paddlewheel-type compounds.

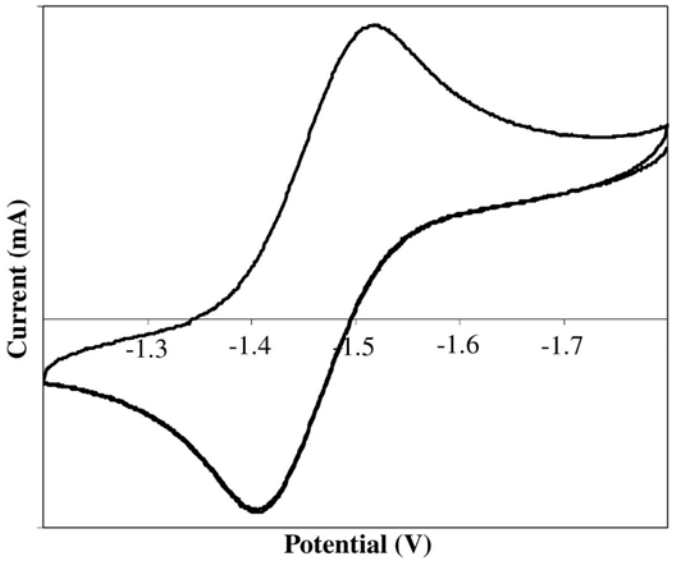

Figure 29. Cyclic voltammogram of $V_2(DPhF)_4$, **20**.

Structural Considerations. The thermal ellipsoid plots of the five new molecules listed in Table 40 are shown in Figures 30 to 34. Each compound has the typical paddlewheel geometry with V–V bond distances ranging from 1.943 Å in **24** to 1.988 Å in **21.** The crystal structure of the V_2^{3+} compound is shown in Figure 35. The structure of the anion is clearly seen as a typical paddlewheel structure, nearly identical to that of **20** except for the decrease in the V to V distance of about 0.05 Å and a small increase in the average V–N distance. The shortening of this bond is consistent with the addition of one electron into a V–V bonding orbital and the increase in the formal bond order from 3 to 3.5. The magnitude of this change suggests that the additional electron resides in the δ-orbital, and that the dimetal core has a $\sigma^2\pi^4\delta^1$ configuration. This situation may be compared to that of the dimolybdenum carboxylates, whose electronic structure is well understood. The difference in bond length between $Mo_2(TiPB)_4^{n+}$ (where TiPB is the anion of 2,4,6-triisopropylbenzoic acid and n = 0 and 1) with a $\sigma^2\pi^4\delta^2$ quadruple bond and the $\sigma^2\pi^4\delta^1$ oxidized species is 0.06 Å.[91] The change in V–N distances is also indicative of the lowering of the overall charge on the dimetal core; the average distance increases from 2.101[3] Å to 2.142[3] Å upon reduction. Similar variations are observed in the series of compounds $M_2(hpp)_4^{n+}$ (n = 0, 1, 2), for M = Mo and W.[92] Finally, the decrease in the torsion angle from about 2.4° in the neutral species to about 1.6° in the reduced species points towards improved δ orbital overlap.

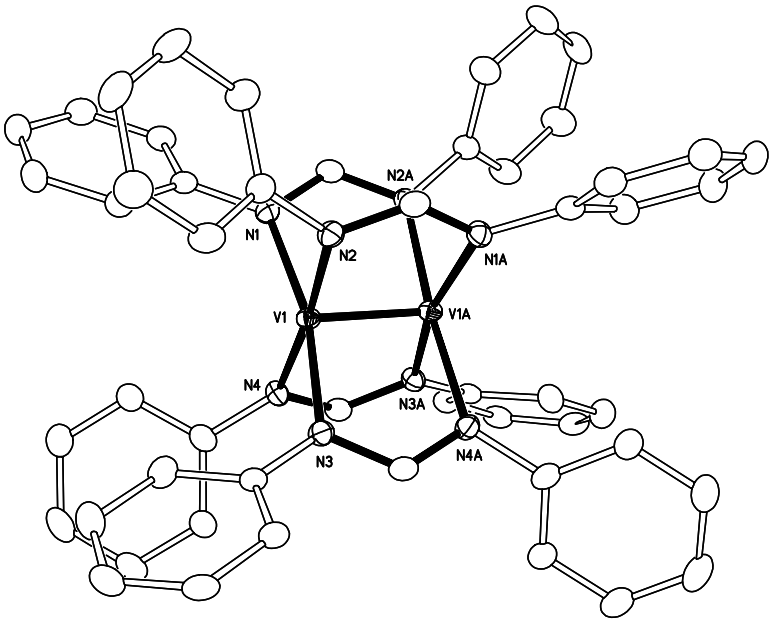

Figure 30. Thermal ellipsoid plot of $V_2(DPhF)_4$, **20**. Thermal ellipsoids are shown at the 30% probability level; hydrogen atoms have been omitted for clarity.

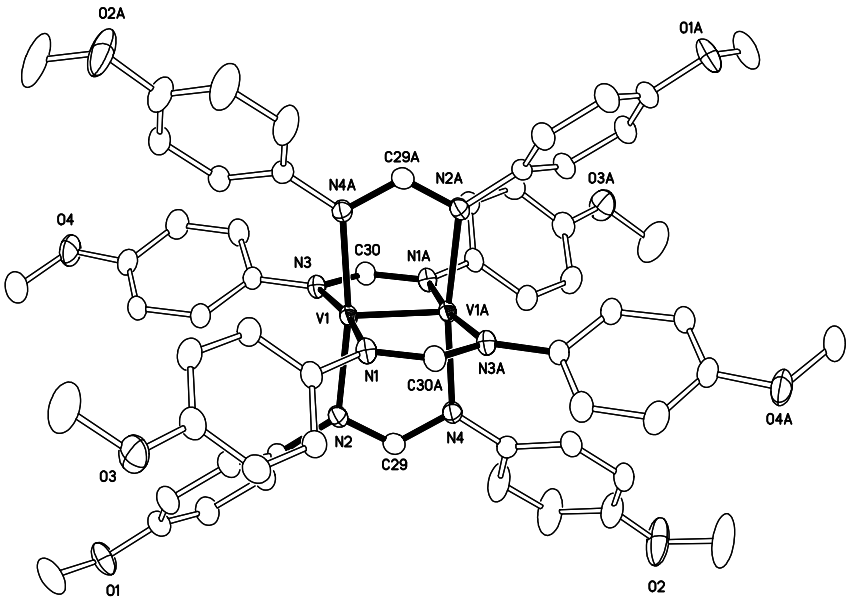

Figure 31. Thermal ellipsoid plot of $V_2(DAniF)_4$, **21**. Thermal ellipsoids are shown at the 30% probability level; hydrogen atoms have been omitted for clarity.

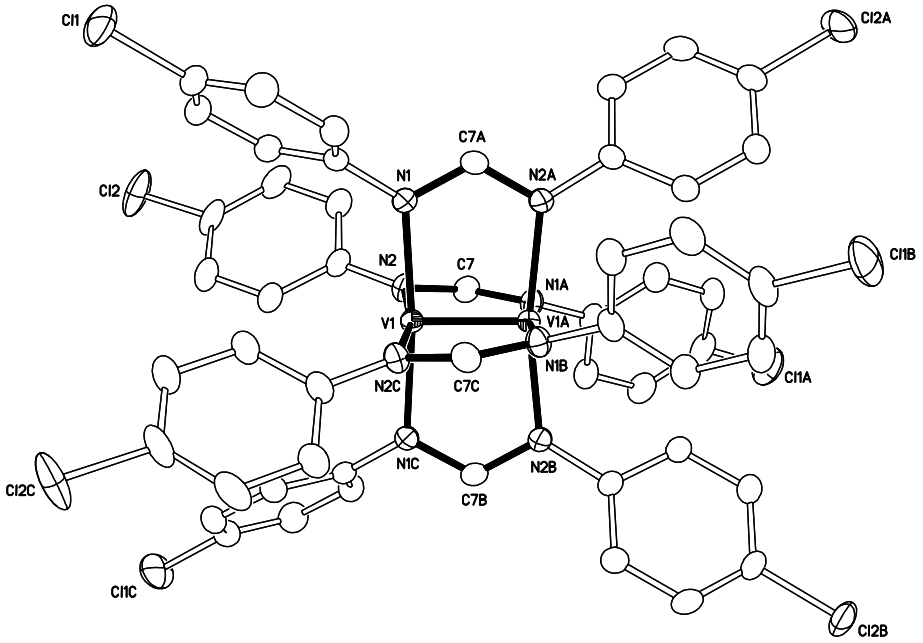

Figure 32. Thermal ellipsoid plot of $V_2(D^{Cl}PhF)_4$, **22**. Thermal ellipsoids are shown at the 30% probability level; hydrogen atoms have been omitted for clarity. Only one of the two independent molecules in the asymmetric unit is shown.

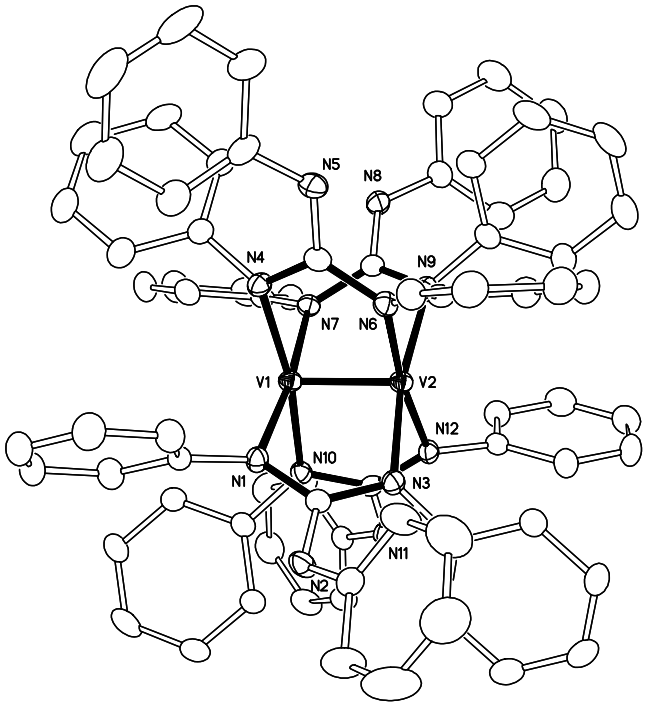

Figure 33. Thermal ellipsoid plot of $V_2(TPG)_4$, in **23**·4benzene. Thermal ellipsoids are shown at the 30% probability level; hydrogen atoms and interstitial benzene molecules have been omitted for clarity.

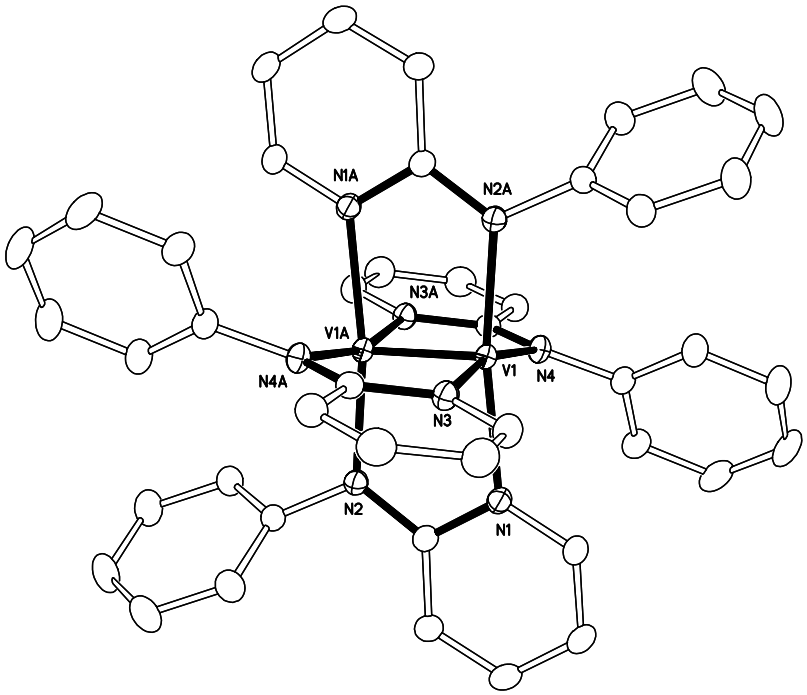

Figure 34. Thermal ellipsoid plot of $V_2(ap)_4$, **24** . Thermal ellipsoids are shown at the 30% probability level; hydrogen atoms have been omitted for clarity.

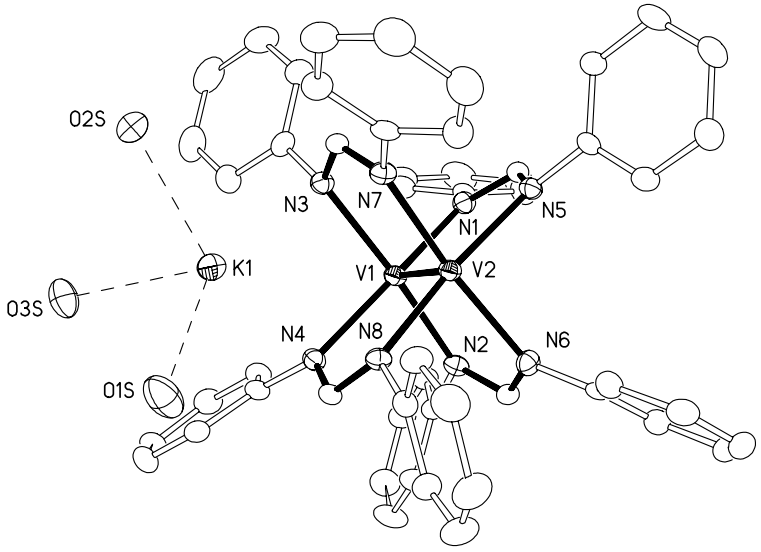

Figure 35. Thermal ellipsoid plot of $[K(THF)_3]V_2(DPhF)_4$, **25**. Thermal ellipsoids are shown at the 30% probability level; hydrogen atoms and THF carbon atoms have been omitted for clarity.

There is an additional feature, namely the presence of the K^+ ion, coordinated by only three THF molecules and associated also with the DPhF ligands. As shown in Figure 35, the K^+ cation is found in one of the pockets between two of the formamidinate groups. This type of association of an alkali metal cation with some of the ligands of an M_2 paddlewheel molecule is not without precedent and has been observed in $Nb_2(hpp)_4$[93] and $W_2(hpp)_4$.[94] Although these compounds were first isolated in crystals of $M_2(hpp)_4 \cdot 2NaEt_3BH$,[95] having Na^+ ions occupying pockets between the paddles, the metal-metal bond distances were essentially identical whether with or without the associated alkali cations. In **25**, there are long K- - -N distances averaging 3.124[3] Å and three THF molecules at a relatively long average distance of 2.729[4] Å, similar to those found in other K(THF) containing compounds.[96] We therefore expect the structure of the V_2^{3+} unit we have found in **25** to be about the same as will be found in a crystal where no such association occurs.

Synthesis. Compounds **20** - **24** were synthesized by the following metathesis reaction, where NXN represents the anion of the bidentate ligand:

$$VCl_2 \cdot THF_n + 2Li(NXN) \xrightarrow{THF,\ r.t.} V_2(NXN)_4 + 2LiCl \qquad (6)$$

Each of the reported compounds are air-sensitive and all reactions were carried out under Ar, and solvents were rigorously dried by fresh distillation over K/Na alloy. For compounds **20**-**24**, removal of the reaction solvent, THF, often yielded an oily red residue, which is best allowed to remain under reduced pressure for a short time, from about 15 min to ½ h. Prolonged exposure of the solid to vacuum may allow the entry of atmospheric oxygen, which causes a darkening of

the surface indicating decomposition. This discolored surface layer can be removed by washing the solid with small amounts of toluene or THF, although, it is best to avoid having to wash the residue at all, because the compound itself is moderately soluble in these solvents. The product can then be separated from the side product, LiCl, by extraction with toluene, filtration over Celite, and diffusion of hexanes or ether to produce X-ray quality crystals.

The combination of KC_8 with **20** yielded a brilliant green solution (within which graphite was suspended) after stirring a few minutes at -78 °C. If a large excess of KC_8 is used, the color change is not observed, although we found by EPR that the anion is still present. It is not clear what additional reactions may be occurring in this situation. Rapid crystallization of **25** was carried out by filtering the THF reaction mixture and adding just enough hexanes to evolve a precipitate. The solution was then placed in the freezer at -10 °C, and crystals appeared after 48 h. Rapid crystallization at low temperature is very important as slower crystallization rates by diffusion of hexanes into the THF solution yielded only the red **20** over several days. Some of **20** is present even when short crystallization times are used.

EPR Spectroscopy. For the reduced species, **25**, our view that the additional electron is introduced into the δ bonding orbital, where it is delocalized in a V_2^{3+} core is further supported by EPR results. A frozen THF glass of **25** at 6 K gave a fifteen line spectrum, shown in Figure 36, which indicates that the electron is coupling with each ^{51}V ($I = 7/2$, ~100%) atom equally. A simulation of the main feature gives a g value of 1.9999. Although this is close to the free-electron value, the complicated hyperfine splitting pattern indicates that the unpaired electron is localized on the dimetal core.

Concluding Remarks. The isolation of the first V_2^{3+} compound is the harbinger of the chemistry of low-valent paddlewheel compounds,[97] thus expanding the available dimetal oxidation states beyond 4, 5, and 6. Additionally, this structure contains one of the very few examples of a vanadium atom with a formal oxidation state of less than 2 in the absence of π-acids.[98] We believe that the presence of a vanadium-vanadium bond plays an important role in delocalizing the extra electron density and thus stabilizing the highly reduced V_2^{3+} unit.

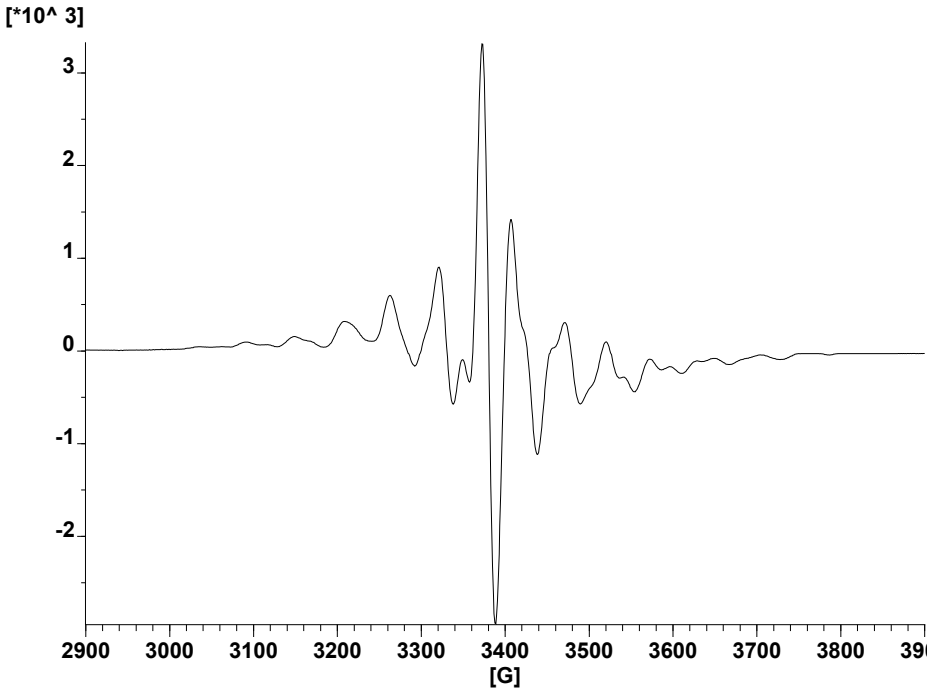

Figure 36. Electron paramagnetic resonance spectrum of **25.** THF glass at 6 K.

CONCLUSIONS

Although much of the focus in metal-metal bonding chemistry today is on systems of higher complexity, such as the design of supramolecular architectures, extended chains of metal atoms, or "molecular wires", and the use of other compounds in catalysis and medicine, there is still a wealth of problems of a more fundamental nature to be examined. The work presented in this dissertation has shown that even the most basic task of synthesizing novel paddlewheel-type compounds remains a rich vein of discovery.

Our work with unsolvated metal carboxylates has focused on how a basic component of the geometric framework can influence the molecular structure and properties. By creating compounds in the solid state without any type of axial ligation, we have had the opportunity to study very well known compounds in a rather extreme situation. Our first investigation, into dichromium systems, yielded an answer to a very old and contentious problem. We found that when deprived of axial ligands, the Cr–Cr bond is very short, almost half an Ångstrom shorter than when axial ligands are present. Although the origin of the variability of the Cr–Cr bond is still poorly understood, we have discovered that the nature and presence of the axial ligands is the major factor controlling its length. The failure of theory to account for the behavior of the Cr–Cr bond underscores how little we yet know about the electronic structure.

The behavior of its congener, molybdenum, could not be more different. Quadruply-bonded molybdenum compounds do not coordinate axial ligands very strongly, and the electronic structures of such compounds are well established. Thus, although the study of unsolvated $Mo_2(O_2CR)_4$ did not give us any more insight on the influence of axial ligation in these systems, we were rewarded in quite a different regard. The steric bulk of the triisopropyl

group was exploited not to prevent axial ligation (although no axial ligands were in fact present), but to kinetically stabilize the Mo_2^{5+} core. Although the oxidation potential of the Mo_2^{4+} parent compound was less accessible than equally reversible waves observed for other dimolybdenum carboxylates, the $Mo_2(TiPB)_4^+$ cation is the first example of the Mo_2^{5+} core in a carboxylato compound.

We found that copper carboxylates had a dramatic response to axial ligand deprivation. Because Cu(II) atoms have a d^9 configuration, no metal-metal bonding is expected (or observed) in the copper carboxylates. However, we were very interested to see what effect axial ligands have on the antiferromagnetic coupling between spin centers. We were surprised to find that the compound adopts an unprecedented trimeric geometry with the copper atoms in a square planar environment. Although this result did not enhance our understanding of the paddlewheel-type superexchange pathways, it provided an even more interesting magnetic system for study, that of the spin frustrated molecule. Detailed magnetic studies on this system have been undertaken by another research group.

Finally, we learned that while the Rh_2^{4+} core displays a tremendous avidity for axial ligation, the absence of axial ligands does not greatly alter the molecular structure. Instead, we were able to provide confirmation of the electronic structure first elucidated by Norman and Kolari. The theoretical expectation of a π^*-type HOMO and σ^* type LUMO for the Rh–Rh single bond is consistent with our results.

Although there are thousands of compounds known to possess metal to metal bonds, there are some areas of the periodic table which still have not been fully investigated. Considering that the study of Cr–Cr bonds has yielded hundreds of compounds, it seems that compounds containing a V–V triple bond should be accessible. Although theoretical work had predicted the stability of such compounds as early as 1985, it was not until 1992 that the first

compound was made. Even though the synthetic strategy had been elucidated, the field has remained neglected for ten years. We have expanded the library of compounds containing metal to metal bonds with the addition of several V_2^{4+} compounds and one V_2^{3+} compound. The triple bond does not appear very sensitive to the electronic properties of the bridging ligand although there is a gradual trend which correlates increasing basicity with shorter metal-metal bonds. The impact of the bridging ligand can be most clearly appreciated by its influence on the reduction potentials of the V_2^{4+} compounds. As the ligand becomes more basic, the reduction potential becomes less accessible, due to what we presume is increased electron density in the metal–metal bond. Although the reduction potentials are very negative, we have isolated and characterized the reduced species. The stability of this compound compared to the dearth of low-valent vanadium compounds suggests that the V–V bond plays an important role in delocalizing the additional charge. The shortening of the V–V bond and the delocalized EPR signal is consistent with the change in bond order from 3 to 3.5.

REFERENCES

(1) Cotton, F. A.; Curtis, N. F.; Harris, C. B; Johnson, B. F. G.; Lippard, S. J.; Maque, J. T.; Robinson, W. T.; Wood, J. S. *Science* **1964**, *145*, 1305.

(2) Cotton, F. A.; Walton, R. A. *Multiple Bonds Between Metal Atoms*, 2nd ed.; Oxford University Press: Oxford, 1993.

(3) (a) Miskowski, V. M.; Hopkins, M. D.; Winkler, J. R.; Gray, H. B. In *Inorganic Electronic Structure and Spectroscopy*, Solomon, E. I.; Lever, A. B. P., Eds. Vol. 2; John Wiley & Sons: New York, 1999, pp. 343-402. (b) Cotton, F. A.; Nocera, D. G. *Acc. Chem. Res.* **2000**, *33*, 483. (c) Hopkins, M. D.; Gray, H. B.; Miskowski, V. M. *Polyhedron* **1987**, *6*, 705.

(4) See for example: (a) Doyle, M. P.; Ren, T. *Prog. Inorg. Chem.* **2001**, *49*, 113. (b) Estevan, F.; Herbst, K; Lahuerta, P.; Barberis, M.; Perez-Prieto, J. *Organometallics* **2001**, *20*, 950. (c) *Catalysis by Di- and Polynuclear Metal Cluster Complexes*; Adams, R. D.; Cotton, F. A., Eds.; Wiley-VCH: New York, 1998.

(5) (a) Asara, J. M.; Hess, J. S.; Lozada, E.; Dunbar, K. R.; Allison, J. *J. Am. Chem. Soc.* **2000**, *122*, 8. (b) Catalan, K. V.; Hess J. S.; Maloney, M. M.; Mindiola, D. J.; Ward, D. L.; Dunbar, K. R. *Inorg. Chem.* **1999**, *38*, 3904. (c) Dale, L. D.; Dyson, T. M.; Tocher, D. A.; Tocher, J. H.; Edwards, D. I. *Anti-Cancer Drug Des.* **1989**, *4*, 295. (d) Aoki, K.; Yamazaki, H. *J. Chem. Soc., Chem. Commun.* **1980**, 186. (e) Howard, R. A.; Kimball, A. P.; Bear, J. L. *Cancer Res.* **1979**, *39*, 2568. (f) Fu, P.; Bradley, P. M.; Turro, C. *Inorg. Chem*. **2001**, *40*, 2476. (g) Aoki, K.; Salam, M. A. *Inorg. Chim. Acta* **2001**, *316*, 50.

(6) (a) Cotton, F. A.; Daniels, L. M.; Murillo, C. A.; Timmons, D. J.; Wilkinson, C. C. *J. Am. Chem. Soc.* **2002** *124*, 9249. (b) Cotton, F. A.; Gruhn, N. E.; Gu, J.; Huang, P.; Lichtenberger, D. L.; Murillo, C. A.; Van Dorn, L. O.; Wilkinson, C. C. *Science* **2002**, *298*, 1971.

(7) (a) Bénard, M. *J. Chem. Phys.* **1979**, *71*, 2546. (b) Bénard, M. *J. Am. Chem. Soc.* **1978**, *100*, 2354. (c) Kok, R. A.; Hall, M. B. *J. Am. Chem. Soc.* **1983**, *105*, 676. (d) Davy, R. B.; Hall, M. B. *J. Am. Chem. Soc.* **1989**, *111*, 1268. (e) Wiest, R.; Bénard, M. *Chem. Phys. Lett.* **1983**, *98*, 102. (f) Kok, R. A.; Hall, M. B. *Inorg. Chem.* **1985**, *24*, 1542.

(8) Cotton, F. A.; DeBoer, B. G.; LaPrade, M. D.; Pipal, J. R.; Ucko, D. A. *Acta Crystallogr.* **1971**, *B27*, 1664.

(9) Cotton, F. A.; Daniels, L. M.; Murillo, C. A. *Angew. Chem.* **1992**, *31*, 737.

(10) Berno, P.; Shoukang, H.; Minhas, R.; Gambarotta, S. *J. Am. Chem. Soc.* **1994**, *116*, 7417.

(11) Cotton, F. A.; Timmons, D. J. *Polyhedron* **1998**, *17*, 179.

(12) (a) Peligot, E. *C. R. Acad. Sci*., **1844**, *19*, 609. (b) Peligot, E. *Ann. Chim. Phys*., **1844**, *12*, 528.

(13) van Niekerk, J. N.; Schoening, F. R. L.; de Wet, J. F. *Acta Crystallogr.* **1953**, *6*, 501.

(14) Cotton, F. A.; Rice, C. E.; Rice, G. W. *J. Am. Chem. Soc*. **1977**, *99*, 4704.

(15) SMART for Windows NT; Bruker AXS Inc., Madison, Wisconsin. 1997-2001.

(16) SAINTPLUS for NT; Bruker AXS Inc., Madison, Wisconsin. 1997-2001.

(17) SADABS, V2.03, Bruker/Siemens area detector absorption and other corrections, Bruker AXS Inc., Madison, Wisconsin. 2000.

(18) XPREP, Bruker AXS Inc., Madison, Wisconsin. 1997-2001.

(19) Sheldrick G.M., SHELXTL; Siemens Industrial Automation Inc., Madison, Wisconsin, 1994-1996.

(20) Sheldrick, G. M.; In *Crystallographic Computing 6*; Flack, H. D.; Parkanyi, L.; Simon, K.; Eds.; Oxford University Press: Oxford, UK, 1993, p. 111.

(21) Ketkar, S. N.; Fink, M. *J. Am. Chem. Soc*. **1985**, *107*, 338.

(22) Baral, S.; Cotton, F. A.; Ilsley, W. H. *Inorg. Chem*., **1981**, *20*, 2696.

(23) Ref. 2, p 277.

(24) (a) Martin, R. L.; Waterman, H. *J. Chem. Soc.* **1957**, 2545. (b) Doedens, R. J. *Prog. Inorg. Chem*. **1976**, *21*, 228. (c) Uekusa, H.; Ohba, S.; Tokii, T.; Muto, Y.; Kato, M.; Husebye, S.; Steward, O. W.; Chang, S.-C.; Rose, J. P.; Pletcher, J. F.; Suzuki, I. *Acta. Crystallogr.* **1992**, *B48*, 650. (d) Agterberg, F. P. W.; Kluit, H. A. J. P.; Driessen, W. L.; Oevering, H.; Buijs, W.; Lakin, M. T.; Spek, A. L.; Reedijk, J. *Inorg. Chem*. **1997**, *36*, 4321. (e) Zubkowski, J. D.; Washington, D.; Njoroge, N.; Valente, E.J.; Cannon, T.; Parks, C.D.; Berdahl, P.; Perry, D.L. *Polyhedron* **1997**, *16*, 2341. (f) Chung, Y.H.; Wei, H. H.; Liu, Y. H.; Lee, G. H.; Wang, Y. *Polyhedron* **1998**, *17*, 449.

(25) (a) Simonov, Y. A.; Malinovskii, T. I. *Soviet Phys.Crystallogr.* **1970**, *15*, 310. (b) Bird, M. J; Lomer, T. R. *Acta Crystallogr.* **1972**, *B28*, 242. (c) Lomer, T. R.; Perera, K. *Acta Crystallogr.* **1974**, *B30*, 2912. (d) Troyanov, S. I.; Il'ina, E. G.; Dunaeva, K. M. *Soviet J. Coord. Chem.* **1991**, *17*, 1692. (e) Il'ina, E. G.; Troyanov, S. I.; Dunaeva, K. M. *Soviet J. Coord. Chem.* **1992**, *18*, 882. (f) Ghermani, N.-E.; Lecomte, C. *Acta Crystallogr.* **1994**, *B50*, 157.

(26) (a) Campbell, G. C.; Haw, J. F. *Inorg. Chem*. **1988**, *27*, 3706. (b) Campbell, G. C.; Reibenspies, J. H.; Haw, J. F. *Inorg. Chem.* **1991**, *30*, 171.

(27) Cotton, F. A.; Dikarev, E. V.; Petrukhina, M. A. *Inorg. Chem.* **2000**, *39*, 6072.

(28) Carruthers, J. R.; Prout, K.; Rossotti, F. J. C. *Acta Crystallogr.* **1975**, *B31*, 2044.

(29) Cotton, F. A.; Hillard, E. A.; Murillo, C. A.; Zhou, H.-C. *J. Am. Chem. Soc.* **2000**, *122*, 416.

(30) Pflugrath, J.; Messerschmidt, A. MADNES, Munich Area Detector (New EEC) System, version EEC 11/9/89, with enhancements by Enraf-Nonius Corp., Delft, The Netherlands. A description of MADNES appears in: Messerschmidt, A.; Pflugrath, J. *J. Appl. Crystallogr.* **1987**, 20, 306.

(31) (a) Kabsch, W. *J. Appl. Crystallogr.* **1988**, 21, 67. (b) Kabsch, W. *J. Appl. Crystallogr.* **1988**, *21*, 916.

(32) Smith, G.; O'Reilly, E. J.; Carrell, H. L.; Carrell, C. J.; Kennard, C. H. L. *Polyhedron* **1996**, *15*, 1995.

(33) Batsanov, A. S.; Timko, G. A.; Struchkov, Yu. T.; Gerbeleu, N. V.; Indrichan, K. M.; Poporich, G. A. *Koord. Khim.* **1989**, *15*, 688.

(34) Batsanov, A. S.; Timko, G. A.; Struchkov, Y. T.; Gerbeleu, N. V.; Indrichan, K. M.; Poporich, G. A. *Koord. Khim.* **1989**, *15*, 688.

(35) (a) Abel, E. W.; Singh, A.; Wilkinson, G. *J. Am.Chem. Soc.* **1959**, *81*, 3097. (b) Bannister, E.; Wilkinson, G. *Chem. Ind. (London)* **1960**, 319. (c) Stephenson, T. A.; Bannister, E.; Wilkinson, G. *J. Am. Chem. Soc.* **1963**, *85*, 6012.

(36) (a) Lawton, D.; Mason, R. *J. Am. Chem. Soc.* **1965**, *87*, 921. (b) Cotton, F. A.; Mester, Z. C.; Webb, T. R. *Acta. Crystallogr.* **1974**, *B30*, 2768.

(37) Norman, Jr., J. G.; Kolari, H. J. *J. Chem. Soc., Chem. Commun.* **1975**, 649.

(38) Cotton, F. A.; Zhong, B. *J. Am. Chem. Soc.* **1990**, *112*, 2256 and references therein.

(39) Lichtenberger, D. L.; Johnston, R. L. In *Metal-Metal Bonds and Clusters in Chemistry and Catalysis*; J. P. Fackler, Jr., Ed.; Plenum Press: New York, 1990, pp. 275-298.

(40) Ref. 2, pp. 161-162.

(41) For a recent reference see: Liwporncharoenvong, T.; Luck, R. L. *J. Am. Chem. Soc.* **2001**, *123*, 3615.

(42) Stephenson, T. A.; Bannister, E.; Wilkinson, G. *J. Chem. Soc.* **1964**, 2538.

(43) Sheldrick G.M., *SHELXS-97*: *Program for Crystal Structure Solution;* University of Göttingen: Göttingen, Germany, 1986-1997.

(44) Angell, C. L.; Cotton, F. A.; Frenz, B. A.; Webb, T. R. *J. Chem. Soc., Chem. Commun.* **1973**, 399.

(45) Cotton, F. A.; Frenz, B. A.; Webb T. R. *J. Am. Chem. Soc.* **1973**, *95*, 4431.

(46) Cotton, F. A.; Timmons, D. J. *Polyhedron* **1998**, *119*, 7889.

(47) Cotton, F. A.; Daniels, L. M.; Murillo, C. A.; Timmons, D. J.; Wilkinson, C. C. *J. Am. Chem. Soc.* **2002**, *124*, 9249.

(48) Bailey, P. J.; Bone, S. F.; Mitchell, L. A.; Parsons, S.; Taylor, K. J.; Yellowlees, L. J. *Inorg. Chem.* **1997**, *36*, 867.

(49) Bailey, P. J.; Bone, S. F.; Mitchell, L. A.; Parsons, S.; Taylor, K. J.; Yellowlees, L. J. *Inorg. Chem.* **1997**, *36*, 5420.

(50) Cotton, F. A.; Pedersen, E. *Inorg. Chem.* **1975**, *14*, 399.

(51) Carvill, A.; Higgins, P.; McCann, G. M.; Ryan, H.; Shiels, A. *J. Chem. Soc., Dalton Trans.* **1989**, 2435.

(52) Santure, D. J.; Huffman, J. C.; Sattelberger, A. P. *Inorg. Chem.* **1985**, *24*, 371.

(53) (a) Cayton, R. H.; Chisholm, M. H.; Darrington, F. D. *Angew. Chem., Int. Ed. Engl.* **1990**, *29*, 1481. (b) Cayton, R. H.; Chisholm, M. H. *J. Am. Chem. Soc.* **1989**, *111*, 8921. (c) Cayton, R. H.; Chisholm, M. H.; Huffman, J. C.; Lobkovsky, E. B. *Angew. Chem., Int. Ed. Engl.* **1991**, *30*, 862.

(54) Cotton, F. A.; Extine, M.; Gage, L. D. *Inorg. Chem.* **1978**, *17*, 172.

(55) See for example the review on the use of $Fe(CN)_6^{3-}$ for the oxidation of organic substrates: Leal, J. M.; Garcia, B.; Domingo, P. L. *Coord. Chem. Rev.* **1998**, *173*, 79.

(56) Cotton, F. A.; Frenz, B. A.; Pedersen, E.; Webb, T. R. *Inorg. Chem.* **1975**, *14*, 391.

(57) Chang, I.-J.; Nocera, D. G. *J. Am. Chem. Soc.* **1987**, *109*, 4901.

(58) Cotton, F. A.; Nocera, D. G. *Acc. Chem. Res.* **2000**, *33*, 483.

(59) Chisholm, M. H.; Huffman, J. C.; Iyer, S. S.; Lynn, M. A. *Inorg. Chim. Acta* **1996**, *243*, 283.

(60) San Filippo, Jr., J.; Sniadoch, H. J. *Inorg. Chem.* **1976**, *15*, 2209.

(61) (a) Boyer, E. B.; Robinson, S. D. *Coord. Chem. Rev.* **1983**, *50*, 109. (b) Felthouse, T. R. *Prog. Inorg. Chem.* **1982**, *29*, 73.

(62) Porai-Koshits, M. A.; Antsyshina, A. S. *Dokl. Akad. Nauk SSSR* **1962**, *146*, 1102 (902 in English translation).

(63) Chernyaev, I. I.; Shenderetskaya, E. V.; Karyagina, A. A. *Russ. J. Inorg. Chem.* **1960**, *5*, 559.

(64) Cotton, F. A.; DeBoer, B. G.; LaPrade, M. D.; Pipal, J. R.; Ucko, D. A. *J. Am. Chem. Soc.* **1970**, *92*, 2926; *Acta Crystallogr.* **1971**, *B27*, 1664.

(65) (a) Cotton, F. A.; Daniels, L. M.; Lin, C.; Murillo, C. A. *J. Am. Chem. Soc.* **1999**, *121*, 4538. (b) Cotton, F. A.; Lin, C.; Murillo, C. A. *Chem. Commun.* **2001**, 11. (c) Cotton, F. A.; Lin, C.; Murillo, C. A. *J. Chem. Soc., Dalton Trans.* **2001**, 499. (d) Cotton, F. A.; Daniels, L. M.; Lin, C.; Murillo, C. A.; Yu, S.-Y. *J. Chem. Soc., Dalton Trans.* **2001**, 502. (e) Bonar-Law, R. P.; McGrath, T. D.; Singh, N.; Bickley, J. F.; Steiner, A. *Chem. Commun.* **1999**, 2457. (f) Bickley, J. F.; Bonar-Law, R. P.; Femoni, C.; MacLean, E. J.; Steiner, A.; Teat, S. J. *J. Chem. Soc., Dalton Trans.* **2000**, 4025. (g) Bonar-Law, R. P.; Bickley, J. F.; Femoni, C.; Steiner, A. *J. Chem. Soc., Dalton Trans.* **2000**, 4244. (h) Bonar-Law, R. P.; McGrath, T. D.; Singh, N; Bickley, J. F.; Femoni, C.; Steiner, A. *J. Chem. Soc., Dalton Trans.* **2000**, 4343. (i) Bonar-Law, R. P.; McGrath, T. D.; Bickley, J. F.; Femoni, C.; Steiner, A. *Inorg. Chem. Comm.* **2001**, *4*, 16.

(66) (a) Cotton, F. A.; Dikarev, E. V.; Petrukhina, M. A. *J. Am. Chem. Soc.* **2001**, 11655. (b) Cotton, F. A.; Dikarev, E. V.; Petrukhina, M. A.; Taylor, R. E. *J. Am. Chem. Soc.* **2001**, *123*, 5831. (c) Cotton, F. A.; Dikarev, E. V.; Petrukhina, M. A. *Angew. Chem. Int. Ed.* **2001**, *40*, 1521. (d) Cotton, F. A.; Dikarev, E. V.; Petrukhina, M. A., Stiriba, S. E. *Polyhedron* **2000**, *19*, 1829. (e) Cotton, F. A.; Dikarev, E. V.; Petrukhina, M. A. *Angew. Chem. Int. Ed.* **2000**, *39*, 2362. (f) Cotton, F. A.; Dikarev, E. V.; Petrukhina, M. A.; Stiriba, S. E. *Organometallics* **2000**, *19*, 1402.

(67) Cotton, F. A.; Wilkinson, G.; Murillo, C. A.; Bochmann, M. *Advanced Inorganic Chemistry*, 6th Ed., John Wiley & Sons: New York, 1999. p 1054.

(68) Cotton, F. A.; Shiu, K.-B. *Rev. Chim. Min.* **1986**, *23*, 14.

(69) Cotton, F. A.; Dikarev, E. V.; Feng, X. *Inorg. Chim. Acta* **1995**, *237*, 19.

(70) (a) It is important to emphasize that the two requirements of bulkiness and the presence of solubilizing substituents must be met. It has been known that bulk alone was not enough to block the axial positions. For example, even with the very bulky carboxylate ligand 2,4,6-tri-tolylbenzoate, pyridine molecules had been found occupying the axial positions of the corresponding tetracarboxylate dirhodium units. See: Callot, H. J.; Albrecht-Gary, A.-M.; Al Joubbeh, M.; Metz, B.; Metz, F. *Inorg. Chem*. **1989**, *28*, 3633.

(71) Rempel, G. A.; Legzdins, P.; Smith, H.; Wilkinson G. *Inorg. Synth.* **1972**, *13*, 90.

(72) (a) Legzdins, P.; Mitchell, R. W.; Rempel, G. L.; Ruddick, J. D.; Wilkinson, G. *J. Chem. Soc., A*. **1970**, 3322. (b) Cotton, F. A.; Dikarev, E. V.; Feng, X. *Inorg. Chim. Acta* **1995**, *237*, 19.

(73) Sheldrick, G. M. *SHELXL-97: Program for Crystal Structure Refinement*; University of Göttingen: Göttingen, Germany, 1997.

(74) (a) Bear, J. L.; Kitchens, J.; Wilcott, III, M. R. *J. Inorg. Nucl. Chem*.**1971**, *33*, 3479. (b) Cotton, F. A.; Norman, Jr., J. G. *J. Am. Chem. Soc.* **1972**, *94*, 5697. (c) Stephenson, T. A.; Morehouse, S. M.; Powell, A. R.; Heffer, J. P.; Wilkinson, G. *J. Chem. Soc*. **1965**, 3632.

(75) Webb, T. R.; Dong, T. Y. *Inorg. Chem*. **1982**, *21*, 114.

(76) Callot, H. J.; Metz, F. *Tetrahedron* **1985**, *20*, 4495.

(77) Johnson, S. A.; Hunt, H. R.; Neumann, H. M. *Inorg. Chem*. **1963**, *2*, 960.

(78) (a) Norman, Jr., J. G.; Kolari, H. J. *J. Am. Chem. Soc*. **1978**, *100*, 791. (b) Trexler, Jr., J. W.; Schreiner, A. F.; Cotton, F. A. *Inorg. Chem*.**1988**, *27*, 3265. (c) Miskowski, V. M.; Schaefer, W. P.; Sadeghi, B.; Santarsiero, B. D.; Gray, H. B. *Inorg. Chem*. **1984**, *23*, 1154. (d) Lichtenberger, D. L.; Pollard, J. R.; Lynn, M. A.; Cotton, F. A.; Feng, X. *J. Am. Chem. Soc*. **2000**, *122*, 3182.

(79) (a) Drago, R. S.; Long, J. R.; Cosmano, R. *Inorg. Chem*. **1982**, *21*, 2196. (b) Drago, R. S.; Long, J. R.; Cosmano, R. *Inorg. Chem*. **1981**, *20*, 2920.

(80) Dubicki, L.; Martin, R. L. *Inorg. Chem*. **1970**, *9*, 673.

(81) Cotton, F. A.; Bratton, W. K. *J. Am. Chem. Soc.* **1965**, *87*, 921.

(82) Cotton, F. A.; Daniels, L. M.; Murillo, C. A. *Angew. Chem., Int. Ed. Engl.* **1992**, *31*, 737.

(83) Berno, P.; Shoukang, H.; Minhas, R.; Gambarotta, S. *J. Am. Chem. Soc.* **1994**, *116*, 7417.

(84) Cotton, F. A.; Timmons, D. J. *Polyhedron* **1998**, *17*, 179.

(85) Cotton, F. A.; Dalal, N. S.; Huang, P.; Murillo, C. A.; Stowe, A. C.; Wang, X. *Inorg. Chem.* **2003**, *42*, 670.

(86) Berry, J. F.; Cotton, F. A.; Huang, P.; Murillo, C. A., unpublished results.

(87) Manzer, L. *Inorg. Synth.* **1982**, *21*, 135.

(88) Bradley, W.; Wright, I. *J. Chem. Soc.* **1956**, 640.

(89) Lin, C.; Protasiewicz, J. D.; Ren, T. *Inorg. Chem.* **1996**, *35*, 7455.

(90) Lin, C.; Protasiewicz, J. D.; Smith, E. T.; Ren, T. *Inorg. Chem.* **1996**, *35*, 6422.

(91) Cotton, F. A.; Daniels, L. M.; Hillard, E. A.; Murillo, C. A. *Inorg. Chem.* **2002**, *41*, 1639.

(92) Cotton, F. A.; Huang, P.; Murillo, C. A. *Inorg. Chem. Commun.* **2003**, *6*, 121.

(93) Cotton, F. A.; Matonic, J. H.; Murillo, C. A. *J. Am. Chem. Soc.* **1997**, *119*, 7889.

(94) Cotton, F. A.; Huang, P.; Murillo, C. A. *Inorg. Chem. Commun.* **2003**, *6*, 121.

(95) (a) Cotton, F. A.; Matonic, J. H.; Murillo, C. A. *J. Am. Chem. Soc.* **1998**, *120*, 6047. (b) Cotton, F. A.; Huang, P.; Murillo, C. A.; Timmons, D. J. *Inorg. Chem. Commun.* **2002**, *5*, 501.

(96) For comparison see Evans, W. J.; Brady, J. C.; Ziller, J. W. *Inorg. Chem.* **2002**, *41*, 3340, Karsch, H. H.; Volker, G. W.; Reisky, M. *Chem. Commun.* **1999**, 1695, and Yélamos, C; Heeg, M. J.; Winter, C. H. *Inorg. Chem.* **1998**, *37*, 3892, where the K–O distances are 2.638(2) Å in $[K(DMI)(THF]_n$ (DMI = 2,3-dimethylindolide), 2.708 Å in $[(THF)K(C_5H_4CH_3CH_2PPh_2)]_n$, and 2.716(5) Å in $[(Ph_2C_3HN_2)K(THF)]_6$, respectively.

(97) Only three other examples of the dimetal core in the 3+ oxidation states are known, but these form a trigonal lantern instead of a paddlewheel geometry. See: Cotton, F. A.; Daniels, L. M.; Falvello, L. R.; Matonic, J. H.; Murillo, C. A. *Inorg. Chim. Acta* **1997**, *256*, 269 and Cotton, F. A.; Daniels, L. M.; Maloney, D. J.; Matonic, J. H.; Murillo, C. A. *Inorg. Chim. Acta* **1997**, *256*, 283.

(98) An example of an isolated V(I) compound can be found in: Reardon, D.; Conan, F.; Gambarotta, S.; Yap, G.; Wang, Q. *J. Am. Chem. Soc.* **1999**, *121*, 9318.

VITA

Elizabeth Anne Hillard began her studies at the University of Alaska-Fairbanks in 1991 and obtained a B.A. in theatre in 1995. She has an extensive theatrical resumé. After graduation, she began a pre-med program, and transferred to a degree program in chemistry at the University of Alaska. She completed her chemistry B.S. degree in May 1999. She can be reached through her parents at

4633 Stanford Dr.

Fairbanks, AK 99709.